An optical approximation to the Casimir effect and related topics

by

Antonello Scardicchio

Submitted to the Department of Physics
in partial fulfillment of the requirements for the degree of

Doctor of Philosophy

at the

MASSACHUSETTS INSTITUTE OF TECHNOLOGY
[June 2006]
May 2006

© Massachusetts Institute of Technology 2006. All rights reserved.

Author .....
Department of Physics
May 15th, 2006

Certified by .....
Robert L. Jaffe
Professor of Physics
Thesis Supervisor

Accepted by .....
Tom Greytak
Associate Dept. Head for Education

MASSACHUSETTS INSTITUTE OF TECHNOLOGY
AUG 10 2006
LIBRARIES

ARCHIVES

An optical approximation to the Casimir effect and related topics

by

Antonello Scardicchio

Submitted to the Department of Physics
on May 15th, 2006, in partial fulfillment of the
requirements for the degree of
Doctor of Philosophy

Abstract

In this thesis, I have studied the dependence of the Casimir force between neutral conductors on their shapes. After reducing the problem to that of finding the density of states of an appropriate hamiltonian I studied it by using semiclassical methods. Some exemplary geometries of interest for the experiments are studied in detail.

Thesis Supervisor: Robert L. Jaffe
Title: Professor of Physics

Acknowledgments

These last years I have been through a series of difficult situations.

However the joy of working and doing physics with wonderful people has led me through them like flying. This is the right place to thank them. So I wish to thank my advisor Bob Jaffe, who has taught me much more than good physics, and also Eddie Fahri, Jeffrey Goldstone, Alan Guth, Mehran Kardar and Frank Wilczek and all the people at CTP. I would also like to thank Michael Berry for his warm hospitality in Bristol and his words of wisdom on physics, life and catastrophe theory.

I wish to thank my friends and fellow physicists Sergio Benvenuti, Alexander Boxer, Mauro Brigante, Qudsia Jabeen Ejaz, Guido Festuccia, Massimo Mannarelli and Claudio Marcantonini;

the staff of CTP, Scott Morley, Joyce Berggreen and Charles Suggs, who are all always extremely helpful;

my brotherly friends Paolo Facchi and Saverio Pascazio.

Last but not least, I want to say thank to my family (my father Vito, my mother Filomena and my brother Francesco) and, obviously

to Linda,
to whom this work is dedicated.

Contents

List of Figures

List of Tables

Chapter 1

Introduction

The story of the Casimir effect begins in 1948, when H. Casimir and D. Polder [1], two researchers at the Philips Laboratories in the Netherlands, were studying the interaction forces between neutral colloidal particles in suspensions. Colloidal particles interact through Van der Waals forces, which are due to exchange of virtual photons between neutral, polarizable objects. Casimir and Polder were led to work on this problem by the experimentalists Verveey and Overbeek, who found that the known formulas for the Van der Waals interactions found by London 20 years earlier did not explain their experiments. Casimir and Polder then decided to calculate the Van der Waals forces in a fully relativistic setup, where the finiteness of the speed of light was taken in account.

The difference between theirs and London's calculation would show up when the particles are far from each other (at a distance large compared to the typical wavelength of the exchanged photons). Indeed Casimir and Polder found that in this limit the Van Der Waals interaction decays faster with the distance of the bodies than it was predicted by the non-relativistic calculations by London and in agreement with Overbeek's experiments.

The importance of this particular limit (the 'retarded limit', since the finiteness of the speed of light shows up explicitly) is clear in the case of metallic particles, when photons are exchanged with wavelengths down to $\lambda_p \sim 100$nm (the plasma wavelength), a small distance for this kind of experiment.

The other important fact to understand the apparent ubiquity of Casimir forces is found in a later paper by Casimir. He showed that the involved, second order perturbation theory calculation which led to the result in the first Casimir-Polder paper can be substituted by the calculation of the shift in energy of the vacuum of the electromagnetic field due to the presence of the two dielectric (or metallic) particles. This vacuum energy is given by the famous formula $\mathcal{E} = \sum \frac{1}{2}\hbar\omega$. This formula is difficult to evaluate in the generic case, essentially because the frequencies ω's are typically not known analytically. Nevertheless it gives a new perspective on Casimir forces: Casimir forces are one-loop corrections to the energy of *any* quantum field in a static, classical background. From this point of view Casimir forces arise everywhere in quantum (and statistical) field theory from colloids, to QCD to string theory.

Going back to the electromagnetic Casimir forces, it must be said that they are *the most relevant* interaction between small metallic objects. They are so important for micro mechanical devices that engineers must take them into account in their projects and arrange configurations that minimize their influence. Due to this necessity, together with the ground-breaking 1997 experiment of S. Lamoreax [2], the experiments to measure Casimir forces have become incredibly more precise. Today the Casimir forces are measured with an error of about 0.5%. With such precise tools at hand it becomes imperative to have equally precise theoretical calculations to compare the data with. Unfortunately we, the theorists, have not yet properly sharpened our tools. We still lack a formula, even approximate, or a fast numerical algorithm, to calculate the Casimir force between arbitrarily shaped conductors. At the moment, although it may seem strange, there is no analytic solution for the most relevant experimental geometry, that of a metallic sphere suspended above a plate.

The obstacles on the path to a solution of this and other relevant experimental configurations are more than one. The main one, I think, is that the calculation of the Casimir force between arbitrarily shaped conductors requires an accurate knowledge of the spectrum of the free wave equation in the open space between the conductors. One could think of finding the spectrum of this problem by means of a numerical

algorithm, like a finite boundary elements method. After having found the numerical valued for the level energies, one should sum them up to a sufficiently high cutoff energy Λ. repeat the operation for different positions of the bodies and extract the part of the energy that depends on the relative distances. The interaction part (independent of Λ in the $\Lambda \to \infty$ limit) being subdominant to the total (which diverges like Λ^4). the computational effort required soon becomes titanic. The difficulty of isolating the interaction part of the Casimir energy for arbitrary conductors has contributed a lot to the mystification of the Casimir effect which has been often regarded as an effect arising from some quite funny properties of Riemann zeta functions (for example identities like $\sum n = \zeta(-1) = -1/12$ have been given status of physical facts). It has also generated great confusion on which cut-off dependent terms have to be renormalized and which ones instead do have a physical significance. This debate cannot be dismissed as academic: it is from this mistreatment of the divergent terms that the well-known claims that Casimir force could be repulsive for some geometries arose. How could the retarded limit of an attractive interaction be repulsive?

The situation is sensibly clearer now than it was 5 or 6 years ago and we know how to isolate divergences effectively and in a consistent way and how to extract the Casimir interaction energy in an approximate way for non exactly solvable problems. In this thesis I will discuss one such approximation to calculate the Casimir force, valid for arbitrary geometries, based on the semiclassical analysis of the density of states. This approximation, dubbed the 'optical approximation' [4], provides a useful tool for investigating novel geometries which could not be addressed with the existing techniques (for example the approximation works well even for bodies without symmetries). In the optical approximation (which I will describe in detail in this thesis) the part of the density of states responsible for the *interaction Casimir energy* (and hence the force) is isolated and approximated by a semiclassical expression. This allows one to attach a Casimir energy contribution to any closed classical path followed by a virtual photon inside the cavity created by the bodies. By using this technique it is easy to make a qualitative picture of the solution. For smooth bodies this picture is also quantitatively correct and can be used to make statements about

novel configurations of conductors.

The exploration of novel geometries made us understand how poor the previously existing approximations are and that the calculation of Casimir force for curved bodies is a subtle problem. It also helped to uncover the difficulties associated with estimates of thermal corrections and to the vectorial nature of the electromagnetic field suggesting possible investigations directions. These last two aspects of the Casimir energy have been definitely overlooked in the past.

The plan of this thesis is as follows: in Chapter 2 I will introduce the problem and the general techniques which will be used to solve it; in Chapter 3 I will discuss the optical approximation, its use and its range of validity for a couple of examples. I will also discuss what is known on the thermal corrections and the interplay of the temperature with the curvature of the bodies and with the finite conductivity. This will conclude the discussion of the *experimental* Casimir effect and the first part of the thesis. In the second part of this thesis I will discuss some more field-theoretic topics related to Casimir energy. In Chapter 4 I will discuss the problem of calculating the Casimir force between small perfect scatterers, in Chapter 5 the force on a single plate due to inhomogeneities of the space and finally in Chapter 6 I will put forward a duality between the Casimir energy and the probability of having certain related configurations of nodal lines in a random superposition of waves. Partial conclusive sections are included in each chapter which give an overview of the work done and future perspectives.

Chapter 2

The Casimir Energy

In this Chapter I will introduce the main tools necessary to calculate the Casimir energy. I will present both the canonical quantization and the path-integral expressions for the Casimir energy, each useful for describing different aspects, and prove their equivalence. The path-integral form makes clear the regularization and renormalization procedure while the canonical form is more suitable for the development of approximated expressions.

2.1 Field Theoretic Setup

As we saw in the Introduction, the most general point of view on the Casimir forces is to regard them as one loop corrections to the energy of a quantum field in a classical background. This allows us to use the techniques developed in the context of quantum field theory and to link a wide variety of problems together. So in this spirit we will consider the influence of matter on the electromagnetic field as that of a classical background. Moreover we will make the simplification of considering a scalar field instead of the full electromagnetic field. Once the problems associated with the gauge invariance are taken care of (by fixing a gauge and by a Faddeev-Popov procedure) in the perfect metal limit the electromagnetic field is (formally) not different from a scalar field.

In this section x is the d-dimensional space coordinate, t the time and no particular

notation is used to define vectors.

Let us start by writing the action functional for a massless real scalar field ϕ coupled to classical matter (represented by the function $\sigma(x)$) in $d+1$ dimensions

$$S[\phi] = \int_0^T dt \int d^d x \left(\frac{1}{2}(\partial\phi)^2 - \frac{1}{2}\sigma(x)\phi^2 \right). \tag{2.1}$$

The function σ represents the influence of the matter on the field ϕ (the "photon"). Eventually we will need σ to be infinite in order to impose the condition $\phi = 0$ on the surface of the bodies which better mimics the conditions on the electric field on the surface of a perfect metal. But for the moment we will assume σ to be a continuous bounded real function.

The effective action $\mathcal{S}_{eff}$ is defined as the path integral

$$e^{i\mathcal{S}_{eff}} = \int \mathcal{D}\phi e^{iS[\phi]} \tag{2.2}$$

and the effective energy (or Casimir energy) $\mathcal{E}$ as [47]

$$\mathcal{E} = -S_{eff}/T. \tag{2.3}$$

We can easily prove that this definition is equivalent to that, more common, obtained by canonical quantization

$$\mathcal{E} = \sum_k \frac{1}{2}\hbar\omega_k, \tag{2.4}$$

where ω_k are the proper frequencies of the scalar field in the static background $\sigma(x)$ (a sufficiently smooth, positive real function), obtained by solving the eigenvalue problem

$$-\nabla^2\phi_k + \sigma\phi_k = \omega_k^2\phi_k, \tag{2.5}$$

where k is an index for the eigenvectors ϕ, in general a d-dimensional vector of integers or real numbers (respectively for discrete or continuous spectrum). For example, if $\sigma = 0$, k would represent the possible wave-vectors of a given free wave. The eigenfunctions ϕ_k form a complete orthonormal set for $L^2(\mathbf{R}^3)$.

To prove the equivalence between (2.4) and (2.3) we write explicitly

$$\begin{aligned} e^{-i\mathcal{E}T} &= \int \mathcal{D}\phi \exp\left(-i\int_0^T dt \int d^dx \frac{1}{2}\phi(\partial_t^2 - \nabla^2 + \sigma - i0^+)\phi\right) \\ &= \det{}^{-1/2}\left(\partial_t^2 - \nabla^2 + \sigma - i0^+\right), \end{aligned} \tag{2.6}$$

(where a small imaginary term has been added to ensure convergence) and hence

$$\begin{aligned} \mathcal{E} &= \frac{i}{T}\ln\det{}^{-1/2}\left(\partial_t^2 - \nabla^2 + \sigma - i0^+\right) \\ &= \frac{-i}{2T}\mathrm{Tr}\ln\left(\partial_t^2 - \nabla^2 + \sigma - i0^+\right). \end{aligned} \tag{2.7}$$

The trace can be done on the basis for $L^2(\mathbf{R}^4)$ of the type $|\omega, k\rangle \equiv |\omega\rangle \otimes |k\rangle$ where $\langle t|\omega\rangle = \frac{1}{\sqrt{2\pi}}e^{i\omega t}$ and $\langle x|k\rangle = \phi_k(x)$ is the complete set of properly normalized solutions of equation (2.5). We get

$$\mathcal{E} = \frac{1}{2iT}\int_{-\infty}^{\infty}\frac{Td\omega}{2\pi}\sum_k \ln(\omega^2 - \omega_k^2 + i0^+). \tag{2.8}$$

By integration by part this last expression can be rewritten as

$$\mathcal{E} = -\sum_k \frac{1}{2}\int_{-\infty}^{\infty}\frac{d\omega}{2\pi i}\omega\frac{2\omega}{\omega^2 - \omega_k^2 + i0^+}. \tag{2.9}$$

The integration can be done explicitly now by closing the contour in the lower semi-plane and picking up the poles $\omega_k - i0^+$, giving equation (2.4).

Neither (2.4) nor (2.3) are finite quantities. They are, as most of the relevant quantities in quantum field theory, affected by divergences. However the interaction energy, which gives rise to the force between separated rigid bodies, is finite. For a careful treatment of these divergences, the definition (2.3) is more suitable, because it can be written in a diagrammatic expansion and the divergences can be identified in each diagram. By writing a perturbation series in powers of σ [47] we obtain the

diagrammatic result of Figure 2.1 which can be rewritten by using

$$\mathrm{Tr}\ln(\partial^2+\sigma) = \mathrm{Tr}\ln(i/G) + \sum_{n\geq 1}\frac{1}{n}\mathrm{Tr}\left(G(-i)\sigma\right)^n \tag{2.10}$$

where in momentum space $G = i/(\omega^2 - k^2)$ is the propagator of the free scalar field. The n-th term in the sum corresponds to the loop with n external lines attached (the factor $1/n$ in the sum is the correct symmetry factor). The first term in (2.10) corresponds to a *cosmological constant* renormalization. It does not concern us here because it is independent on the details of the matter distribution σ but its effects would be important in a gravitational theory. For the moment we assume we can dispose of it without further comments.

In the rest of this section we will prove that for $d = 3$ the 'cosmological constant' term above and the $n = 1$ term in (2.10) are the only ones which need regularization and renormalization. We will also prove that they do not depend on the relative positions of the bodies (this statement is self-evident for the first term in (2.10)) and hence do not contribute to the force between rigid bodies [77]. This is not the case for the divergences that occur in common Casimir calculations which make use of zeta-function regularization techniques. First of all there are more of the latter as they arise from the lack of smoothness of the distribution of matter σ. Second, they are not the kind of divergences that can be regularized and one must check if they have physical effects (as it happens when one approaches the problem of the stress on a single body). If they do then the problem is ill-posed and the the Casimir forces depend on fine details of the response function of the matter. In particular no perfect metal limit can be implemented.

So let us start from a matter distribution which is static, infinitely smooth and of compact support ($\sigma(x) = 0$ outside a compact subset of $\mathbf{R}^3$). This means that the Fourier transform of the function $\sigma(x)$, which we will denote as $\sigma(\omega, k) = \delta(\omega)\tilde{\sigma}(k)$, vanishes faster than any power of $|k|$ at large wave numbers $|k|$. The $n = 1$ term in (2.10) can be written as

$$\frac{T}{2\pi}\int \frac{d\omega d^d k}{(2\pi)^{d+1}} G(\omega, k)\tilde{\sigma}(0). \tag{2.11}$$

The factor $T/2\pi$ comes from the $\delta(0)$ in $\sigma(\omega, k)$. For static distributions of matter every term in the expansion (2.10) will be linear in T, giving an energy $\mathcal{E}$ which is independent of T (extensiveness of the action in the time direction). The integral in (2.11) is quadratically divergent (for $d = 3$) however it depends only on the *total amount of matter* $\tilde{\sigma}(0) = \int d^d x \sigma(x)$. We can reabsorb this divergence by a term $\int dt dx \sigma$ in the action (this is known as "no tadpole condition"). In the case of separated rigid bodies this divergence is not observable since moving the bodies rigidly does not change the total amount of matter. We now go on and examine the second term in the sum over n of (2.10). The $n = 2$ term in that expression is

$$\frac{T}{2\pi}\int \frac{d^d k}{(2\pi)^d}\int \frac{d\omega' d^d k'}{(2\pi)^{d+1}} G(\omega', k')G(\omega', k'+k)|\tilde{\sigma}(k)|^2 \quad = \\ = \frac{T}{2\pi}\int \frac{d^d k}{(2\pi)^d}|\tilde{\sigma}(k)|^2 \int \frac{d\omega' d^d k'}{(2\pi)^{d+1}} \frac{i}{\omega'^2 - k'^2}\frac{i}{\omega'^2 - (k'+k)^2} \tag{2.12}$$

(again linear in T) and under the smoothness conditions established above for σ it is a finite integral in $d < 4$ and in particular $d = 3$ (divergences can only arise from the k' integral). This is in perfect accord with the rules of perturbative quantum field theory [47].

So the Casimir interaction is well defined if and only if we are calculating the force between rigid bodies *i.e.* if we do not change the total amount of matter.[1] We are not allowed to discard divergences which arise in the case of single bodies expanding or contracting, in doing it we would obtain wrong results. Even though we will not pursue this observation further (a recent example with discussions is contained in [53]) we notice that it allows us to dismiss all the known cases in which the Casimir force was found to be repulsive. This in turn has enormous relevance for the experiments.

In the rest of this Chapter we will move on to express Eq. (2.4) in a form even more suitable for calculations.

[1]Conservation of the quantity of matter alone would not forbid a change in the shape of the bodies. A more accurate analysis does indeed show that one cannot change the shape of the bodies either, leaving as only alternative rigid displacement. We will show this in Chapter 3, when we will have more tools to analyze the shape dependence of the Casimir energy.

2.2 From the Casimir energy to the density of states

In this section we will rewrite the Casimir energy (2.4) in a form which makes explicit use of the density of states of a Schrodinger equation on a domain with appropriate boundary conditions. Such a problem has been analyzed extensively in the literature in the realm of semiclassical quantum mechanics and in mathematics it is known as the 'spectral problem' for hermitian operators.

Let us start from (2.4)

$$\mathcal{E} = \sum_k \frac{1}{2}\hbar\omega_k, \tag{2.13}$$

where ω_k are the positive roots of the eigenvalues of the Schrodinger equation (2.5). This last equation we will rewrite by defining $\omega = \sqrt{E}$

$$-\nabla^2\phi(x) + \sigma(x)\phi(x) = E\phi(x), \tag{2.14}$$

or

$$H\phi(x) = E\phi(x). \tag{2.15}$$

We make a further simplification, now, assuming $\sigma \to +\infty$ on the bodies, in such a way to make them impenetrable. This mimics the case of a perfect metal, corrections expected when the distances of the bodies becomes comparable to the plasma wavelength (or $1/\sqrt{\sigma}$ in our Lagrangian). The space between the bodies is then represented by a domain $\mathcal{D} \subset \mathbf{R}^3$ and the functions must vanish continuously outside $\mathcal{D}$ and hence on the boundary $\partial\mathcal{D}$.

We then have to study the problem

$$\begin{aligned} H\phi(x) &= E\phi(x) \\ H &= -\nabla^2 \\ \phi(x) &= 0 \qquad \text{for} \quad x \in \partial\mathcal{D}. \end{aligned} \tag{2.16}$$

The positivity of the hermitian operators $-\nabla^2$ (with these boundary conditions)

ensures the reality of the Casimir energy. We can rewrite (2.13) as

$$\mathcal{E} = \frac{1}{2}\hbar \int_0^\infty dE \rho(E) \sqrt{E}, \tag{2.17}$$

where $\rho(E)$ is the density of states of (2.16) and by writing

$$\rho(E) = \frac{1}{\pi} \text{Im Tr} \frac{1}{H - E - i0^+}, \tag{2.18}$$

it is evident that our original field theory problem is now a problem in quantum mechanics or, if you prefer, scattering theory. The relevant quantity is the propagator

$$G(x', x; E) \equiv \langle x' | \frac{1}{H - E} | x \rangle \tag{2.19}$$

(we have used the same letter G that denoted the two-points function in the previous section, confident that there will be no confusion since we are not going to use the two-points correlation function anymore).

Our goal in this thesis is to develop an approximation to G which is able to separate the divergences from the finite interaction part in a sensible and accurate way. We know indeed from the previous Section that for rigid bodies this can be done. We anticipate that we will do this by rewriting G as a path integral and saturate it with a sum over from classical paths. This will make it exact in the case of parallel plates and a very good approximation for gently curved bodies.

Let us write the Fourier transform of $G(x', x; E)$ as a path integral

$$G(x', x; t) = \langle x' | e^{-iHt} | x \rangle = \int_{x(0)=x}^{x(t)=x'} \mathcal{D}x(t) \exp\left(i \int_0^t dt \frac{\dot{x}^2}{4} \right). \tag{2.20}$$

The boundary conditions on the function $\phi(x)$ turn into boundary conditions for the propagator $G(x', x; t)$ for any one of the points x' and x on the boundary $\partial\mathcal{D}$. The particle is free inside $\mathcal{D}$ but the fact that it cannot penetrate in the bodies makes it impossible to evaluate (2.20) exactly. We will see however that the boundary conditions can be imposed by considering classical paths which bounce on the "walls"

$\mathcal{D}$ and get a phase factor (-1) for each bounce. We will analyze the implications of this picture in the next Chapter. We anticipate that we will have to take the semiclassical approximation of $G(x', x; t)$, then Fourier transform to $G(x', x; E)$ and insert this expression in $\rho(E)$ and finally in $\mathcal{E}$ to obtain the optical approximation to the Casimir energy.

Chapter 3

The Optical Approximation to the Casimir Energy

In this chapter I will introduce and develop the optical approximation for the calculation of the Casimir energy between conductors of arbitrary shape. The need for such an approximation, as underlined in the previous chapters, stems from the fact that the problem is unsolvable in the generic case.

After the introduction of the optical approximation for the Schrödinger equation propagator and the resulting approximation for the Casimir energy, I will analyze some examples and discuss the limits of validity of the approximation itself.

I will then go on to study how to use the approximation for other observables. In particular I will calculate the optical approximation for the energy-momentum tensor and focus on the pressure as an alternative way of calculating the Casimir force. Some examples will be proposed that parallel those in the first part of the chapter. I will also consider the introduction of a temperature and discuss the correction to the force for small temperatures. We will see that these corrections come from the low momentum part of the propagator and hence are not captured correctly by our approximation.

3.1 Introduction

Revolutionary new experimental techniques have made possible precise measurements of Casimir forces[40]. Casimir's original prediction for the force between grounded conducting plates due to modifications of the zero point energy of the electromagnetic field has already been verified to an accuracy of a few percent. Variations with the conductor geometry and the effects of finite conductivity and finite temperature will soon be measured as well. Progress has been slower on the theoretical side. Despite years of effort, Casimir forces can only be calculated for the simplest geometries. Beyond Casimir's original study of parallel plates[1], we are only aware of useful calculations for a corrugated plate[41] and for a sphere and a plate[42]. The former was obtained with functional integral techniques quite special to that geometry and the latter was obtained by computationally intensive numerical methods. Simple and experimentally interesting geometries like two spheres, a finite inclined plane opposite an infinite plane, and a pencil point and a plane, remain elusive. The Proximity Force Approximation[3] (PFA), which has been used for half a century to estimate the dependence of Casimir forces on geometry, was shown in many examples [41, 42] to deviate significantly from precise numerical results. Thus at present neither exact results nor reliable approximations are available for generic geometries. It was in this context that we recently proposed a new approach to Casimir effects based on classical optics[4]. The basic idea is extremely simple: first the Casimir energy is recast as a trace of the Green's function; then the Green's function is replaced by the sum over contributions from optical paths labelled by the number of (specular) reflections from the conducting surfaces. The integral over the wave numbers of zero point fluctuations can be performed analytically, leaving

$$\mathcal{E}_{\rm opt} = -\frac{\hbar c}{2\pi^2}\sum_r (-1)^r \int_{\mathcal{D}_r} d^3x \frac{\Delta_r^{1/2}(x)}{\ell_r^3(x)}. \tag{3.1}$$

Here $\ell_r(x)$ is the length of the closed geometric optics ray beginning and ending at the point x and reflecting r times from the surfaces. $\Delta_r(x)$ is the enlargement factor of

classical optics[5, 6], also associated with the r-reflection path beginning and ending at x. $\mathcal{D}_r$ is the subset of the domain, $\mathcal{D}$, between the plates in which r reflections can occur. The factor $(-1)^r$ implements a Dirichlet boundary condition on the plates; different boundary conditions require different factors. Both $\ell_r(x)$ and $\Delta_r(x)$ are very easy to compute either analytically in simple cases, or numerically in general. $\Delta_r(x)$, although well known in optics, may not be familiar in the context of Casimir effects. We will describe its properties in some detail.

Eq. (3.1) turns out to be a powerful tool to compute Casimir effects for generic geometries, and to identify, interpret and dispose of, divergences. Eq. (3.1) is not exact. Instead it is an approximation which is valid when the natural scales of diffraction are large compared to the scales that measure the strength of the Casimir force. In practice this will typically be measured by the ratio of the separation between the conductors, a, to their curvature, R. Although approximate, the optical approach is surprisingly accurate, as well as physically transparent and versatile. It generalizes naturally to the study of Casimir thermodynamics, to the study of energy, pressure, and momentum densities, to various boundary conditions, to fermions, and to compact and/or curved manifolds. In the first sections of this chapter we will focus on fundamentals: how to derive the optical approximation and how to apply it to practical calculations of Casimir forces. In the later sections we study Casimir effects at finite temperature, the calculation of local observables like the energy density and pressure, and the generalization to conducting and other boundary conditions. Our first aim is to familiarize the reader with the use of the optical approximation, since this method of calculation is unfamiliar. In Section II we present some examples of the use of the optical approximation. First we review in more detail the treatment of parallel plates already presented in Ref. [4]. Although it is no great triumph to rederive this classic result, the optical derivation illustrates several characteristic features of the method: rapid convergence, simple disposal of divergences and ease of computation, in particular. Next we present the case of a sphere and a plate. This too was summarized in Ref. [4]. Here we concentrate especially on the enlargement factor, both its interpretation and how to compute it. Also we illustrate the generic way that

divergences can be eliminated. The numerical results we present here are more accurate than those of Ref. [4]. Finally we apply the optical method to the case of a finite plate suspended above an infinite conducting plane – the "Casimir pendulum". We show how all reflections can be computed and how the optical result differs from the proximity force approximation. In collaboration with O. Schroeder we are preparing a thorough study of the hyperboloid ("pencil point") near an infinite plane[7]. In Section III we discuss the derivation of the optical approximation from exact expressions for the Casimir energy. We show how a uniform approximation to the propagator turns into a uniform approximation for the Casimir energy. The derivation illustrates the nature of the approximation and shows the way toward improvements, which, in essence, amount to including the effects of diffraction. We present results for a massive scalar field in N dimensions in Section III. We discuss the general problem of divergences. The Casimir energy is generically divergent — or more properly, it depends in detail on the cutoffs that limit the conductivity of real materials at high frequency. However it is known that the Casimir *force* between rigid conductors is cutoff independent[8]. In the optical approximation the cutoff dependent terms in the Casimir energy can easily be isolated and shown to be independent of the separation between conductors. They therefore do not contribute to forces and can be dropped. Corrections to the optical approximation will bring in new surface divergences. In Section 3.3.3 we discuss the relation of the optical approximation to previous works on "semiclassical" approximations to the Casimir energy[9]. In the last section we summarize our results, discuss their implications, and mention extensions to other interesting geometries.

3.2 Three examples

In this section we present three examples of the use of the optical approximation, eq. (3.1). Our aim is expressly pedagogical: we want to demonstrate that this method can yield interesting and accurate results without onerous calculations.

3.2.1 Parallel plates

Casimir's original result for parallel plates can be derived in many ways. We present a derivation from the optical approximation in order to illustrate several generic features of the approach in the simplest possible context. The points we wish to stress are: ease of calculation; the rapid convergence in r, the number of reflections; and the simple and accurate treatment of divergences. The "semiclassical" method[9] and the method of images[10] generate exactly the same calculation as ours for parallel plates. However they do not generalize to less trivial geometries (although one might say that our method *is* the correct generalization of the method of images). We study a massless scalar field for simplicity, and quote the generalization to a massive scalar in a later section. For a flat surface the enlargement factor Δ_r reduces to $1/\ell_r^2(x)$, so the contribution of the r reflection path is

$$\mathcal{E}_r = -\frac{\hbar c}{2\pi^2}(-1)^r M_r \int_{\mathcal{D}_r} d^3x \frac{1}{\ell_r(x)^4}, \tag{3.1}$$

where M_r is the multiplicity of the path. It is convenient to separate the paths into "odd" ($r = 2n+1$) and "even" ($r = 2n$) according to the number of reflections. Some of these paths are shown in Fig. 3-1. Odd and even paths differ dramatically in their contribution to the Casimir effect: they differ in sign and in multiplicity: $M_r = 1$ for odd paths and $M_r = 2$ for even paths, as shown in the figure. The length of an even path depends only on n, whereas the length of an odd path varies with position. Finally, odd paths contribute a divergence to $\mathcal{E}$, but do not contribute to the Casimir force. The even paths are finite and give the entire Casimir force. First consider the even paths. The length of the $2n$ reflection path is $\ell_{2n} = 2na$ independent of x, as can easily be seen in Fig. 3-1. The volume of each domain, $\mathcal{D}_{2n}$, is the volume between the plates, Sa. Hence the contribution from even paths is

$$\mathcal{E}_{\text{even}} = -\frac{\hbar c}{2\pi^2} 2Sa \sum_{n=1}^{\infty} \frac{1}{(2na)^4} = -\frac{\hbar c \pi^2}{1440 a^3} S. \tag{3.2}$$

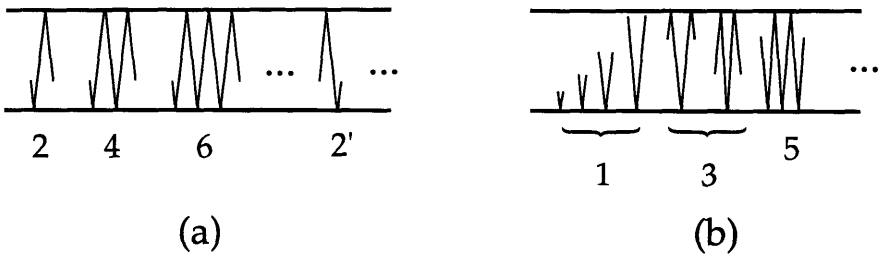

Figure 3-1: Optical paths for parallel plates. The initial and final points on the paths, which coincide, have been separated so the paths can be seen. a) Even reflections 2, 4, and 6. Path 2' is distinct from 2 and illustrates the origin of $M_{2n} = 2$. b) Odd reflection paths. The paths shown form a family of continuously increasing length. Another family begins with the first reflection from the top.

which is the famous result due to Casimir[1] [1]. Next consider the odd paths. There are two families. One is illustrated in Fig. 3-1. The other family begins with the first reflection from the top plate. Their contributions are identical, giving an overall factor of two. The $r = 2n + 1$ reflection paths range in length from $2na$ to $2(n + 1)a$ as can be seen from Fig. 3-1, and contribute

$$\mathcal{E}_{2n+1} = \frac{\hbar c}{2\pi^2} 2S \int_{na}^{(n+1)a} dz \frac{1}{(2z)^4}, \text{ for } n = 0, 1, 2, \ldots \tag{3.3}$$

The first reflection contribution diverges at the lower limit. As discussed in the Introduction (and further in Section III) the divergence indicates dependence on the properties of the material composing the plates and is cutoff at a distance scale ϵ determined by the microphysics. For example we can take ϵ to be the skin depth or regard ϵ as $\sim c/\Lambda$, where Λ is a frequency cutoff, for example the plasma frequency of the metal. Inserting ϵ as the lower limit for $n = 0$ and summing over n, we obtain the contribution of odd paths,

$$\mathcal{E}_{\text{odd}} = \frac{\hbar c}{2\pi^2} 2S \int_{\epsilon}^{\infty} dz \frac{1}{(2z)^4} = \frac{\hbar c}{48\pi^2 \epsilon^3} S \tag{3.4}$$

[1]In the case of the electromagnetic field treated by Casimir there is an extra factor of two due to the two independent polarizations.

This contribution displays the cubic surface divergence expected for a scalar field obeying a Dirichlet boundary condition[11]. However, the divergent term — and indeed the sum of all odd reflections — is independent of a and therefore does not contribute to the *force* between the plates. Until now we have not considered the contributions from one-reflection paths that lie below the bottom plate or above of the top plate. It is easy to see that the sum of these contributions is identical to eq. (3.4) and does not contribute to the force. This simple calculation illustrates some general features of the optical approach:

- The even reflections dominate, give rise to attraction, and their sum converges rapidly in n. They are also attractive for Neumann boundary conditions, where the factor $(-1)^r$ is absent. They would be repulsive if one surface were Neumann and the other Dirichlet.[2] In the case of parallel plates 92% of the Casimir effect comes from the second reflection, 98% from the second and fourth, and 99.3% from the second, fourth and sixth reflections. Similar results will be found to hold in more complicated geometries.

- The only divergent contribution comes from the first reflection. It does not depend on the separation and therefore does not contribute to the Casimir force. This result is quite general. To see the general argument, reconsider the first reflection from the bottom plate, $\mathcal{S}_1$

$$\mathcal{E}_{1,\mathcal{S}_1} = \frac{\hbar c}{2\pi^2} S \int_\epsilon^a dz \frac{1}{(2z)^4} = \frac{\hbar c}{2\pi^2} S \int_\epsilon^\infty dz \frac{1}{(2z)^4} - \frac{\hbar c}{2\pi^2} S \int_a^\infty dz \frac{1}{(2z)^4}. \quad (3.5)$$

  The first term in eq. (3.5) combined with the contribution of the 1-reflection path outside of the plates (from the lower face of the bottom plate) is the cutoff dependent energy of an isolated plate. It is manifestly independent of the presence of any other conductor, and gives no contribution to Casimir forces. The second term is a finite effect of the first reflection. For parallel plates the finite

[2]The expression for parallel plates contains series $-1+1/2^4-1/3^4+\ldots = -\frac{7}{8}\frac{\pi^4}{90}$ so for a Dirichlet-Neumann configuration we have a *repulsive* force 7/8 of the attractive force for Dirichlet-Dirichlet and Neumann-Neumann. This result was found by Boyer [30] in his analysis of a perfectly conducting plate facing a perfectly permeable plate.

contribution of the first reflection is cancelled by higher odd reflections. This occurs whenever the enlargement factor is $1/\ell_n^2$, that is, when all the conductors are planar. For non-planar surfaces the first reflection gives a (relatively small) cutoff independent contribution to the force.

- The optical approach gives the exact answer for infinite plates. However it will fail when $S^{1/2} \approx a$ for the same reason that the capacitance of two finite, parallel metallic plates contains corrections of order a^2/S[12]: It is a poor approximation to consider the electric field inside two far separated plates ($a \gg S^{1/2}$) as constant inside and zero outside. Likewise, in the same limit it is a poor approximation to expect the Green's function for the field ϕ to have contributions only from optical paths. The corrections, or edge effects, can be regarded as due to diffractive rays coming from the edges of the plates [13]. We discuss corrections to the optical approximation in further detail in Section III.

- The difference between even and odd paths has a fundamental origin, as already noticed in work on the "semiclassical" approximation to the Casimir energy [9]. The even paths are truly periodic, in the sense that the momentum of the particle, after going around the path, returns to its initial value. These are therefore the paths that according to Gutzwiller [14] contribute most to the oscillations of the density of states. The connection between these paths, the oscillation of the density of states, and the finite part of the Casimir energy has been noted many times[15] and is exact for parallel plates and related geometries (*eg.* flat manifolds with various topologies). However, the exactness of this result is an accident due to the particularly simple geometry. For example, there are very simple geometries in which periodic paths do not exist at all (*eg.* the Casimir pendulum: a finite plane inclined at an angle above an infinite surface). The relation between the optical approach and the "semiclassical" approach is discussed further in Section III.

3.2.2 The sphere and the plane

Next we analyze a problem with non-planar conductors — typical of real experimental configurations[40] — a sphere of radius R separated by a distance a from an infinite plane. In Ref. [4] we tested the optical approximation by computing the Casimir force between a sphere and a plane up through the fourth reflection. We showed that the optical approximation is in very good agreement with the numerical results of Ref. [42] for $a/R < 1$. In fact the numerical results presented in Ref. [4] suffered from an insufficiently accurate numerical integration algorithm. The results presented here supercede Ref. [4] and show that the optical approximation is even more accurate than we originally claimed. For example, the optical approximation and the numerical data differ by only 30% at $a/R \approx 5$. Here we explain in detail how to compute the first and second reflection contributions. The relevant paths are shown along with some other aspects of the geometry in Fig. 3-2. For each reflection we must compute a) the

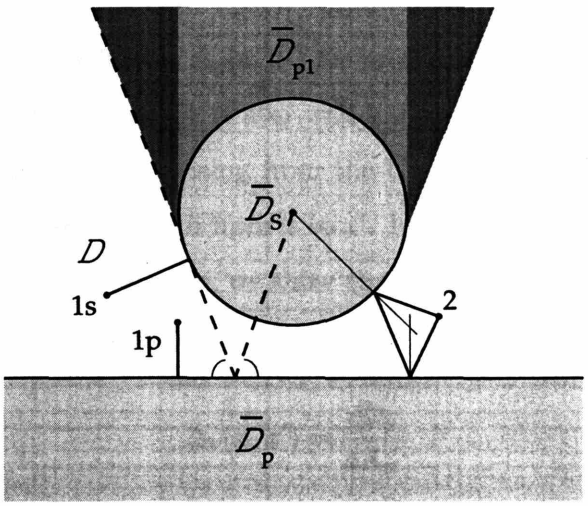

Figure 3-2: Geometry and reflections for a sphere and a plane. The regions and geometrical constructions are defined in the text.

optical path length, $\ell_r(x)$, b) the enlargement factor, $\Delta_r(x)$, and c) the domain of integration $\mathcal{D}_r$ for which r-reflections are possible. The $\mathcal{D}_r$ are subsets of the domain $\mathcal{D}$ above the plane and outside the sphere.

Optical path lengths, $\ell_r(x)$

Finding the r-reflection optical path from x back to x, $\ell_r(x)$, is elementary in principle. One just draws straight lines from x to a given surface, from the arrival point on this surface to another surface, and so on, returning after r reflections to the original point x. One then moves the points of reflection on the surfaces until one reaches the minimum total length (an elastic string would do the job). The minimum length path suffers specular reflection upon each encounter with a surface. In all but the simplest geometries this problem must be solved numerically. However it is a problem amenable to extremely quick numerical solution: it is easily defined and the minimum is unique (at least for convex surfaces). This procedure also defines the points of reflection, $x_{r,1}(x)$, $x_{r,2}(x)$, etc. The first reflection paths from the sphere ($1s$) and the plane ($1p$) and the two reflection path are shown in Fig. 3-2.

Enlargement factor, $\Delta_r(x)$

The enlargement factor for the closed path beginning and ending at x is a special case of the general enlargement factor, $\Delta_r(x,x')$ for propagation from x to x', well known in optics[5, 6]. In another guise, it is also well known to field theorists: $\Delta_r(x,x')$ is just the van Vleck determinant arising from the Gaussian fluctuations of the action about the classical r-reflection path from x to x'. In Section III, where we discuss the origins of the optical approximation, we show that the evaluation of the determinant gives the standard optics definition,

$$\Delta_r(x,x') = \frac{d\Omega_x}{dA_{x'}} \tag{3.6}$$

From this definition it is clear that in order to obtain $\Delta_r(x,x')$ one must follow the spread of an infinitesmal pencil of rays of opening $d\Omega_x$ from their origin at x, along this path, and measure the spread in area $dA_{x'}$ when they arrive at x'. Having already identified the points of reflection in 3.2.2 it is relatively easy to compute $\Delta(x,x')|_{x'=x}$ numerically by tracing the paths of a few nearby rays[7]. It is also possible to solve this problem analytically. Here we present the analytic solution for the first and second

reflections from a sphere and plane. Beyond this level, it is probably more efficient to proceed numerically. One reflection from the plane is trivial: $\Delta(x,x) = 1/\ell_1^2(x)$ One reflection from the sphere is simplified by a) normal incidence, and b) $x = x'$. The second reflection can be simplified by regarding it as a single reflection from the sphere starting from x and ending at the *image* $\tilde{x}$ of the original point x in the plane. In that case we need $\Delta_1(x,\tilde{x})$. Consider the path from x to the sphere at the point Q, and then to x'. To obtain Δ one must follow the wavefront radii of curvature along the ray. We consider a ray that impacts the sphere at an angle θ to the normal. It travels a distance σ_1 before and σ_2 after, with $\ell = \sigma_1 + \sigma_2$. These variables are defined in Fig. 3-3(a). Consider a pencil of rays originating at x, spanning two infinitesmal arcs of angular widths $d\phi_{1,2}$ along perpendicular directions. Let dx'_1 and dx'_2 be the associated arc lengths observed at x'. Then

$$\Delta_r(x) = \left.\frac{d\Omega_x}{dA_{x'}}\right|_{x'=x} = \left.\frac{d\phi_1}{dx'_1}\frac{d\phi_2}{dx'_2}\right|_{x'=x}. \tag{3.7}$$

Since both the initial ray and the sphere have equal radii of curvature we have the freedom to choose the directions defining $d\phi_1$ and $d\phi_2$. We choose "latitude" and "longitude" as follows: Latitude is the direction perpendicular to the plane formed by x, x' and the center of the sphere (see Fig. 3-3(a)). Longitude is the direction in the plane. Consider the pencil of rays of varying latitude as shown in Fig. 3-3(b). The variables are defined in the figure. It is easy to see that

$$dx'_1 = \sigma_1 d\phi_1 + \sigma_2 d\alpha, \tag{3.8}$$

and considering that $d\alpha = 2d\beta\cos\theta + d\phi_1$ and $Rd\beta = \sigma_1 d\phi_1$, we find

$$\frac{d\alpha}{d\phi_1} = 1 + \frac{2\sigma_1\cos\theta}{R}, \tag{3.9}$$

and hence

$$\frac{d\phi_1}{dx'_1} = \frac{1}{\ell + \frac{2\sigma_1\sigma_2\cos\theta}{R}} \tag{3.10}$$

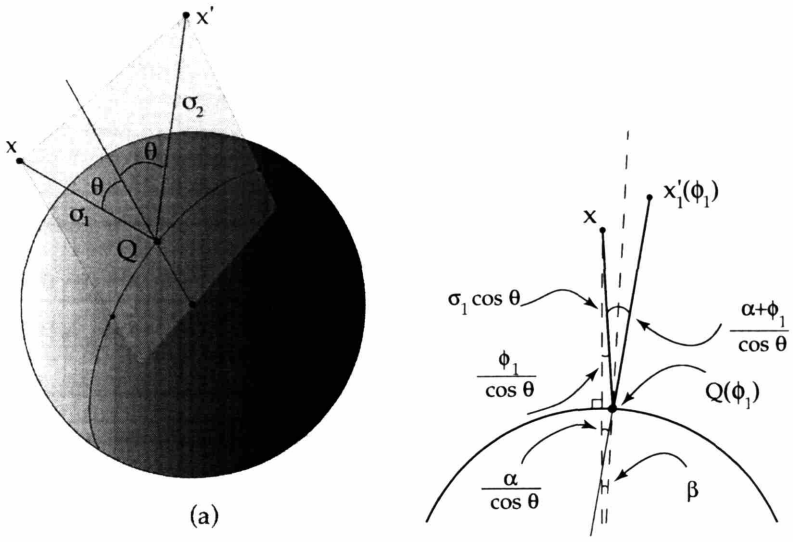

Figure 3-3: Geometry for reflection in a sphere. (a) The ray from x to x' reflecting at Q. Nearby rays originating at x and lying in the plane vary in longitude. Nearby rays out of the plane vary in latitude. (b) Variables for the calculations of the enlargment factor associated with latitude. The xx' plane has been projected along the vertical. A nearby ray originating at x heading out of the $xx'Q$ plane by an angle ϕ_1 is shown. This ray reflects from the sphere at $Q(\phi_1)$. The angle subtended by x and $Q(\phi_1)$ from the center of the sphere is β. The angle formed by the vector from the center of the sphere to x and the ray from $Q(\phi)$ to $x_1'(\phi_1)$ is α. In the diagram the distance σ_1 and the angles α and ϕ_1 are modified by factors of $\cos\theta$ due to the projection.

The same calculation applies for the longitudinal displacement except that the relation between $d\phi_1$ and $d\beta$ is replaced by $Rd\beta = \sigma_1 d\phi_2/\cos\theta$ and $d\alpha = 2d\beta + d\phi_1$, with the result

$$\frac{d\phi_2}{dx_2'} = \frac{1}{\ell + \frac{2\sigma_1\sigma_2}{R\cos\theta}} \tag{3.11}$$

Putting these formulas together we find for a single reflection on the sphere (the subscript s indicates reflection from the sphere) with angle of reflection θ

$$\Delta_{1s}(x,x') = \frac{1}{(\ell + \frac{2\sigma_1\sigma_2}{R\cos\theta})(\ell + \frac{2\sigma_1\sigma_2\cos\theta}{R})}. \tag{3.12}$$

Note that $\Delta(x,x')$ is symmetric with respect to the interchange of x and x' as it must, because the propagator possesses this symmetry. For the first reflection from

the sphere we have $\cos\theta = 1$ and $\sigma_1 = \sigma_2 = \ell/2$, so

$$\Delta_{1s}(x) = \frac{1}{(\ell + \ell^2/2R)^2} \tag{3.13}$$

and, as mentioned above, the enlargement factor for the second reflection (on the sphere and then on the plane or *vice versa*), is given by the first reflection from x to its image $\tilde{x}$ in the plane, $\Delta_2(x) = \Delta_{1s}(x, \tilde{x})$. A similar approach to higher reflections would require further analysis. The original wavefront leaving x is spherical. The first reflection from the sphere produces a new wavefront with, in general, two unequal radii of curvature. When next incident upon the sphere, the asymmetric wavefront will be transformed in a manner yet to be described. The ease with which $\Delta_r(x)$ can be computed numerically makes this unnecessary.

Domain of the r^{th} reflection, $\mathcal{D}_r$

The next step is the integration over the domains appropriate to each reflection. The first reflections give rise to cutoff dependent but a-independent contributions which must be analyzed at this point. Consider the first reflection from the plane. The appropriate domain is all of space except the interior of the sphere $\overline{\mathcal{D}}_s$ and the region shadowed by the sphere $\overline{\mathcal{D}}_{p1}$ (see Fig. 3-2). The integral can then be written as the difference between the integral over all space and the integral over $\overline{\mathcal{D}}_s \bigcup \overline{\mathcal{D}}_{p1}$. The integral over the whole space is the divergent constant discussed in 3.2.1 which does not contribute to the force. It is to be ignored in the following. So the correct domain for the first reflection from the plane is the region, $\overline{\mathcal{D}}_s \bigcup \overline{\mathcal{D}}_{p1}$, in the shadow of the sphere, *and the sign is to be reversed.* Similarly, the integral of the first reflection on the sphere must be performed on the domain consisting of the whole space minus the interior of the sphere ($\overline{\mathcal{D}}_s$) and the region below the plate ($\overline{\mathcal{D}}_p$). The irrelevant divergence is given by the integral over all the space minus the interior of the sphere and the finite, a-dependent part, which contributes to the Casimir force, is given by the negative of the integral over the region, $\overline{\mathcal{D}}_p$, below the plane. So the correct domain for the first reflection from the sphere is $\overline{\mathcal{D}}_p$ *and the sign of the contribution*

is reversed. Hence we can write

$$\mathcal{E}_{1s} + \mathcal{E}_{1p} = -\frac{\hbar c}{2\pi^2} \int_{\overline{\mathcal{D}}_s \cup \overline{\mathcal{D}}_{p1}} d^3x \frac{1}{(2z)^4} - \frac{\hbar c}{2\pi^2} \int_{\overline{\mathcal{D}}_p} d^3x \frac{\Delta_{1s}^{1/2}(x)}{\ell_{1s}^3(x)}. \tag{3.14}$$

The second reflection gives a finite contribution to $\mathcal{E}$. The path length, $\ell_2(x)$, never vanishes so there are no divergences at short distances, and the integrand, $\Delta_2^{1/2}(x)/\ell^3(x)$, falls rapidly at large distances. The result is typically approximately 90% of the total result. Higher reflections can be analyzed in a similar fashion. The integration domains become progressively more restricted. For example, three reflection paths that reflect twice from the plane and once from the sphere do not exist in the shadow of the sphere ($\overline{\mathcal{D}}_{p1}$) nor in the darkly shaded regions in Fig. 3-2 determined by the geometrical construction indicated by the dashed lines. It is not hard to carry out the constructions and calculations necessary to construct the optical approximation for the sphere and plane to any required order.

Discussion of numerical results

In Ref. [4] we presented initial results on the optical approximation for the sphere and plane. Here we present final results (see Fig. 3-4), discuss them in more detail, and compare them with the results of Ref. [42] and with the proximity force approximation (PFA). In presenting our results we display the sum of all the reflections (even and odd) up to (and including) the fourth. Since the energy must approach the parallel plate limit as $a \to 0$ we can estimate the error in neglecting higher reflections in this limit. The error in neglecting the fifth and higher odd reflections is a +3.8% excess (because the sign of the odd reflections contribution is opposite to that of the total energy) as $a \to 0$. Neglecting the even reflections (6th, 8th, etc.) as $a \to 0$ gives an error of -1.8%, negative because these contributions have the same sign of the total energy. Altogether the sum of the first four reflections overestimates the energy by $3.8\% - 1.8\% = 2\%$ as $a \to 0$. To illustrate this estimate of accuracy we have plotted our results as a band 2% in width in Fig. 3-4. Since the fractional contribution of higher reflections decreases with a, we believe this is a conservative

estimate for larger a. Obviously, calculating the higher reflections will reduce this uncertainty interval, leaving eventually only the error due to diffraction which we are not able to estimate. The proximity force approximation has been the standard tool for estimating the effects of departure from planar geometry for Casimir effects for many years[16]. In this approach one views the sphere and plate as a superposition of infinitesimal parallel plates:

$$\mathcal{E}_{\rm PFA} = -\frac{\pi^2\hbar c}{1440}\int_{\mathcal{S}} d^2S \frac{1}{d(x)^3}. \tag{3.15}$$

where $d(x)$ is the distance from the plate to the sphere at a point x on the surface $\mathcal{S}$. This formulation is ambiguous since the surface $\mathcal{S}$ could be taken to be either the sphere or the plate. Whichever surface is chosen, the distance is measured normal to that surface. The ambiguity is useful since it gives a measure of the uncertainty in the PFA. In either case the relevant integrals are easily performed. For the plate we obtain,

$$\mathcal{E}^{\rm plate}_{\rm PFA} = -\frac{\pi^3\hbar c R}{1440a^2}\frac{1}{1+a/R} \tag{3.16}$$

while for the sphere we obtain

$$\mathcal{E}^{\rm sphere}_{\rm PFA} = -\frac{\pi^3\hbar c R}{1440a^2}\left(1 - 3\frac{a}{R} - 6\frac{a^2}{R^2}\left(1 + (1+\frac{a}{R})\ln\frac{a}{R+a}\right)\right) \tag{3.17}$$

In the limit $a/R \to 0$ both estimates agree to lowest order. The $a \to 0$ limit is usually called the proximity force *theorem* and has been much discussed over the years. It is usually stated as a result for the Casimir *force* in the limit $a/R \to 0$: $\mathcal{F}_{\rm PFA} \sim 2\pi R\mathcal{E}/A = -\pi^3\hbar c R/720a^3$ (where $\mathcal{E}/A$ is the Casimir energy per unit area for parallel plates). This limit provides a convenient parametrization of the Casimir force when a is not so small,

$$\mathcal{F} = -f(\frac{a}{R})\frac{\pi^3\hbar c R}{720a^3} \tag{3.18}$$

Modern experiments are approaching accuracies where the deviations of $f(a/R)$ from unity may be important. The accuracy of the PFA beyond the $a/R \to 0$ limit is unknown, and the two different versions give different $\mathcal{O}(a/R)$ corrections:

$$f_{\rm PFA}^{\rm plate}(a/R) = 1 - \frac{1}{2}\frac{a}{R} + \mathcal{O}(\frac{a^2}{R^2}) \tag{3.19}$$

$$f_{\rm PFA}^{\rm sphere}(a/R) = 1 - \frac{3}{2}\frac{a}{R} + \mathcal{O}(\frac{a^2}{R^2}) \tag{3.20}$$

An important application of the optical approximation is to obtain a more accurate estimate of $f(a/R)$. The optical approximation to the Casimir energy and the data of Ref. [42] both fall like $1/a^2$ at large a. In fact both are roughly proportional to $1/a^2$ for all a. In contrast the PFA estimates of the energy falls like $1/a^3$ already at $a/R \simeq 1$ and departs from the Gies et al. data at relatively small a/R. For purposes of display we therefore scale the estimates of the energy by the factor $-1440a^2/\pi^3 R\hbar c$. The results are shown in Fig. 3-4. At large a/R the optical approximation has the

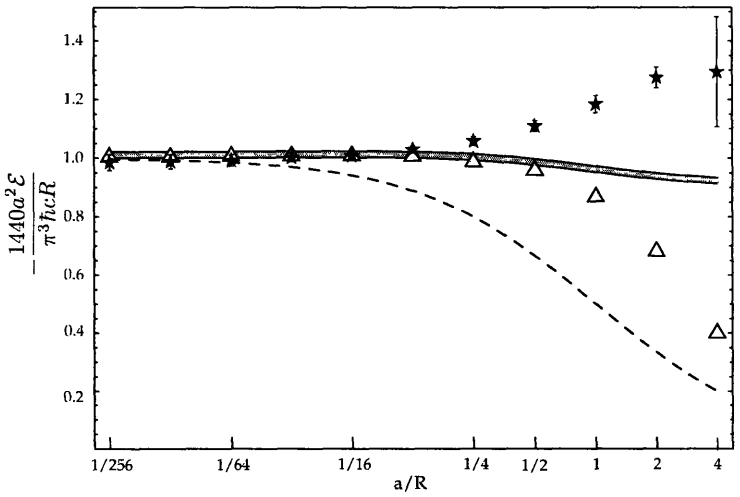

Figure 3-4: Casimir energy for a sphere of radius R a distance a above an infinite plane. $1440a^2\mathcal{E}/\pi^3 R\hbar c$ is plotted versus a/R. The stars with error bars are the data of Ref. [42]. The thick solid curve is the optical approximation through the fourth reflection. The width of the curve indicates our estimate of the error in the optical approximation from neglect of the odd and even reflections with $n \geq 5$. The dashed curve is the plate-based proximity force approximation. The triangles are the results we published in Ref. [4], which are superceded by this work.

same scaling behavior as the data and differs from Ref. [42] by no more than 30%

at the largest a/R. At small a/R, given our estimate of the accuracy of the optical approximation, we find that

$$f^{\text{optical}}(a/R) = 1 + 0.05a/R + \mathcal{O}\left((a/R)^2\right), \tag{3.21}$$

which must be compared with the predictions of PFA eqns.(3.19) and (3.20). In Fig. 3-5 we show the contributions to the optical approximation of the different reflections we have computed. As expected the dominant contribution, always greater than 90%, comes from the second reflection. The fourth reflection contributes about 6% for $a/R \ll 1$ and less as a/R increases. The contributions of the first and third reflections are very small for all a/R. A relevant result, confirmed by the analytical analysis on the energy momentum tensor (within the optical approximation) is that the asymptotic behavior of $\mathcal{E}$ as $a/R \gg 1$ predicted by the optical approximation is $\propto 1/a^2$. This is in contrast with the Casimir-Polder law which predicts $1/a^4$ at large a [1]. The discrepancy must be attributed to diffraction effects.

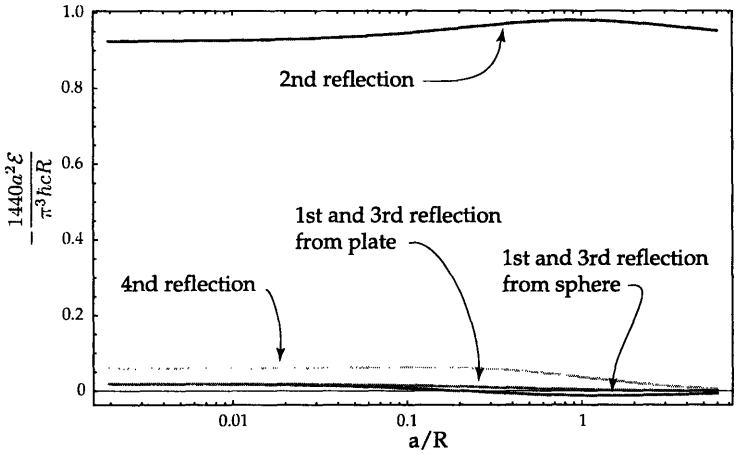

Figure 3-5: Contributions of specific reflections to the optical approximation.

3.2.3 Casimir Pendulum

In this section we treat a problem for which the exact answer is unknown. The configuration is shown in Fig. 3-6. The base plate is taken to be infinite. The upper plate is held at its midpoint a distance a above the base plate. The width of the

upper plate is w and its depth, d (out of the page), is assumed to be infinite. We define the Casimir energy per unit depth, $\varepsilon = \mathcal{E}/d$. θ is the angle of inclination of the upper plate. It will be convenient to use $z = \frac{1}{2}w\sin\theta$ as a variable as well. It is also possible to view this configuration as a finite slice between $\ell_1 = a/\sin\theta - w/2$ and $\ell_2 = a/\sin\theta + w/2$ of a wedge of opening angle θ. In this section we will discuss both the Casimir energy and the "Casimir torque", $\nu = \frac{1}{d}\frac{d\mathcal{E}}{d\theta}$, per unit depth. We are aware

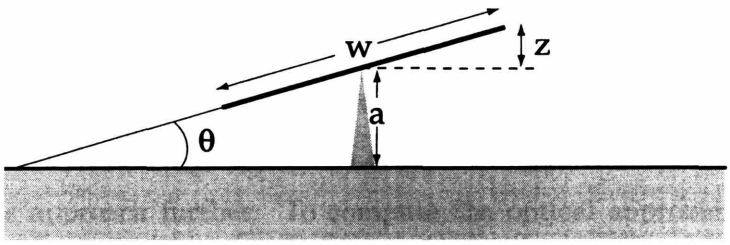

Figure 3-6: Geometry for the Casimir Pendulum.

of two *ad hoc* approximate approaches to this problem. The first is the PFA which treats each element of the system perpendicular to the lower plate as an infinitesmal parallel plate Casimir system. It is easy to show that

$$\begin{aligned} \varepsilon_{\rm PFA} &= -\frac{\pi^2\hbar c}{1440}\frac{w\cos\theta}{a^3}\left(1-\frac{w^2\sin^2\theta}{4a^2}\right)^{-2} \\ &= -\frac{\pi^2\hbar c a}{1440}\frac{\sqrt{w^2-4z^2}}{(a^2-z^2)^2} \end{aligned} \tag{3.22}$$

which gives a torque,

$$\nu_{\rm PFA}(a,w,z) = -\frac{\pi^2\hbar c}{720}\,\frac{az(w^2-a^2-3z^2)}{(a^2-z^2)^3} \tag{3.23}$$

where the minus sign denotes that the torque is destabilizing: $z = 0$ is a point of unstable equilibrium. As in the case of the sphere and the plane, the PFA is ambiguous. A more symmetric treatment of the two planes in the present geometry would integrate over the surface that bisects the wedge and take the distance normal to that surface. The result is the replacement of $\cos\theta$ by $\cos^4(\theta/2)$ in eq. (3.22) and a similar modification of the torque. A second "approximate" treatment of the Casimir

Pendulum can be extracted from the known exact solution for the Casimir energy density for the "Dirichlet wedge"[17], which consists of two semi-infinite plates with opening angle θ meeting at the origin. One can obtain an estimate of the energy for the pendulum by integrating the energy density over the two dimensional domain bounded (in polar coordinates, (ρ, ϕ)) by $0 < \phi < \theta$ and $\ell_1 < \rho < \ell_2$. This approach takes no account of the modification of the energy density due to the finitenss of the upper plate. Furthermore it is inherently ambiguous because the energy density for a scalar field is only defined up to a total derivative. The calculation in Ref. [17] used the conformally invariant stress tensor. One would obtain a different answer if one used, for example, the Noether stress tensor. In light of these difficulties, we do not pursue this approach further. To compute the optical approximation we need the enlargement factor, the lengths of optical paths, and the integration domain, $\mathcal{D}_r$. Since all the conducting surfaces are planar, the enlargement factor is trivial in this case, $\Delta_r(x) \to 1/\ell_r^2(x)$. The path lengths are also easy to compute. The only non-trivial step is the determination of the integration domains. As in the case of parallel plates, the odd reflections do not contribute to forces or torques for the Casimir pendulum. Instead they sum to a cutoff dependent constant associated with each plate. Any odd reflection path "turns around" with a reflection at normal incidence from one plate or the other. Consider all the points, x, which are the origins of paths that turn around at a given point P on either surface. These paths are shown, for the case where P is on the lower, infinite plane, in Fig. 3-7. They comprise one reflection paths lying on the interval $\overline{PQ_1}$, three reflection paths lying on the interval $\overline{Q_1Q_2}$, *etc.* The contributions to ε from these intervals integrates to the same result as the integral over z for odd paths in the case of parallel plates. It is independent of a, w, and θ and can be set aside. The fact that the enlargement factor is trivial is crucial for this argument.

Even optical path lengths, $\ell_r(x)$

The analysis of paths that reflect an even number of times makes use of simple geometrical concepts. For any point $x \equiv (\rho, \phi)$, we define an infinite sequence of

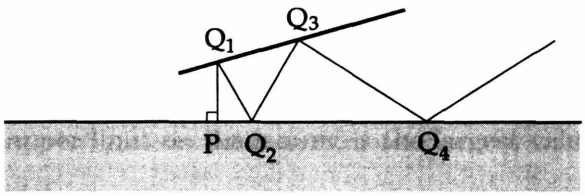

Figure 3-7: Odd reflection paths for the Casimir Pendulum.

images in the upper and lower planes as shown in Fig. 3-8, ignoring for the moment that the upper plane is finite. The images below the lower plane are denoted $\bar{x}_1, \bar{x}_2, \ldots$ and those above the upper plane are denoted $x_1, x_2, \ldots$. In sequence, $\bar{x}_1 = \overline{\mathbf{R}}x$, $x_1 = \mathbf{R}x$, $x_2 = \mathbf{R}\bar{x}_1$, $\bar{x}_2 = \overline{\mathbf{R}}x_1$, *etc.* with $\overline{\mathbf{R}}$ denoting reflection in the lower plane and $\mathbf{R}$ denoting reflection in the upper plane. All of the images lie on the circle of radius ρ about the origin. The length of the $2n$ reflection path can easily be seen to be given by

$$\ell_{2n}(x) = ||x_n - \bar{x}_n|| = 4\rho^2 \sin^2 n\theta \tag{3.24}$$

independent of ϕ. Substituting into eq. (3.1) we obtain the expression for the Casimir

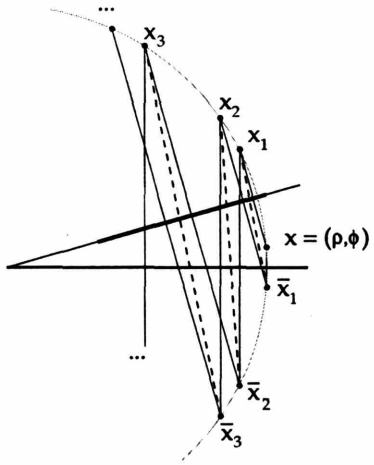

Figure 3-8: Images of the point x in the Casimir Pendulum configuration. The dashed lines have the same length as the $r = 2, 4, 6, \ldots$ reflection paths.

energy per unit depth,

$$\varepsilon_{\text{opt}} = -\frac{\hbar c}{16\pi^2} \sum_{n=1}^{N_{\max}} \frac{1}{\sin^4 n\theta} \int_0^\theta d\phi \int_0^\infty d\rho \frac{1}{\rho^3} \Theta(\mathcal{D}_{2n}) \tag{3.25}$$

The step function $\Theta(\mathcal{D}_{2n})$ vanishes when the point x is not in the domain where $2n$-reflection paths are possible. As we show in the following section, for n large enough, $\mathcal{D}_{2n} \to \emptyset$. $N_{\max}$, the upper limit on the n-sum, is the largest value of n for which any $2n$-reflection paths exist.

Domain of the $2n^{\text{th}}$ reflection, $\mathcal{D}_{2n}$

The domain in which the $2n$-reflection path exists is determined by the constraint that the points of reflection at the upper plate must lie between ℓ_1 and ℓ_2, the inner and outer radii that define its boundaries. Note, of course, that $\ell_2 > \ell_1$. Although the calculation is elementary, it is tricky, so we only quote the results. The constraints depend on whether n is even or odd, so we summarize them independently.

- **n-odd** When n is odd, the integration domain $\mathcal{D}_{2n}$ is defined by the inequalities:

$$\ell_1 \cos\phi \le \rho \cos n\theta \le \ell_2 \cos((n-1)\theta + \phi) \tag{3.26}$$

  where the lower limit ensures that the innermost reflection occurs at $\rho \ge \ell_1$ and the upper limit ensures that the outermost reflection occurs at $\rho \le \ell_2$. The inequality cannot be satisifed for any ρ or $\phi(\le \theta)$ unless

$$\ell_2 \cos(n-1)\theta > \ell_1 \tag{3.27}$$

  When eq. (3.27) is satisfied the contribution of the $2n^{\text{th}}$ reflection (n-odd) is

$$\varepsilon^{\text{odd}}_{\text{opt } n} = -\frac{\hbar c}{32\pi^2}\frac{\cos^2 n\theta}{\sin^4 n\theta}\begin{cases} \frac{1}{\ell_1^2}\tan\theta - \frac{1}{\ell_2^2}\left(\tan n\theta - \tan(n-1)\theta\right) & \text{for } \ell_2\cos n\theta \ge \ell_1\cos\theta \\ \frac{(\ell_2\cos(n-1)\theta - \ell_1)^2}{\ell_1^2\ell_2^2\,\cos(n-1)\theta\,\sin(n-1)\theta} & \text{for } \ell_2\cos n\theta \le \ell_1\cos\theta \end{cases} \tag{3.28}$$

- **n-even** When n is even, the integration domain $\mathcal{D}_{2n}$ is defined by the inequalities:

$$\ell_1 \cos(\theta - \phi) \le \rho \cos n\theta \le \ell_2 \cos((n-1)\theta + \phi) \tag{3.29}$$

where, as before, the lower limit ensures that the innermost reflection occurs at $\rho \geq \ell_1$ and the upper limit ensures that the outermost reflection occurs at $\rho \leq \ell_2$. The inequality cannot be satisifed at all unless

$$\ell_2 \cos(n-1)\theta > \ell_1 \cos\theta \tag{3.30}$$

When eq. (3.30) is satisfied the contribution of the $2n^{\text{th}}$ reflection (n-even) is

$$\varepsilon^{\text{even}}_{\text{opt } n} = -\frac{\hbar c}{32\pi^2}\frac{\cos^2 n\theta}{\sin^4 n\theta}\begin{cases} \frac{1}{\ell_1^2}\tan\theta - \frac{1}{\ell_2^2}\left(\tan n\theta - \tan(n-1)\theta\right) & \text{for } \ell_2\cos n\theta \geq \ell_1 \\ \frac{(\ell_2\cos(n-1)\theta - \ell_1\cos\theta)^2}{\ell_1^2\ell_2^2\,\cos(n-1)\theta\,\sin n\theta\,\cos\theta} & \text{for } \ell_2\cos n\theta \leq \ell_1 \end{cases} \tag{3.31}$$

The torque is obtained by differentiating with respect to θ at fixed a and w, remembering that ℓ_1 and ℓ_2 depend on θ. Of course the θ-derivative of eqs. (3.31) and (3.28) are complicated and need not be written down explicitly. The resulting expressions for $\nu^{\text{odd}}_{\text{opt } n}$ and $\nu^{\text{even}}_{\text{opt } n}$ must be summed over n subject to the constraints in eqs. (3.28) and (3.31). This sum must be performed numerically. The results are discussed in the following subsection.

Discussion

Fig. 3-9 shows the pendulum Casimir energy as a function of z for $a = 1$ and several values of w. The weak dependence on z at small z is to be expected. So is the divergence as $z \to 1$ which we do not show in the figure. When the plates touch at $z/a = 1$, the Casimir energy of perfectly sharp, perfectly conducting plates would in fact diverge, as would the Casimir torque. The optical approximation for the pendulum turns out to be very close to the plate based PFA. It is convenient therefore to scale out a factor of $-1440a^3/\hbar c\pi^2 w$ (see eq. (3.22)) when displaying or results for the energy per unit depth, ε_{opt}, and a factor $-720a^5/\hbar c\pi^2 w^2$ when displaying results for the torque per unit depth. The energy and torque are plotted for representative values of w ($w = 1.5a, 2.5a, 5a$, and $10a$) as a function of z/a in Fig. 3-9. The plots are shown only up to $z/a = 0.5$. Above $z/a \sim 0.5$ both grow rapidly and diverge at $z = a$. The PFA gives an excellent approximation for the pendulum over a wide

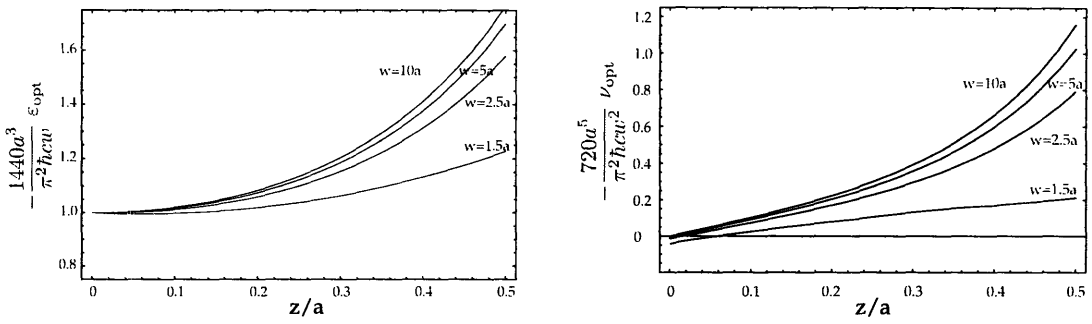

Figure 3-9: Casimir energy and torque in scaled units for a Casimir pendulum of width $w = 1.5a, 2.5a, 5a$ and $10a$. Positive values of the scaled torque are destabilizing.

range of the parameter space. This can be seen by examining the ratio of $\varepsilon_{\rm opt}/\varepsilon_{\rm PFA}$ as shown in Fig. 3-10. The reason behind this success is that the second (optical) reflection is proportional to the PFA result (eq. (3.22)) for all z. The constant of proportionality is the familiar $90/\pi^4 = 0.924$. The sum of the higher even reflections

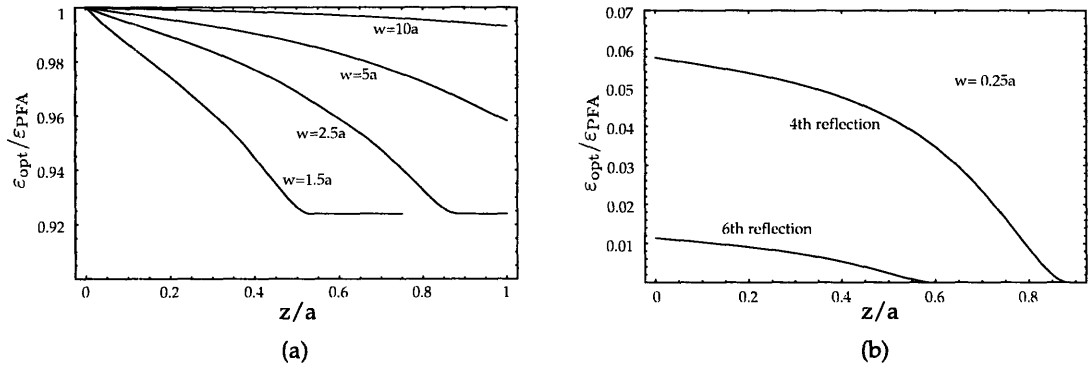

Figure 3-10: The ratio of the optical approximation to the PFA. (a) for a pendulum of different widths as a function of z/a. The breaks in the curves for $w = 1.5a$ and $2.5a$ occur when only the second reflection can contribute. The $w = 1.5a$ curve ends at the $z = 0.75a$ when $z = w/2$. (b) The contributions of the 4th and 6th reflections for $w = 2.5a$. The 2nd reflection contributes $0.924\ldots$ independent of z. This is the only case we found in which the optical approximation gives an energy smaller than the PFA.

combines with the second to equal the PFA at $z = 0$ and drops away slowly with increasing z/a. So the optical estimate coincides with the PFA at $z = 0$ and drops slowly with z. The contributions of the first few reflections are shown for $w = 2.5a$ in Fig. 3-10. A careful study of Fig. 3-9 reveals one peculiar feature, namely the fact that the torque does not vanish for $z/a = 0$, implying a cusp in the Casimir energy

for $z = 0$. We believe this is an artifact of our approximation. Since the already tiny effect vanishes quickly for large values of w/a, it is most probably an edge effect.

3.3 Origins of the optical approximation

Most studies of Casimir energies do not consider approximations. Instead they focus on ways to regulate and compute the sum over modes, $\sum \frac{1}{2}\hbar\omega$[16]. These methods have proved very difficult to apply to geometries other than parallel plates. The main reason for this *impasse* lies in the high degree of divergence of this sum. Even though the Casimir *force* between rigid bodies is known to be finite and the divergences can be regulated and analyzed, for example with the multiple reflection expansion (MRE) of Balian and Bloch[28], they make the calculation intractable unless the spectrum is known analytically. Finding the spectrum of the Laplace operator for non-separable problems is not merely a technical difficulty, it is more one of principle. In fact there are strict relations between this problem and those of chaotic billiards theory. The existence of an exact solution for the Casimir problem with a non-trivial geometry would imply the existence of an exact solution for the same family of quantum billiards and hence of classical billiards. Thirty years of work on the ergodicity of classical billiards and the implications for the density of states in the corresponding quantum billiards suggest this task is hopeless (see [14]). Consider an attempt to proceed numerically: One could easily compute the spectrum $\{\omega\}$ to some high, but finite, accuracy, and attempt to compute the sum. However the sum diverges – the leading non-trivial divergence in N dimensions is of order Λ^N. One could hope to compute it by introducing a cutoff, computing the energy at nearby separations, a and $a + da$, taking the difference, $\mathcal{E}(a + da, \Lambda) - \mathcal{E}(a, \Lambda)$, and finally taking $\Lambda \to \infty$. However such numerical problems are hopelessly unstable: tiny errors in the asymptotic spectrum lead to significant ambiguities in the finite parts. The force, indeed, is given by the small oscillatory ripple in the density of state numerically shadowed by the 'bulk' contributions which give rise to distance-independent divergencies. So we focused our attention on ways to get approximate solutions of the Laplace-Dirichlet

problem which are apt to capture the oscillatory contributions in the density of states, providing physical insights and accurate numerical estimates. We have not found any previous use of ideas from classical optics. In this section we give a derivation of the optical approximation based on a path integral representation of the Helmholtz Greens function. Schaden and Spruch have developed an approximation for Casimir energies [9] using Gutzwiller's semiclassical treatment[14] of the density of states. It is misleading to call the approach of Ref. [9] "semiclassical" because, as can be seen for example from eq. (3.1), the only $\hbar$ in the Casimir problem for a massless field is the multiplicative factor in $\frac{1}{2}\hbar\omega$. However, since the authors of Ref. [9] use the term following Gutzwiller, we will continue to refer to their approach as "semiclassical". This work differs in important ways from ours and in general is not as accurate, however the relationship between the two approaches is interesting, and is explored later in this section.

3.3.1 Derivation

We begin with the well-known definition of the Casimir energy in terms of a space and wavenumber dependent density of states[18], $\tilde{\rho}(x,k)$,

$$\mathcal{E}_{\mathcal{D}}[\psi] = \int_0^\infty dk \int_{\mathcal{D}} d^N x \frac{1}{2}\hbar\, \omega(k)\tilde{\rho}(x,k), \tag{3.1}$$

where $\omega(k) = c\sqrt{k^2+\mu^2}$, and the density of states $\tilde{\rho}(x,k)$ is related to the propagator $G(x',x,k)$ by

$$\tilde{\rho}(x,k) = \frac{2k}{\pi}\ \mathrm{Im}\ \tilde{G}(x,x,k). \tag{3.2}$$

Since we are considering a scalar field, G is the Greens function for the Helmholtz equation. We choose G to be analytic in the upper-half k^2-plane (or equivalently take k^2 to have a small positive imaginary part). The tildes on $\tilde{\rho}(x,k)$ and $\tilde{G}(x,x',k)$ denote the subtraction of the contribution of the free propagator, $G_0(x',x,k)$. The Casimir energy depends on the boundary conditions obeyed by the field ψ and on the arrangement of the boundaries, $\mathcal{S} \equiv \partial\mathcal{D}$ (not necessarily finite), of the domain $\mathcal{D}$.

From the outset we recognize that $\mathcal{E}$ must be regulated, and will in general be cutoff dependent, as discussed in the Introduction. We will not denote the cutoff dependence explicitly except when necessary. ρ is the familiar density of states associated with the problem

$$\begin{aligned} (\Delta + k^2)\psi(x) &= 0 \quad \text{for} \quad x \in \mathcal{D} \\ \psi(x) &= 0 \quad \text{for} \quad x \in \mathcal{S}, \end{aligned} \tag{3.3}$$

so that G satisfies the equation

$$\begin{aligned} (\Delta' + k^2)G(x', x, k) &= -\delta^N(x' - x) \quad \text{for} \quad x', x \in \mathcal{D}, \\ G(x', x, k) &= 0 \quad \text{for} \quad x' \text{ or } x \in \mathcal{S}, \end{aligned} \tag{3.4}$$

and

$$\tilde{G}(x', x, k) = G(x', x, k) - G_0(x', x, k), \tag{3.5}$$

where G_0 is the free scalar propagator in the absence of boundaries. The spectral representation expresses G as a sum over a complete set of eigenfunctions ψ_n with eigenvalues k_n

$$G(x', x, k) = \sum_n \frac{\psi_n(x')\psi_n(x)}{k_n^2 - k^2 - i\epsilon}. \tag{3.6}$$

Notice that since the problem (3.3) is real we have chosen a complete set of *real* eigenfunctions and removed the usual complex conjugation from (3.6). We can regard this problem as the study of a quantum mechanical free particle with $\hbar = 1$, mass $m = 1/2$, and energy $E = k^2$, living in the domain $\mathcal{D}$ with Dirichlet boundary conditions on $\partial\mathcal{D}$. Dirichlet boundary conditions are an idealization of interactions which prevent the quantum particle from penetrating beyond the surfaces $\mathcal{S}$. This idealization is adequate for low energies but fails for the divergent, *i.e.* cutoff dependent, contributions to the Casimir energy[77]. As we have already seen in Section II, the divergences can be simply disposed of in the optical approach, and the physically measurable contributions to Casimir effects are dominated by $k \sim 1/a$, where a, a

typical plate separation, will satisfy $1/a \ll \Lambda$ where Λ is the momentum cutoff characterizing the material. So the boundary condition idealization is quite adequate for our purposes. Following this quantum mechanics analogy we introduce a fictitious time, t, and consider the functional integral representation of the propagator[19]. The space-time propagator is

$$G(x', x, t) = \int_{-\infty}^{\infty} \frac{dE}{2\pi i} G(x', x, \sqrt{E}) e^{-iEt}, \tag{3.7}$$

where $E = k^2$. Since G is analytic in the upper half k^2-plane, it is evident that $G(x', x, t) = 0$ when $t < 0$. The inverse Fourier transform reads

$$G(x', x, k) = i \int_0^{\infty} dt\ e^{ik^2 t} G(x', x, t). \tag{3.8}$$

$G(x', x, t)$ obeys the free Schrödinger equation in $\mathcal{D}$ bounded by $\mathcal{S}$. It can be written as a functional integral over paths from x' to x with action $S(x', x, t) = \frac{1}{4}\int dt \dot{x}^2$. The optical approximation is obtained by taking the stationary phase approximation of the propagator G *in the fictitious time domain.* Hence we assume that the functional integral is dominated by the contribution of classical paths between x' and x. These are straight line paths, reflecting r times from the boundaries, and traversed at constant speed, $v = \ell_r(x', x)/t$. where $\ell_r(x', x)$ is the length of the path. Then the optical approximation to the propagator is given by,

$$G_{\text{opt}}(x', x, t) = \sum_r D_r(x', x, t) e^{iS_r(x'x,t)}. \tag{3.9}$$

The action is

$$S_r(x', x, t) = \frac{\ell_r(x', x)^2}{4t} \tag{3.10}$$

and D is the van Vleck determinant

$$D_r(x', x, t) \propto \det \left(\frac{\partial^2 \ell_r^2}{\partial x_i' \partial x_j} \right)^{1/2} \tag{3.11}$$

This approximation is exact to the extent one can assume the classical action of the path S_r to be quadratic in x', x. This is the case for flat and infinite plates. Thus the non-quadratic part of the classical action comes from the curvature or the finite extent of the boundaries, which we parameterize generically by R, $\partial^3 S/\partial x^3 \sim 1/Rt$. Hence, in a stationary phase approximation $\delta x \sim \sqrt{t}$ and the corrections are of order $\delta^3 S \sim \mathcal{O}\left(\sqrt{t}/R\right)$. Back in k-space the corrections hence will be $\mathcal{O}\left(1/kR\right)$, and the important values of k for the Casimir energy are of order $1/a$, where a is a measure of the separation between the surfaces. Thus the figure of merit for the optical approximation is a/R. At the moment there is no good way to estimate the order in a/R of the corrections to the optical approximation (possibly fractional, plus exponentially small terms). Certainly some of the curvature effects are captured by the van Vleck determinant, and as we saw in section 3.5.3 for the sphere-plare problem, the optical approximation works in practice out to $a/R \sim 1$. This is topic for further investigation. Eq. (3.9) is, in fact, the usual approximation of ray optics, the van Vleck determinant being precisely the enlargement factor of classical optics, as we now show. Since $\partial \ell_r(x', x)/\partial x' = \mathbf{n}'$ and $\partial \ell_r(x', x)/\partial x = -\mathbf{n}$, where $\mathbf{n}$ and $\mathbf{n}'$ are the unit tangent vectors to the path in the points x and x', we have

$$D_r(x', x, t) \propto \det\left(n_i n'_j + \ell_r \frac{\partial n_j}{\partial x'_i}\right)^{1/2}, \tag{3.12}$$

We perform the analysis in three dimensions. Other values of N are analogous, and we quote the general result at the end. The matrix $\frac{\partial n_j}{\partial x'_i}$ is

$$\frac{d\phi_1}{dx'_1}\mathbf{t}_1 \otimes \mathbf{t}'_1 + \frac{d\phi_2}{dx'_2}\mathbf{t}_2 \otimes \mathbf{t}'_2, \tag{3.13}$$

where $\mathbf{t}_{1,2}$ and $\mathbf{t}'_{1,2}$ are orthonormal tangent vectors perpendicular to $\mathbf{n}$ and $\mathbf{n}'$ respectively and with them form two orthonormal bases centered in x and x', and $d\phi_i/dx'_i$ is the derivative of the angle subtended at the point x when we shift the point x' along the direction $\mathbf{t}'_i$. Taking the determinant is now easy: it is the product of the three eigenvalues of the matrix, but given the fact that $\{\mathbf{n}, \mathbf{t}_1, \mathbf{t}_2\}$ (and their primed

correspondents) are an orthonormal triple these are just $\{1, \ell_r d\phi_1/dx'_1, \ell_r d\phi_2/dx'_2\}$, so

$$D_r(x', x, t) \propto \left(\ell_r^2 \frac{d\Omega_x}{dA'_x}\right)^{1/2}. \tag{3.14}$$

The coefficient of proportionality is independent of the path[3] r and must depend on t in such a way that for the direct path we obtain the free propagator. Therefore,

$$D_r(x', x, t) = \frac{(-1)^r}{(4\pi i t)^{N/2}} \left(\ell_r^{N-1} \frac{d\Omega_x}{dA'_x}\right)^{1/2}, \tag{3.15}$$

where we have returned to N-dimensions. We have introduced the factor $(-1)^r$ to implement a Dirichlet boundary condition. In the case of a Neumann boundary condition, this factor would not be present. Although we did not label $d\Omega/dA$ with an index r, it should be clear from the derivation that it does depend on the path r. Putting all together we find the space-time form of the optical propagator to be

$$G_{\text{opt}}(x', x, t) = \sum_r \frac{(-1)^r}{(4\pi i t)^{N/2}} \left(\ell_r^{N-1} \frac{d\Omega_x}{dA'_x}\right)^{1/2} e^{i\ell_r^2/4t}. \tag{3.16}$$

When dealing with infinite, parallel, flat plates this approximation becomes exact. For a single infinite plate, for example, the length-squared of the only two paths going from x to x' are

$$\begin{aligned} \ell^2_{\text{direct}} &= ||x' - x||^2 \\ \ell^2_{\text{1reflection}} &= ||x' - \tilde{x}||^2, \end{aligned} \tag{3.17}$$

where $\tilde{x}$ is the image of x. Both are quadratic functions of the points x, x' and the optical approximation is indeed exact. In order to calculate the density of states we must return to k-space. $G(x', x, k)$ is obtained by Fourier transformation (see eq. (3.8)), and can be expressed in terms of Hankel functions, giving us the final form

[3]We are not discussing the Maslov indexes other than the $(-1)^r$ here. If the ray r would touch a caustic it would be necessary to introduce the appropriate phase factor.

for our approximation

$$\begin{aligned} G_{\rm opt}(x',x,k) &= \sum_r \frac{(-1)^r i\pi}{(4\pi)^{N/2}} \left(\ell_r^{N-1}\Delta_r\right)^{1/2} \left(\frac{\ell_r}{2k}\right)^{1-N/2} H^{(1)}_{\frac{N}{2}-1}(k\ell_r)\,, \\ &\equiv \sum_r G_r(x',x,k), \end{aligned} \tag{3.18}$$

where Δ_r is the enlargement factor

$$\Delta_r(x',x) = \frac{d\Omega_x}{dA_{x'}} \tag{3.19}$$

and we have suppressed the arguments x and x' on ℓ_r and Δ_r in (3.11). This can be thought of as a particular case of the general results in Ref. [20].

For $N = 1$ and $N = 3$ the Hankel function reduces to an exponential. For example, when $N = 3$ we find

$$G_r(x',x,k) = (-1)^{n_r}\frac{\Delta_r^{1/2}}{4\pi}e^{ik\ell_r}. \tag{3.20}$$

However, had we attempted a stationary phase approximation directly in k-space we would have obtained an exponential *for any* N,

$$G_{\rm semicl}(x',x,t) = \sum_{\text{paths } r} D_r(x',x,k)e^{ik\ell_r(x'x)},$$

which does not reduce to the exact expression in the limit in which we have only infinite, non-intersecting (hence parallel), flat planes, because in k space it is not a gaussian problem even for quadratic ℓ^2. This is an important advantage of applying the stationary phase approximation in the time domain where it leads to the optical approximation. Also we believe the optical approximation to be a more favorable starting point for considering systematic corrections to the stationary phase approximation uniformly[4] in $1/R$. The expressions (3.9) and (3.11) are the first term of a systematic expansion of the propagator in $1/kR$. For gently curved geometries we expect them to provide a good approximation, the final test, in absence of exact solu-

[4]The technique of passing to the Fourier transform to obtain uniform approximations is certainly not new in wave optics [21].

tions. coming only from comparison with the experiments. The corrections come from two different (but related) effects [22]: a) we have to expand the function $S_r(x', x)$ in the exponential to include cubic (and higher order) terms and b) we have to include other stationary paths of non-classical origin, like paths running all around the bodies one or more times (these can be considered as a non-perturbative, exponentially small correction to the propagator). Both phenomena are due to the curvature of the boundary surfaces and we go back to the previous estimate that the parameter controlling the accuracy of the our approximation is indeed $1/kR$ (wedges and discontinuities must be considered as regions in which $R \to 0$ and the expansion is somewhat different). Two intertwined branches of wave optics have dealt with finding corrections to the geometric optics predictions for curved boundaries. The first [13, 6] deals both with perturbative *a)* and nonperturbative *b)* corrections to next to leading order in $1/kR$ of particular importance in the shadow region. The second deals with edges and holes in locally flat surfaces, originated by Sommerfeld's work [5] (see also [23] and references therein). Both must be considered relevant to future studies of Casimir forces, since high-curvature and finite-size effects will soon be relevant in the next generation of precision experiments [24, 25]. Another phenomenon to be taken in account, even in the case of gently curved surfaces, the optical approximations fails when either x or x' are in the shadow region or we are in presence of a caustic, the set of points where the Hessian $\partial^2 S_r/\partial x \partial x'$ has one or more vanishing eigenvalues [26]. In these regions of the parameters (x, x') the gaussian approximation fails and one cannot ignore cubic terms in the action. There are various ways of treating this phenomenon, whose importance in wave optics[27, 21] as well as quantum mechanics [20, 22] is today clear. The most interesting prediction related to the presence of caustics (for what concerns us here) is the fact that a ray crossing a caustic acquires a non-trivial phase shift. This could possibly result in a change of the sign of the Casimir force for concave geometry. Unfortunately, the existing formalism does not seem to be easily translated into our language and more work is needed in this direction.

The famous multiple reflection expansion [28] is also intimately related to the opti-

cal approximation developed here. It is relatively easy to see that our approximation arises as the first term in a uniform $1/kR$ expansion for the propagator. Most of the effort in applying the MRE to Casimir energies has focused on the divergent terms associated with general geometrical properties of the bodies [29] or on the Casimir force at large distances where only the lowest reflections contribute. To our knowledge no one has been able to develop a useful expansion beyond the optical limit from the MRE.

3.3.2 The optical Casimir energy

The substitution of (3.11) into (3.2) and then in (3.1) gives rise to a series expansion of the Casimir energy associated with classical closed (but not necessarily periodic) paths

$$\mathcal{E}_{\rm opt} = \sum_{\text{paths } r} \mathcal{E}_r, \tag{3.21}$$

where each term of this series will be in the form of

$$\mathcal{E}_r = \frac{1}{2}\hbar \,\mathrm{Im} \int_0^\infty dk\omega(k)\frac{2k}{\pi}\int_{\mathcal{D}_r} d^N x \;\; G_r(x,x,k). \tag{3.22}$$

Here the integration has been restricted to the domain $\mathcal{D}_r$ where the given classical path r exists. At this point it is useful to separate potentially divergent contributions from those which are finite. Because G is analytic in the upper half k-plane, the k integration can be taken along a contour with $\mathrm{Im}k > 0$. The Hankel function $H_n^{(1)}(k\ell)$ falls exponentially in the upper half plane, so the x integral converges absolutely and uniformly at fixed-k unless there are x-values where $\ell_r(x)$ can vanish. One can easily convince oneself that for smooth surfaces[5] only the paths that reflect *once* on any surface can give vanishing path length. So for the moment, we put aside the first reflection and consider the cutoff independent contributions from $r > 1$. In that case we can interchange the k and volume integrals. The resulting k-integral is also

[5]It suffices that the vector $\mathbf{n}$ normal to the surface is continuous, i.e. no wedges are present.

uniformly convergent.

$$\mathcal{E}_r = \frac{\pi\hbar}{2}\frac{(-1)^r}{(4\pi)^{N/2}}\,\Re\int_{\mathcal{D}_r} d^N x \frac{(\ell_r^{N-1}\Delta_r)^{1/2}}{\ell_r^{N/2-1}}\int_0^\infty dk\omega(k)\frac{2k}{\pi}(2k)^{N/2-1}H^{(1)}_{N/2-1}(k\ell_r), \tag{3.23}$$

for $r > 1$. The k-integral can be performed in general, but is particularly simple for the massless case, $\omega(k) = ck$,

$$\mathcal{E}_r = \hbar c\frac{(-1)^{r+1}}{2\pi^{N/2+1/2}}\Gamma\left(\frac{N+1}{2}\right)\int_{\mathcal{D}_r} d^N x\frac{\Delta_r^{1/2}}{\ell_r^{(N+3)/2}}, \tag{3.24}$$

which is the Casimir energy associated to the optical path $r > 1$, and generalizes our fundamental result, eq. (3.1) to dimensions other than three. The generalization to the massive case for $N = 3$ is given by

$$\mathcal{E}_r = (-1)^{r+1}\frac{\hbar c\mu^2}{4\pi^2}\int_{\mathcal{D}_r} d^3x\frac{\Delta_r^{1/2}}{\ell_r}K_2(\mu\ell_r), \tag{3.25}$$

which reduces to the $N = 3$ case of eq. (3.24) as $\mu \to 0$. It is worth noting that for $\mu > 0$ the paths with length $\ell > 1/\mu$ are exponentially damped. Now we return to analyze the potentially divergent first reflection. For simplicity of notation we specialize to $N = 3$ although the analysis is completely general. Let the boundary of $\mathcal{D}$ be the surfaces of a set of rigid bodies $B_1, B_2, ..., B_n$. The divergent contributions come from the paths $1B_i$ that reflect once on any of the bodies B_i. To regulate possible divergences we insert a simple exponential cutoff in k. It is easy to see that our results are independent of the form of the cutoff. Then for a massless field, reflecting from body B,

$$\mathcal{E}_{1B} = (-1)\frac{\hbar c}{4\pi^2}\int_{\mathcal{D}_{1B}} d^3x\Delta_{1B}^{1/2}(x,x)\int_0^\infty dk\; e^{-k/\Lambda}k^2\;\sin(k\ell_{1B}(x,x)). \tag{3.26}$$

The k-integration can be performed,

$$\mathcal{E}_{1B} = -\frac{\hbar c}{4\pi^2}\int_{\mathcal{D}_{1B}} d^3x\;\Delta_{1B}^{1/2}\frac{2\ell_{1B}\Lambda^4(3-(\ell_{1B}\Lambda)^2)}{(1+(\ell_{1B}\Lambda)^2)^3}. \tag{3.27}$$

Notice that for $\ell_{1B}\Lambda \gg 1$ we reobtain the standard result, eq. (3.1) as we should. When $\ell_{1B}\Lambda < 1$ however the structure of the function changes completely. In particular the *sign* changes at $\ell_{1B}\Lambda = \sqrt{3}$. There is a non trivial consequence of this fact: from eq. (3.1) one expects a positive divergence ($r = 1$ here) as $\ell \to 0$, however the small ℓ divergence in eq. (3.27) is negative. This effect, that the cutoff dependent contribution to the Casimir energy density changes sign near the bounding surface, is well known and has figured centrally in recent discussions of Casimir energy densities[8]. Of course the bulk contribution to the vacuum fluctuation energy comes from the zero-reflection term, which is positive. The negative surface correction is well known and has many physical consequences. For example it contributes to the surface tension of heavy nuclei[31].

To analyze the divergent first reflection, eq. (3.26) further, we need an expression for $\Delta(x,x)$ near a generally curved surface. This entails a small change in Δ_{1s} (see eq. (3.12)) to take in account two different principal radii of curvature, say R_a and R_b (here $x' = x$ so $\theta = 0$ and $\sigma_1 = \sigma_2 = \ell/2$),

$$\Delta_{1B}(x,x) = \frac{1}{(\ell_{1B} + \ell_{1B}^2/2R_a)(\ell_{1B} + \ell_{1B}^2/2R_b)}. \tag{3.28}$$

Substituting back into eq. (3.27) and replacing $d^3x = dS(\ell)d\ell/2$, where $dS(\ell) = (\ell/2R_a + 1)(\ell/2R_b + 1)dS$, and dS is the surface area element on the body, we get (up to finite terms arising from upper bounds on the integration in $d\ell$)

$$\mathcal{E} \sim -\frac{\hbar c}{4\pi^2}\int dS \int_0^\infty d\ell \sqrt{(1+\ell/2R_a)(1+\ell/2R_b)}\frac{\Lambda^4(3-(\ell\Lambda)^2)}{(1+(\ell\Lambda)^2)^3}. \tag{3.29}$$

where we have suppressed the subscript $1B$. The ℓ-integration may be evaluated at large Λ to obtain an asymptotic expansion of the cutoff dependent terms in the first reflection,

$$\begin{aligned}\mathcal{E} &\sim -\frac{\hbar c}{4\pi^2}\int dS\left(\frac{\pi}{2}\Lambda^3 + \frac{1}{8}\Lambda^2\left(\frac{1}{R_a}+\frac{1}{R_b}\right) + \mathcal{O}(\ln\Lambda)\right) \\ &= -\frac{S}{8\pi}\hbar c\Lambda^3 - \Lambda^2\frac{1}{32\pi^2}\hbar c\int dS\left(\frac{1}{R_a}+\frac{1}{R_b}\right) + \mathcal{O}(\ln\Lambda)\end{aligned} \tag{3.30}$$

Eq. (3.30) summarizes the cutoff dependent contributions to the Casimir energy in the optical approximation. As discussed in Section II, these terms do not contribute to the forces between rigid objects. Also they are trivial to isolate and discard from the calculation of forces. The form of eq. (3.30) invites comparison with the work of Balian and Bloch[28] on the asymptotic expansion of the density of states based on their multiple reflection expansion. The MRE propagator includes not only specular paths, but also contributions from diffraction which also yield cutoff dependent contributions to the Casimir Energy. Scaling arguments indicate that terms up to at least the third "reflection" in the MRE are cutoff dependent. These higher divergences are omitted from the optical approximation, which is convenient since they do not contribute to Casimir forces in any case. The first few terms in the MRE expansion of the density of states are given by,

$$\tilde{\rho}_{\mathrm{MRE}}(k) \sim 2k\left(-\frac{S}{16\pi} - \frac{1}{12\pi^2 k}\int dS \frac{1}{2}\left(\frac{1}{R_a}+\frac{1}{R_b}\right) + \mathcal{O}\left(1/k^2\right)\right), \tag{3.31}$$

so the leading cutoff dependent terms in the Casimir energy are[6]

$$\begin{aligned}\mathcal{E} &\sim \frac{1}{2}\hbar c \int_0^\infty dk k\ \tilde{\rho}_{\mathrm{MRE}}(k)\ e^{-k/\Lambda} \\ &\sim -\frac{S}{8\pi}\hbar c\Lambda^3 - \frac{1}{24\pi^2}\hbar c\Lambda^2 \int dS\left(\frac{1}{R_a}+\frac{1}{R_b}\right) + \mathcal{O}\left(\Lambda\right)\end{aligned} \tag{3.32}$$

Comparing with the optical result, eq. (3.30) we see that the first terms agree and the second terms differ by a factor of 3/4. Apparently our optical approximation to the propagator, despite its simplicity, captures the leading divergence and the order of magnitude of the subleading divergence.[7] The discrepancy between our approximation and the MRE (exact) result for the quadratically divergent term in $\mathcal{E}$ is not surprising. To get the divergences right, it is necessary to capture paths of zero

[6]The sign of the second term here is opposite that of Ref. [28] because we are dealing with convex rather than concave geometries

[7]One might think to claim more than order of magnitude success here. However it should be noted that for Neumann boundary conditions both terms in (3.30) change signs while only the surface terms in (3.32) changes sign. This is due to the fact that 2 'reflections' in the MRE expansion contribute to the curvature divergence as well and their sign is the same for Dirichlet or Neumann boundary conditions.

length that occur in higher reflections. However only the first reflection is classical. The finite part of the Casimir energy (the one responsible for Casimir forces) however comes from paths of finite length, whose corresponding terms in the expansion for the propagator we believe are captured quite well by the optical approximation. This could help explain why the approximation works better than one would expect from a naive error estimate.

3.3.3 Connections with other semiclassical approximations.

Stationary phase approximations are not new in the study of Casimir energy both at zero and non-zero temperature [9, 32]. These works certainly share with ours the attempt to switch the attention toward general properties and approximations to the Helmholtz equation. On the other hand, relying more or less heavily on Gutzwiller's trace formula, they suffer from two significant problems. First, they treat symmetric and nearly symmetric geometries in radically different ways, and fail to provide a natural deformation away from the symmetric limit (not to mention that they give the exact result for parallel plates only for odd number of space dimensions). Second, they require a certain amount of strongly geometry-dependent work (to calculate monodromy matrices for example). We discuss both these problems further below. In order to study these points we will rewrite a given contribution $\mathcal{E}_r$ (specializing to $N = 3$ and suppressing the index r) as

$$\mathcal{E} = \mathrm{Im}(-1)^n \int_0^\infty dk\ \hbar c k^2 e^{-k/\Lambda} \int_0^\infty d\ell\ J(\ell) e^{ik\ell}, \tag{3.33}$$

where

$$J(\ell) \equiv \int_{\mathcal{D}_r} d^3x\ \delta(\ell - \ell_r(x,x)) \frac{\Delta_r^{1/2}(x,x,k)}{4\pi^2}. \tag{3.34}$$

Our strategy has been to dominate the functional integral over paths from x back to x by the classical paths, then perform the k integral analytically, and to leave the integration over x for numerical evaluation. The standard "semiclassical" approach [14, 9] is to perform all spatial integrations by stationary phase including the one over

the argument of the Greens function itself. This leaves a function only of k which can be integrated analytically. The fact that we can do the x integral numerically allows us to capture much more detailed information about the system. We will show this in detail in the following. To underline the differences, let us repeat briefly the line of reasoning leading to Gutzwiller's trace formula. We start by writing an asymptotic expansion for $k\ell \gg 1$. The asymptotic contributions to the ℓ-integral come [33] both from a) boundaries at ℓ_m, ℓ_M (minimum and maximum length achieved by the path r) that is *integration by part* terms and b) integrable divergences in the function $J(\ell)$ that is *stationary phase* (SP) points at ℓ_j. So that

$$\int_0^\infty d\ell\ J(\ell)e^{ik\ell} \sim \sum_{n\geq 0} \left(A_n(k)e^{ik\ell_M} - B_n(k)e^{ik\ell_m}\right) + \sum_{\text{SP points } j} C_j(k)e^{ik\ell_j}. \qquad (3.35)$$

A, B, C are polynomials in k, $1/k$ and ℓ_m, ℓ_M, ℓ_j respectively. Schaden and Spruch [9] approach based on Gutzwiller trace formula [14] consists in taking only the stationary phase contributions, b), to the energy, the coefficients $C_j(k)$'s then being related to the 'monodromy matrix'.[8] These terms correspond to closed classical paths, for which the final momentum is equal to the initial one (the action is $S \propto \ell$). The stationary phase approximation requires the periodic orbits to be well-separated in units of wavelength. However as one approaches a situation in which one exact symmetry exists, the space, $\mathbf{R}^2$ in 3 dimensions, perpendicular to the closed orbit at a given point breaks into the product of two subspaces $A \times B$, and ℓ is constant with respect to the B coordinates b. In the symmetric situation the SP points then form lines (or planes if more than one symmetry is present) parameterized by b. The problem can again be solved easily just by writing $d^2x \propto dadb$ and factoring out the integral over db[9, 34] leaving the integral over da to be evaluated by stationary phase approximation again.[9] However,

[8]To be precise the stationary phase integral is done on the directions transverse to the periodic orbit. The integration over the direction parallel to the orbit is eventually performed by means of a trick [14].

[9]The simplest example is that of a cylinder facing a plane. Then the periodic orbits are lines perpendicular both to the cylinder and the plane, b is parallel to the axis of the cylinder and a is the direction perpendicular to this. In the case of parallel plates both the directions a and b are symmetry directions so they both factor out and no stationary phase approximation is performed. In this case the former analysis gives an exact result, as is well known.

when the symmetry is slightly broken the length ℓ acquires a small b dependence and the integral over db can no longer be factored out. Moreover a naive stationary phase approximation in both $dadb$ is not reliable because arbitrarily close to the breaking point, the dependence of ℓ on b is small and the Hessian matrix $\partial^2\ell(x,x)/\partial x^2$ has one (or more) very small eigenvalues in the old b directions. There exists [35] a theory for Gutzwiller trace formula for approximate symmetries. However, we found that it is not easy to implement in the study of the Casimir energy for arbitrary surfaces. In the

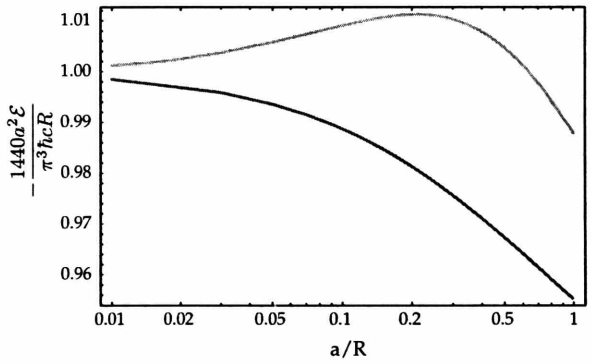

Figure 3-11: Comparison between the optical approximation (upper curve) and the "semiclassical" approximation of Schaden and Spruch (lower curve) for the sphere and plane. The scaled Casimir energy is plotted versus a/R. For the optical approximation, the sum of the first four reflections has been rescaled to go to unity as $a \to 0$. It is possible to show that in the limit $a/R \gg 1$ the optical approximation and Schaden and Spruch's formula agree (in the figure they both tend to $90/\pi^4 = 0.92...$). The most notable and relevant discrepancies are in the derivative at small a/R.

cases in which these problems can be avoided, like a sphere of fixed radius in front of a plane, and for $a/R \ll 1$ the semiclassical approximation *à la* Schaden and Spruch provides quite a good approximation (see figure) since in the expansion (3.35) the stationary phase approximation gives a much larger contribution than the integration by parts terms. A much stronger disagreement has to be expected if the sphere gets substituted by a plate of width w bent with a curvature of order $R \gg w$. Indeed the method of Ref. [9] differs dramatically from the optical approximation for the case of a hyperboloid[7]. This is not a diffraction effect but rather a 'precocious' breakdown of the semiclassical approximation which is cured by a uniform approximation of the kind we have described.

3.4 Local Observables

Local properties of the quantum vacuum induced by the presence of boundaries are of broad interest in quantum field theory [46]. For example gravity couples locally to the energy-momentum tensor. Vacuum polarization induces local charge densities near boundaries, provided the symmetries of the theory allow it. Also, local densities are free from some of the cutoff dependencies that plague many other Casimir effects. Any local observable that can be expressed in terms of the Greens function can be estimated using the optical approach. In this section we study the energy, momentum and stress densities for a scalar field.

Some local observables are not unambiguously defined [47]. For example the charge density (in a theory with a conserved charge) is unambiguously defined while the energy density, in general, is not (while its integral over the volume, the total energy, is). In this chapter we use the Noether definition of the energy-momentum tensor, similar results would be obtained with other interesting definitions.

3.4.1 Energy-momentum tensor

We study the Noether energy-momentum tensor of a free, real scalar field ϕ in a domain $\mathcal{D}$ with Dirichlet boundary conditions (BC) on $\mathcal{S} = \partial\mathcal{D}$ made of (in general disconnected) surfaces. Other BC (Neumann, Robin) can be discussed but for simplicity we restrict ourselves to Dirichlet BC here.

The lagrangian is (we use $\hbar = c = 1$)

$$\mathcal{L} = \frac{1}{2}\partial_\mu\phi\partial^\mu\phi - \frac{1}{2}m^2\phi^2, \tag{3.1}$$

where Greek letters are used for 4-dimensional indices while the vector notation will be used for spatial vectors.

The Noether energy-momentum tensor for this real scalar field is

$$T_{\mu\nu} = \frac{\partial\mathcal{L}}{\partial(\partial^\mu\phi)}\partial_\nu\phi - g_{\mu\nu}\mathcal{L} \tag{3.2}$$

$$T_{\mu\nu} = \partial_\mu\phi\ \partial_\nu\phi - g_{\mu\nu}\frac{1}{2}\left(\partial_\alpha\phi\ \partial^\alpha\phi - m^2\phi^2\right) \tag{3.3}$$

from which we identify the energy density T_{00}, the momentum density T_{0i}, and the stress tensor T_{ij}. The definition of these quadratic operators involves divergences that we will regulate by point splitting. We hence replace quadratic operators like $\phi(x)^2$ by $\lim_{x'\to x}\phi(x')\phi(x)$. The energy density operator, for example, is

$$\begin{aligned} T_{00}(x,t) &= \lim_{x'\to x}\left[\frac{1}{2}\partial_0\phi(x',t)\partial_0\phi(x,t) + \frac{1}{2}\vec{\nabla}'\cdot\vec{\nabla}\phi(x',t)\phi(x,t) + \frac{1}{2}m^2\phi(x',t)\phi(x,t)\right] \\ &= \lim_{x'\to x}\left[\frac{1}{2}\partial_0\phi(x',t)\partial_0\phi(x,t) - \frac{1}{2}\phi(x',t)\vec{\nabla}^2\phi(x,t) + \right. \\ &\quad \left. + \frac{1}{2}m^2\phi(x',t)\phi(x,t) + \frac{1}{2}(\vec{\nabla}'+\vec{\nabla})\cdot\phi(x',t)\vec{\nabla}\phi(x,t)\right] \end{aligned} \tag{3.4}$$

The field ϕ satisfies the free wave equation in $\mathcal{D}$

$$\partial^2\phi + m^2\phi = 0 \tag{3.5}$$

and hence it can be decomposed into normal modes

$$\phi(x,t) = \sum_j \frac{1}{\sqrt{2E_j}}\left(\psi_j(x)e^{-iE_jt}a_j + \psi_j^*(x)e^{iE_jt}a_j^\dagger\right), \tag{3.6}$$

where ψ_j and E_j are the eigenfunctions and eigenvalues of the problem

$$(-\vec{\nabla}^2 + m^2)\psi_j = E_j^2\psi_j \quad \text{for } x\in\mathcal{D}; \qquad \psi_j(x) = 0 \quad \text{for } x\in\mathcal{S}. \tag{3.7}$$

We also use the definition $E(k) = \sqrt{k^2+m^2}$, and $E_j = \sqrt{k_j^2+m^2}$ so that the eigenvalue equation reads

$$-\vec{\nabla}^2\psi_j = k_j^2\psi_j, \tag{3.8}$$

and because of the positivity of the operator $-\vec{\nabla}^2$, the spectrum $\{E_j\}$ is contained in the half-line $\{E\geq m\}$.

We now introduce the propagator $G(x',x,k)$, defined as in Ref. [4] to be the

Green's function of the problem (3.7) or (3.8):

$$\begin{aligned}(-\vec{\nabla}'^2 - k^2)G(x', x, k) &= \delta(x' - x) \\ G(x', x) &= 0 \quad \text{for } x' \text{ or } x \in \mathcal{S},\end{aligned} \tag{3.9}$$

which can be written using the spectral decomposition as

$$G(x', x, k) = \sum_n \frac{\psi_n(x')\psi_n(x)}{k_n^2 - k^2 - i\epsilon} \tag{3.10}$$

In Ref. [4] we have developed an approximation for the propagator $G(x', x, k)$ in terms of optical paths (closed, in the limit $x' \to x$). The derivation can be found in Ref. [4], the general result valid for N spatial dimensions being

$$\begin{aligned}G_{\text{opt}}(x', x, k) &= \sum_r \frac{(-1)^{n_r}}{2^{N/2+1}\pi^{N/2-1}} (\ell_r \Delta_r)^{1/2} k^{N/2-1} H^{(1)}_{\frac{N}{2}-1}(k\ell_r), \\ &\equiv \sum_r G_r(x', x, k),\end{aligned} \tag{3.11}$$

where H is a Hankel function, r labels the paths from x to x', n_r is the number of reflections of the path r, $\ell_r(x', x)$ is its length and $\Delta_r(x', x)$ is the *enlargement factor* familiar from classical optics,

$$\Delta_r(x', x) = \frac{d\Omega_x}{dA_{x'}}. \tag{3.12}$$

$\Delta_r(x', x)$ is the ratio between the angular opening of a pencil of rays at the point x and the area spanned at the final point x' following the path r. For $N = 3$ we have

$$G_r(x', x, k) = (-1)^{n_r} \frac{\Delta_r^{1/2}(x', x)}{4\pi} e^{ik\ell_r(x', x)}. \tag{3.13}$$

With this explicit form for the propagator G, we now have to rewrite the elements of the quadratic operator $T_{\mu\nu}$ as functions of G and its derivatives. It is useful to pass from the point-splitting to a frequency cutoff by inserting the latter in the normal

modes decomposition (3.6) as

$$e^{-k_j/\Lambda} = \int_0^\infty dk e^{-k/\Lambda} 2k\ \delta(k^2 - k_j^2). \tag{3.14}$$

The limit $x' \to x$ can then be exchanged with the dk integral and we get for the energy density,

$$\langle 0|T_{00}(x,t)|0\rangle = \int_0^\infty dk e^{-k/\Lambda} \frac{1}{2} E(k)\rho(x,k) + \int_0^\infty dk e^{-k/\Lambda} \frac{k}{2E(k)} \vec{\nabla} \cdot \vec{j}(x,k). \tag{3.15}$$

The density ρ and the vector $\vec{j}$ are defined as

$$\rho(x,k) = \frac{2k}{\pi} \text{Im}\ G(x,x,k) \tag{3.16}$$

$$\vec{j}(x,k) = \lim_{x' \to x} \frac{1}{\pi} \text{Im} \vec{\nabla} G(x',x,k) = \frac{1}{2\pi} \text{Im} \vec{\nabla}\ G(x,x,k). \tag{3.17}$$

$\mathcal{E}$ is obtained by integrating T_{00} over the whole volume between the bodies:

$$\mathcal{E} = \int_{\mathcal{D}} d^3x \int_0^\infty dk e^{-k/\Lambda} \frac{1}{2} E(k)\rho(x,k) + \int_0^\infty dk e^{-k/\Lambda} \frac{k}{2E(k)} \int_{\mathcal{S}} d\vec{S} \cdot \vec{j}(x,k). \tag{3.18}$$

We have turned the integral over the divergence of $\vec{j}$ into a surface integral using Gauss's theorem. In the case of Dirichlet or Neumann boundary conditions, since $d\vec{S} \propto \vec{n}$ we have (here $\partial_{\vec{n}} \equiv \vec{n} \cdot \vec{\nabla}$ and $j_{\vec{n}} = \vec{n} \cdot \vec{j}$)

$$j_{\vec{n}}(x,k) = \frac{1}{\pi} \text{Im}\ \partial_{\vec{n}} G(x,x,k) = 0, \qquad x \in \mathcal{S} \tag{3.19}$$

and the surface integral term disappears. It should be noted that the vanishing of the $\vec{j}$ contribution to the total energy relies on the continuity of the propagator for $x', x \in \mathcal{D}$. In some approximations, including the optical one, this continuity is lost. Hence spurious surface terms arise on the boundary of certain domains $\mathcal{D}' \subset \mathcal{D}$. This region is what in wave optics is called the 'penumbra' region. Diffractive contributions are also not negligible in this region and they cancel the discontinuities in G, hence

eliminating the surface terms.[10] The surface terms in the energy are hence of the same order of the diffractive contributions which define the error in our approximation.

The divergence $\vec{\nabla} \cdot \vec{j}$ could also be eliminated from T_{00} by changing the energy-momentum tensor according to

$$\tilde{T}_{\mu\nu} = T_{\mu\nu} + \partial^{\alpha}\psi_{\alpha\mu\nu}, \tag{3.20}$$

with

$$\psi_{\alpha\mu\nu} = \frac{1}{2}\phi\left(g_{\mu\nu}\partial_{\alpha} - g_{\alpha\nu}\partial_{\mu}\right)\phi. \tag{3.21}$$

The total energy $\mathcal{E}$ and momentum are not affected by this redefinition however the new tensor $T_{\mu\nu}$ is not symmetric.

It can be seen that the stress tensor T_{ij} is normal on the surface $\mathcal{S}$ (for both Dirichlet and Neumann BC) so locally the force on the surface is given by the pressure alone

$$\frac{d\vec{F}}{dS} = \vec{n}P = \langle 0|T_{\vec{n},\vec{n}}|0\rangle. \tag{3.22}$$

The operator $T_{\vec{n}\vec{n}}$ regulated by point splitting is

$$\begin{aligned} T_{\vec{n}.\vec{n}}(x,t) &= \lim_{x'\to x}\left[\partial'_{\vec{n}}\phi'\partial_{\vec{n}}\phi - \frac{1}{2}g_{\vec{n},\vec{n}}\left(\partial'_0\phi'\partial_0\phi - \vec{\nabla}'\phi'\cdot\vec{\nabla}\phi - m^2\phi^2\right)\right] \\ &= \lim_{x'\to x}\left[\partial'_{\vec{n}}\phi'\partial_{\vec{n}}\phi + \frac{1}{2}\left(\partial'_0\phi'\partial_0\phi + \phi'\vec{\nabla}^2\phi - m^2\phi^2\right)\right. \\ &- \left.\frac{1}{2}\left(\vec{\nabla}' + \vec{\nabla}\right)\phi'\vec{\nabla}\phi\right] \end{aligned} \tag{3.23}$$

where ϕ' is shorthand for $\phi(x',t)$. The second term in brackets is zero when averaged over an eigenstate of the number operator $|\{n_j\}\rangle$, by virtue of the equations of motion. For Dirichlet BC the term $\phi\vec{\nabla}^2\phi = 0$ on the boundaries, so we have ($\vec{\nabla} = \vec{n}\partial_{\vec{n}} + \vec{\nabla}_t$)

$$\langle 0|T_{\vec{n},\vec{n}}|0\rangle = \lim_{x'\to x}\sum_j \frac{1}{4E_j}\left(\partial'_{\vec{n}}\partial_{\vec{n}} - \vec{\nabla}'_t\cdot\vec{\nabla}_t + k_j^2\right)\psi_j(x')\psi_j(x). \tag{3.24}$$

[10] As an example see Kirchoff's treatment of the diffraction from a hole in Ref. [5].

Since also $\vec{\nabla}_t \psi_j(x) = 0$ on the boundaries this expression simplifies to

$$P(x) = \lim_{x' \to x} \sum_j \frac{1}{4E_j} \partial'_{\vec{n}} \partial_{\vec{n}} \psi_j(x') \psi_j(x). \tag{3.25}$$

This expression can be rewritten, in terms of the propagator G, regulated by a frequency cutoff as we did for T_{00},

$$P(x) = \lim_{x' \to x} \partial'_{\vec{n}} \partial_{\vec{n}} \int_0^\infty dk e^{-k/\Lambda} \frac{k}{2\pi E(k)} \mathrm{Im} G(x', x, k). \tag{3.26}$$

In this regulated expression we can exchange the derivatives, limit and integral safely. Below we discuss what the divergences are when $\Lambda \to \infty$ and how to interpret and dispose them.

All the above expressions are exact. Once the propagator G is known, we can calculate the energy-momentum tensor components from them. However as discussed above in the interesting cases it is difficult to find an exact expression for G and some approximations must be used.

For smooth impenetrable bodies we use the optical approximation to the propagator developed in Ref. [4] and recalled in eq. (3.11). This gives G as a series of optical paths and hence the pressure P as a sum of contributions due to optical paths which reflect over the smooth, metallic surfaces[11]

$$P \simeq \sum_r P_r \tag{3.27}$$

$$P_r = (-1)^{n_r} \lim_{x' \to x} \partial'_{\vec{n}} \partial_{\vec{n}} \int_0^\infty dk e^{-k/\Lambda} \frac{k}{2\pi E(k)} \frac{\Delta_r^{1/2}(x', x)}{4\pi} \sin\left(k \ell_r(x', x)\right), \tag{3.28}$$

An important feature of the optical approximation is that all divergences are isolated in the low reflection terms whose classical path length can vanish as $x', x \to \mathcal{S}$. In practice only the zeroth and first reflection are potentially divergent. Before

[11] If the conducting surfaces are rough and the average height h of the roughness is much smaller than the important wavelengths $\sim a$, then the surfaces can be considered, for what we are concerned, smooth [44]. The corrections to the Casimir energy in the optical approximation are still not known but they must be very small, $\mathcal{O}\left(\langle h^2 \rangle\right)$ since $\langle h \rangle = 0$ the average being on regions of size $\sim a$.

performing the integral in k and taking $\Lambda \to \infty$ then we have to put aside the divergent zero and one reflection terms P_0 and P_1 for a moment (in the next section we will show how their contributions are to be interpreted).

For the remaining families of paths (that we will denote as $r \in \mathcal{R}$) the integral over k can be done and the limit $\Lambda \to \infty$ taken safely. The result is finite and reads

$$P(x) = \sum_{r\in\mathcal{R}} \lim_{x'\to x} \partial'_{\vec{n}}\partial_{\vec{n}}(-1)^{n_r}\frac{\Delta_r^{1/2}(x',x)}{8\pi^2\ell_r(x',x)}. \tag{3.29}$$

We can further simplify this expression. For simplicity let us call z the normal direction. Notice that for any sufficiently smooth function $f(z',z)$ vanishing for either z' or z on the surface $z=0$

$$\partial_{z'}\partial_z f(z',z)\Big|_{z'=z=0} = \frac{1}{2}\partial_z^2 f(z,z)\Big|_{z=0}. \tag{3.30}$$

The proof is trivial: consider that the lowest order term in the expansion of $f(z',z)$ near $z',z=0$ is $\propto z'z$. The propagator $G(x',x,k)$ satisfies all these properties and hence we can use this result to get rid of the limit $x' \to x$ and assume $x'=x$ from the beginning. We can therefore rewrite Eq. (3.29) as,

$$P(x) = \sum_{r\in\mathcal{R}}(-1)^{n_r}\partial_z^2\frac{\Delta_r^{1/2}(x,x)}{16\pi^2\ell_r(x,x)}. \tag{3.31}$$

Equation (3.31) is one of the main results of this chapter. In Ref. [4] we reduced the computation of Casimir energy to a volume integral. The force is then found by taking the derivative with respect to the distance between the bodies. Calculating the pressure instead gives the force by means of just a double integral of a local function. The problem is then computationally lighter and sometimes (as we will see in the examples) can even lead to analytic results.

Essentially the problem has been reduced to finding the lengths and enlargement factors associated with the optical paths *for points close to the boundary.* In the case of the pressure (eq. (3.29) or (3.31)) it is necessary to know their derivatives in

the direction transverse to the surfaces. We will see that this problem can be easily tackled numerically when it cannot be solved analytically.

3.4.2 Regulate and eliminate divergences

As in the energy calculations [4], the only divergences occurring in the pressure come from by paths whose lengths $\ell \ll 1/\Lambda$, where Λ is the plasma frequency of the material.[12] There are only two such families of paths: the zero and one reflection paths. In this section we show that these divergent contributions are independent of the distances between the bodies. This fact is easily understood: in order for a path to have arbitrarily small length all of its points must be on the same body. So in order to study these terms we need only consider a single, isolated body (and a massless field). We are also careful in maintaining the double derivative $\partial^2_{z',z}$ since we are calculating the terms P_0 and P_1 separately.

For $r = 0$, the zero reflection term, introducing an exponential cutoff Λ on the material reflection coefficient we obtain

$$P_0 = \int_0^\infty e^{-k/\Lambda} dk \frac{k}{2\pi E(k)} \lim_{x' \to x \in \mathcal{S}} \partial_{z'} \partial_z \left(\frac{\sin k|z' - z|}{4\pi |z' - z|} \right) = \frac{\Lambda^4}{4\pi^2}. \tag{3.32}$$

The same calculation for the $r = 1$ or one reflection term gives:

$$P_1 = \int_0^\infty e^{-k/\Lambda} dk \frac{k}{2\pi E(k)} \lim_{x' \to x \in \mathcal{S}} \partial_{z'} \partial_z \left(-\frac{\sin k|z' + z|}{4\pi |z' + z|} \right) = \frac{\Lambda^4}{4\pi^2}. \tag{3.33}$$

Notice that these two terms are equal, so we could have substituted $\partial_{z',z} \to \frac{1}{2}\partial_z^2$ for their sum, after having properly regulated the divergence.

This positive, cut-off dependent pressure, $P_\Lambda \equiv P_0 + P_1$, must be dynamically

[12] It is well known that the forces between rigid bodies remain finite and do not depend on the characteristics of the material in the perfect metal limit. On the contrary, stresses on the isolated bodies are strongly dependent on the dielectric constants and in general diverge in the perfect metal limit [48]. However, in the case of finite dielectric constants the calculation of the Casimir force is possible only in the parallel plates case [49]: a description of the interplay of finite conductivity effects and geometry dependence, even within the optical approximation, is still lacking. So in this chapter we limit ourselves to the case of infinite conductivity (which is however a very good approximation for the experiments) and we neglect the infinite self-stresses induced by this idealization.

balanced locally by a pressure generated by the material, lest it collapse. Moreover the total force obtained by integrating this quantity over the (closed) surface $\mathcal{S}$ of the whole body gives zero. However, if the space around the body were inhomogeneous, as in the presence of a gravitational field, a finite term survives the surface integration, giving rise to a "vacuum Archimedes effect" in which the pressure on one side is, due to gravitational effects, larger than on the other side, so the body feels a net force. We have analyzed this effect in detail in Ref. [50] and called it "Casimir buoyancy".

Finally note that another important element of this class of quadratic operators is the Feynman propagator. In studying a field theory in a cavity or in between impenetrable bodies (for example hadrons as bags, photons in cavities or Bose-Einstein condensates in traps), we can consider expanding the Feynman propagator in a series of classical optical paths reflecting off the boundaries. The first term, related to the direct path is the familiar free propagator, the others give the finite volume corrections.

3.5 Examples

In this section we calculate the Casimir force from the pressure, using the formalism developed in the previous section, for three examples that were already addressed in Ref. [4] using the energy method.

3.5.1 Parallel Plates

The parallel plates calculation is a classic example, whose result is well known and constitutes the basis the widely used proximity force approximation (PFA) [3]. We use this standard example to establish the rank among contributions to the total pressure and show the similarity and differences with the energy method [4].

We calculate the force acting on the lower plate, denoted by d or *down*, by calculating the pressure on its surface. We discard the zero and $1d$ (one reflection on the lower plate itself) reflection terms. The first term to be considered is the path that bounces once on the upper plate (u or *up*) $1u$. For parallel plates $\Delta = 1/\ell^2$ and we

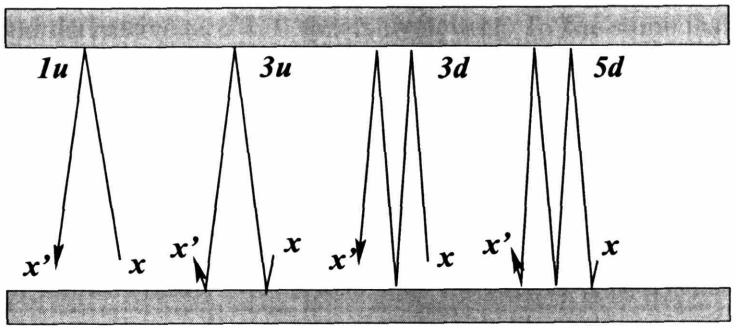

Figure 3-12: Odd reflection paths that contribute to the Casimir force between the two plates in the pressure calculations with the optical approximation. The points x' and x will eventually be taken coincident and lying on the lower plate.

have

$$P(x) = \sum_{r \geq 1u} (-1)^{n_r} \partial_z^2 \frac{1}{16\pi^2 \ell_r^2(x,x)}. \tag{3.1}$$

The length $\ell_r(x,x)$ for the paths that bounce an even number of times is a constant in z and hence the derivatives vanish: they do not contribute to the pressure. This seemingly innocuous observation simplifies the calculations considerably and it is a test for any other geometry which reduces to parallel plates in some limit: in this limit the even reflections contributions must vanish. Generically their contributions are small. This parallels the role of the odd reflection paths in the energy method [4].

Figure 3-12 shows the odd reflection paths labelled with our conventions. For the path $1u$ we have

$$P_{1u}(x) = \lim_{z \to 0} -\partial_z^2 \frac{1}{16\pi^2(2a-2z)^2} = -\frac{3}{32\pi^2 a^4}. \tag{3.2}$$

The next path to be considered is the path that bounces 3 times, first on d, then on u and again on d, $dud = 3u$ (3 stands for 3 reflections and u for the plate where the middle reflection occurs) which gives a contribution

$$P_{3u}(x) = \lim_{z \to 0} -\partial_z^2 \frac{1}{16\pi^2(2a+2z)^2} = -\frac{3}{32\pi^2 a^4}. \tag{3.3}$$

The two contributions Eq. (3.2) and Eq. (3.3) are equal. The reason is easily uncovered. One can recover Eq. (3.3) from Eq. (3.2) sending $z \to -z$ but for the purpose of

taking the second derivative at $z = 0$ this is irrelevant. In the same fashion $P_{3d} = P_{5d}$, $P_{5u} = P_{7u}$ etc. and hence we find

$$P(x) = -2\frac{3}{32\pi^2 a^4} - 2\frac{3}{32\pi^2 (2a)^4} - 2\frac{3}{32\pi^2 (3a)^4} + ... = -\frac{3}{16\pi^2 a^4}\frac{\pi^4}{90}, \tag{3.4}$$

which is the well-known result. Notice also that the rate of convergence is the same as in the calculation making use of the Casimir energy in Ref. [4] (n-th term contributes $1/n^4$ of the first term, in this case $1u + 3u$). These observations that allow us to determine the rank of the contributions are fundamental, and they apply as well to the other examples in this section.

3.5.2 The Casimir Torsion Pendulum

In this section we study a geometry already considered in Ref. [4]: a plate inclined at an angle θ above another infinite plate. We have called this configuration a 'Casimir torsion pendulum' because the Casimir force will generate a torque which can be experimentally measured. The configuration is analogous to the parallel plates case but the upper plate must be considered tilted at an angle θ from the horizontal. The length of the upper plate must be taken finite, we denote it by w, while the length of the lower plate can be infinite which we choose for simplicity. There is only one substantial difference with the parallel plates case: the even reflection paths do contribute in the pendulum, since their length varies as we move the final points x', x.

We calculate the force exerted on the lower, infinite plate for simplicity. We then obtain the energy $\mathcal{E}$, by integrating over the distance along the normal to the lower plate and from this we can calculate the torque as

$$\mathcal{T} = -\frac{\partial \mathcal{E}}{\partial \theta}. \tag{3.5}$$

The lower plate is taken infinite, the upper plate width is w, and the distance between the height at the midpoint of the upper plate is a. We will choose as the origin of the coordinates one point on the intersection line between the lower plate

and the line obtained by prolonging the upper plate. This defines a fictitious wedge of opening angle θ. We call x the horizontal and z the vertical coordinate, the third direction, along which one has translational symmetry, being y.

Since the surfaces are locally flat we have $\Delta = 1/\ell^2$ as in the case of the parallel plates, and again the odd reflections are exactly as in the case of the parallel plates. However now the even reflections contribute (the notation is the same as in the parallel plates case, in the even reflections $2u$ means the first reflection is on the upper plate etc.):

$$P = P_{1u+3u} + P_{2u+2d} + P_{3d+5d} + ... \tag{3.6}$$

where we have grouped the terms with the symbolic notation $P_{a+b} = P_a + P_b$ when $P_a = P_b$. It is useful to recapitulate what we have learned about the rank of these contributions: P_{1u+3u} dominates, P_{3d+5d} is smaller by $\sim 1/16$, P_{5u+7u} is smaller by $\sim 1/81$, *etc.* The even reflections are generically much smaller than the odd reflections, and vanish as $\theta \to 0$.

The first term in (3.6) is

$$P_{1u+3u} = -2\frac{1}{16\pi^2}\partial_z^2 \frac{1}{\ell_1^2(z,x)}, \tag{3.7}$$

with $\ell_1 = 2(x\sin\theta - z/\cos\theta)$, and an overall factor of 2 takes into account the identity $P_{1u} = P_{3u}$. Taking the derivative and then setting $z = 0$ we find

$$P_{1u+3u} = -\frac{3}{16\pi^2}\frac{1}{x^4\sin^4\theta\cos^2\theta}, \tag{3.8}$$

and integrating from $x_m = (a/\sin\theta - w/2)/\cos\theta$ to $x_M = (a/\sin\theta + w/2)/\cos\theta$ we find the force per unit length in the y direction

$$F_{1u+3u} = -\frac{\cos\theta}{32\pi^2\sin^4\theta}\left(\frac{1}{(a/\sin\theta - w/2)^2} - \frac{1}{(a/\sin\theta + w/2)^2}\right). \tag{3.9}$$

Since term by term $F = -\partial\mathcal{E}/\partial a$ we find the first term in optical expansion of the

Casimir energy $\mathcal{E}$ (the arbitrary constant is chosen so that $\mathcal{E} \to 0$ when $a \to \infty$) as

$$\mathcal{E}_{1u+3u} = -\frac{aw\cos^4\theta}{2\pi^2\left(4a^2 - w^2\sin^2\theta\right)^2} \tag{3.10}$$

and from this one obtains the torque

$$\mathcal{T}_{1u+3u} = \frac{2aw\left(w^2 - 4a^2\right)\cos^3\theta\sin\theta}{\pi^2\left(4a^2 - w^2\sin^2\theta\right)^3} \tag{3.11}$$

Analogously we can calculate the contribution to the pressure P of the two reflections paths $2u$ and $2d$. Again the contributions of the two paths are identical and the result simplifies to

$$P_{2u+2d} = \frac{2}{8\pi^2}\frac{1}{2}\partial_z^2\frac{1}{\ell_2^2(z,x)}, \tag{3.12}$$

and using $\ell_2 = 2\sqrt{x^2+z^2}\sin\theta$ we find

$$P_{2u+2d} = -\frac{1}{16\pi^2\sin^2\theta\ x^4} \tag{3.13}$$

which integrated from $x_m = (a/\sin\theta - w/2)/\cos\theta$ and $x_M = (a/\sin\theta + w/2)/\cos\theta$ gives the force along the z axis due to these paths:

$$F_{2u+2d} = -\frac{\cos^3\theta}{48\pi^2\sin^2\theta}\left(\frac{1}{(a/\sin\theta - w/2)^3} - \frac{1}{(a/\sin\theta + w/2)^3}\right). \tag{3.14}$$

This expression can now be expanded for $\theta \ll 1$ (quasi-parallel plates)

$$F_{2u+2d} \simeq -\frac{1}{16\pi^2}\left(\frac{w}{a^4}\theta^2 + \frac{5w^3 - 11wa^2}{6a^6}\theta^4 + ...\right). \tag{3.15}$$

Notice that this expression vanishes when $\theta \to 0$, as it should since for parallel plates all the contributions of even reflections paths vanish.

The next term in the series is F_{3d+5d}, whose calculation is performed in the same

fashion. The result is:

$$F_{3d+5d} = -\frac{3}{16\pi^2}\frac{\cos^5 2\theta}{\sin^4 2\theta}\left(\frac{1}{(a/\sin\theta - w/2)^3} - \frac{1}{(a/\sin\theta + w/2)^3}\right), \quad (3.16)$$

$$\simeq -\frac{1}{16\pi^2}\left(\frac{3w}{16a^4} + \frac{5w^3 - 48a^2w}{32a^6}\theta^2 + ...\right). \quad (3.17)$$

We can also present the term given by the 4 reflections paths,

$$F_{4u+4d} = -\frac{\cos^3 2\theta}{48\pi^2 \sin^2 2\theta}\left(\frac{1}{(a/\sin\theta - w/2)^3} - \frac{1}{(a/\sin\theta + w/2)^3}\right) \simeq -\frac{1}{16\pi^2}\left(\frac{w}{4a^4}\theta^2 + ...\right). \quad (3.18)$$

The terms independent of θ can be seen to reconstruct the parallel limit case $F = -(1 + 1/16 + 1/81 + ...)3/16\pi^2 a^4$.

Term by term, this series for the force reproduces the series in Ref. [4]. The series for the energy and the torque agree as well. The results of the pressure method then coincide with those of the energy method (as for all the examples analyzed in this chapter). In Ref. [4] we discussed at some length the predictions of the optical method for the Casimir torsion pendulum. We will not repeat them here, referring the reader to that paper for further details.

3.5.3 Sphere and Plane

The sphere facing a plane is an important example for several reasons: it has been analyzed theoretically with various exact or approximate numerical techniques [9, 42]; it is an experimentally relevant configuration; the exact solution is unknown and probably will escape analytical methods for a long time to come. We have already calculated the optical approximation to the Casimir energy in Ref. [4] up to 5 reflections. In this chapter we study this problem for mainly pedagogical purposes, leaving a more accurate and complete numerical analysis for the future. We believe it is worth studying this example because, contrary to the previous two examples, the enlargement factor plays an important role and moreover we will reanalyze this example with finite temperature in Section IV B 2.

We calculate the pressure (and by integrating, the force) exerted on the plate by

the sphere which, of course, equals the force exerted by the plate on the sphere. We start from the qualitative observation that the rank of the contributions is the same as in the parallel plates case in the limit $a/R \to 0$. In all the examples we have analyzed this rank is preserved for any value of a/R. Moreover the ratios of the contributions to the force $F_{3+5}(a,R)/F_{1+3}(a,R)$, $F_4(a,R)/F_2(a,R)$ etc. decrease quickly as a/R increases, we believe due to the growing importance of the enlargement factor.

Here we calculate analytically the $1s$ term (here s stands for 'sphere' and p for 'plate') and by using the relation $P_{1s+3s} \equiv P_{1s} + P_{3s} = 2P_{1s}$ proved in Section 3.4 (the notation is the same as in that section) we are able to include the $3s$ term as well.

Using the expressions for the length and enlargement factor for the $1s$ path obtained in Ref. [4] we get

$$\begin{aligned} P_{1s+3s} &= -2\frac{R}{16\pi^2}\frac{\partial^2}{\partial z^2}\frac{\Delta_{1s}^{1/2}}{\ell_{1s}} \\ &= -\frac{R}{32\pi^2}\frac{\partial^2}{\partial z^2}\left(R-\sqrt{(a+R-z)^2+\rho^2}\right)^{-2}\left((a+R-z)^2+\rho^2\right)^{-1/2}\Big|_{z=0} \end{aligned} \tag{3.19}$$

The final expression for the pressure P_{1s+3s} obtained after the derivatives are taken is rather long, however the contribution to the force on the plate, F_{1s+3s} (obtained by integration of P_{1s+3s} over the infinite plate) is quite simple:

$$F_{1s+3s} = 2\pi\int_0^\infty d\rho\rho P_{1s+3s} = -\frac{\hbar c R}{8\pi a^3}. \tag{3.20}$$

This is the largest of the contributions and increasing a/R improves the convergence of the series due to the presence of the enlargement factor, so the asymptotic behavior at large a/R predicted by the optical approximation is that given by this formula, *i.e.* $F \propto R/a^3$ or $E \propto R/a^2$. This asymptotic law is in accordance with the numerics of Ref. [4] and the predictions of other semiclassical methods [9]. However, eq. (3.20) is in disagreement with the Casimir-Polder law [1] which predicts $E \propto R^3/a^4$ for $a \gg R$. This is no great surprise, since our method is not valid for $a/R \gg 1$, the semiclassical reflections being corrected and eventually overshadowed by diffractive contributions [13, 38].

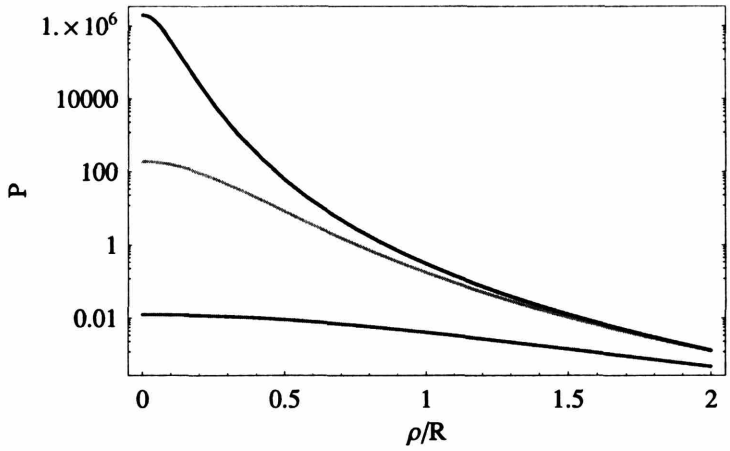

Figure 3-13: The magnitude of the total pressure up to reflection $5p$ in units of $\hbar c/R^4$ as a function of the radial coordinate on the plate, ρ/R. Upward, or red to blue $a/R = 1$, $a/R = 0.1$ and $a/R = 0.01$.

We have calculated the contribution of the two reflections paths analytically as well. The calculation is more involved than the one reflection term but a big simplification occurs if one notices that, for the purpose of taking the second derivative with respect to z at $z = 0$, one can leave the reflection point on the sphere fixed. We could not prove a similar result for any other reflection. It is certainly not true for *odd* reflections but one can conjecture it to be true for *even* reflections. In this chapter we have not calculated the 4 reflection terms and hence we could not check this conjecture for more than 2 reflections.

And finally, we have calculated the $3p$ (or *sps*) and hence obtained the $5p$, or *pspsp*, paths contribution P_{3p+5p}; P_{3p+5p} in the parallel plates limit should account for $\sim 1/16$ of the total force. This contribution, unlike the previous ones, must be calculated partly numerically, mainly because finding the reflection point on the sphere requires the (unique) solution of a transcendental equation. This task is achieved much more quickly by a numerical algorithm than by patching together the several branches of the analytic solution.

The total pressure is plotted in Fig. in 3-13 while the various contributions (keeping in mind that P_{1s+3s} and P_{3p+5p} are negative and P_{2+2} is mainly positive) are shown in Fig. 3-14. Figure 3-13 reveals some interesting features of the pressure in this

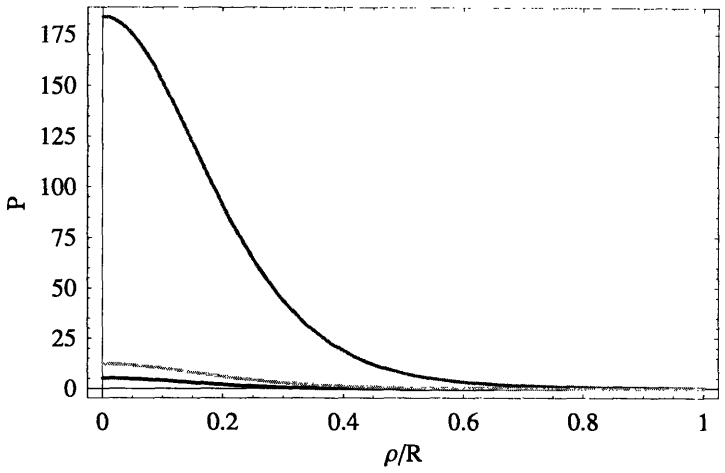

Figure 3-14: Contributions to the pressure in units of $\hbar c/R^4$ as a function of ρ/R, for fixed $a/R = 0.1$. Downward or red to blue, we have $-P_{1s+3s}$, $-P_{3p+5p}$ and P_{2+2}. Although unnoticeable in this figure, the curve P_{2+2} changes sign at around $\rho/R \simeq 0.4$ (see Figure 3-15 for a similar situation).

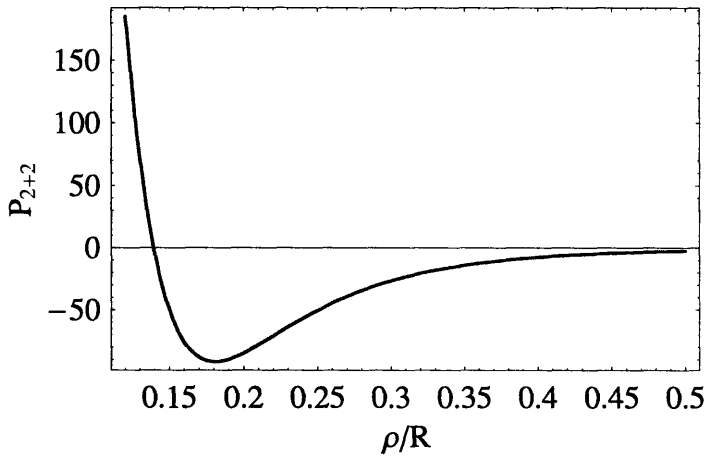

Figure 3-15: Contribution of the two reflection path(s) to the pressure in units of $\hbar c/R^4$ as a function of ρ/R, for fixed $a/R = 0.01$. The pressure becomes negative, showing that the sign of the pressure is not determined by the number of reflection only.

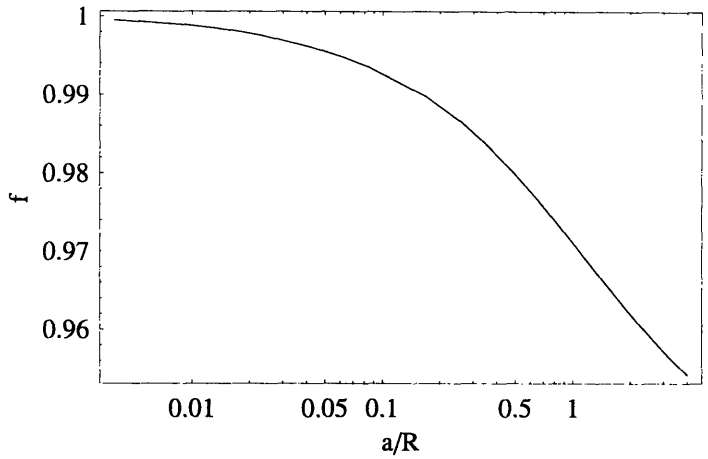

Figure 3-16: The ratio between the optical force up to the $5p$ reflection and the most divergent term in the PFA, as defined by eq. (3.21).

geometry: the total pressure decays very quickly with the distance as $P \sim \rho^{-\alpha}$: the exponent α seems to depend upon the distance a/R, but for $a/R \leq 0.1$ a good fit is obtained with $\alpha = 6$, in accordance with the asymptotic expansion of the $1 + 3$ reflection term Eq. (3.19); by decreasing the distance between the sphere and the plate, the pressure becomes more and more concentrated near the tip, giving us reasons to trust our approximation and supporting the use of the PFA as a first approximation in the limit $a/R \to 0$. Figure 3-14 shows the relative importance of the contributions due to the different paths. As expected the contribution to the total pressure decreases quite fast by increasing the number of reflections. In Fig. 3-15 one can also see that the sign of the pressure is not determined simply by the number of reflections of the underlying optical path — as for the contribution to the energy density.

By integrating the pressure over the whole plate we obtain the force F. It is useful to factor out the most divergent term of the force, as predicted by the PFA, so we define the quantity $f(a/R)$ as

$$F(a) = -\frac{\pi^3 R}{720 a^3} f(a/R). \tag{3.21}$$

Since we include only a finite number of reflections it is convenient to factor out the

constant $\zeta(4)/(1+1/16)$ such that f is normalized with $f(0)=1$. The function $f(a/R)$, calculated including paths $1s$, $3s$, 2, $3p$ and $5p$, is plotted in Figure 3-16. When $a/R \to 0$ f is fitted by

$$f(a/R) = 1 - 0.10\ a/R + \mathcal{O}\left((a/R)^2\right)\ . \tag{3.22}$$

By comparing to the results of [4]

$$f_{\text{energy}}(a/R) = 1 + 0.05\ a/R + \mathcal{O}\left((a/R)^2\right) \tag{3.23}$$

there is the difference in the sub-leading term.

By neglecting the $5s+7p$ reflection paths (which in the parallel plates case contribute $\sim 2\%$ of the total force) we can only assert that the functions f in (3.22) and (3.23) represent the optical approximation with an error of 2%. When plotted on the whole range of a/R where the optical approximation is to be trusted the pressure and energy method curves never differ more than 2%. However there is no such a bound on the sub-leading term which, on the contary, depends on the higher reflections contributions which have not been included in this calculations.[13] With the terms calculated at this point, we cannot make a precise statement about the sub-leading term. We can however safely say that the subleading term a/R coefficient is quite small and our method disagrees with the PFA prediction $-0.5a/R$. The sphere opposite plate is such an experimentally relevant geometry that further, more accurate studies need to be performed to compare with experimental data.

In conclusion, the lessons to be learned from this example are two: 1) The calculations with the pressure method are even quicker and simpler than the energy method and sometimes can give analytic results for non-trivial geometries and 2) the sub-leading terms must be compared only between calculations performed with the same accuracy.[14]

[13]For example consider that including only $1s$, $3p$, and 2 and reflections would have given a sub-leading term $-0.16a/R$ instead of $-0.10a/R$ in Eq. (3.22). The sub-leading term then changes of 50% by adding the $3s+5p$ reflection terms which contributes only up to 8% of the total.

[14]AS would like to thank M. Schaden and S. Fulling for conversations on this point during the

3.6 Casimir Thermodynamics

As measurements of Casimir forces increase in accuracy they become sensitive to thermal effects. The natural scale for Casimir thermodynamics is a distance, $\tilde{\beta} = \hbar c/\pi T$, which at room temperature is about 2.5 microns. [To avoid confusion with the wave number k, we set Boltzmann's constant equal to unity and measure temperature in units of energy. We continue to keep $\hbar$ and c explicit.] So, assuming the corrections are of $\mathcal{O}\left((a/\tilde{\beta})^{\alpha}\right)$, depending on the value of α thermal effects might be expected between the 10% (for $\alpha = 1$) and 0.3% (for $\alpha = 4$, the standard parallel plates result) level for Casimir force measurements on the micron scale. In open geometries, like the sphere and plane, even longer distance scales are probed by Casimir effects, and this gives rise to interesting changes in the temperature dependence of the Casimir free energy in comparison with the case of parallel plates[16]. The optical approximation is well suited for discussion of thermodynamics since the thermodynamic observables, like the Casimir energy, can be expressed in terms of the propagator. Here we consider again a non-interacting, scalar field outside rigid bodies on which it obeys Dirichlet boundary conditions.

Before entering into a technical discussion of temperature effects, it is useful to anticipate one of our central results which follows from qualitative observations alone. As $T \to 0$ the temperature effects probe ever longer distances. Even at room temperature the natural thermal scale is an order of magnitude larger than the separation between the surfaces in present experiments (see Ref. [40]). Since long paths contribute little to the Casimir force, we can be confident that thermal effects vanish quickly at low temperature. However, the leading T-dependence at small T comes from regions beyond the range of validity of the optical (or any other) approximation, so we are unable to say definitively how they vanish for geometries where no exact solution is possible (*i.e.* other than infinite parallel plates).

---

workshop 'Semiclassical Approximations to Vacuum Energy' held at Texas A & M, College Station, TX, January 2005. The concerns about the errors to be associated with the optical, semiclassical or proximity force approximation is still open to debate and is strictly connected to one of the most challenging open problems in spectral theory *i.e.* how to go beyond the semiclassical approximation to the density of states of a positive Hermitian operator.

This section is organized as follows: First we discuss the free energy and check our methods on the parallel plates geometry; then we discuss the temperature dependence of the pressure, which we apply to the sphere and plate case. Finally we discuss the difficulties associated with the $T \to 0$ limit.

3.6.1 Free Energy

The free energy is all one needs to calculate both thermodynamic corrections to the Casimir force and Casimir contributions to thermodynamic properties like the specific heat and pressure. However like the Casimir *energy*, Casimir contributions to the specific heat, pressure, *etc.*, are cutoff dependent and cannot be defined (or measured) independent of the materials which make up the full system. So we confine ourselves here to the thermal corrections to the Casimir force. The problem of parallel plates has been addressed before and our results agree with those[16].

Derivation

We start from the expression of the free energy for the scalar field as a sum over modes

$$\begin{aligned}
\mathcal{F}_{\text{tot}} &= -\beta^{-1} \sum_n \ln \left(\frac{e^{-\beta \frac{1}{2} \hbar \omega_n}}{1 - e^{-\beta(\omega_n - \mu)}} \right), \\
&= \beta^{-1} \sum_n \ln \left(1 - e^{-\beta(\hbar\omega_n - \mu)} \right) + \sum_n \frac{1}{2} \hbar \omega_n, \\
&\equiv \mathcal{F} + \mathcal{E}, \qquad (3.1)
\end{aligned}$$

where μ is the chemical potential, and the last term is the Casimir energy, or the free energy at zero temperature, since $\mathcal{F} = 0$ for $T = 0$. The Casimir energy $\mathcal{E}$, being independent of the temperature, does not contribute to the thermodynamic properties of the system. It however does contribute to the pressures and forces between two bodies. The force between two bodies, say a and b, is obtained by taking the gradient

of the free energy with respect to the relative distance $\vec{r}_{ab}$

$$\vec{f}_{ab} = -\vec{\nabla}_{ab}\mathcal{F}. \tag{3.2}$$

At $T = 0$ we recover the familiar result $\vec{f} = -\vec{\nabla}\mathcal{E}$.

Next we turn the sum over modes into a sum over optical paths. Following the same steps that led from Eq. (3.4) to Eq. (3.15) we obtain

$$\mathcal{F} = \beta^{-1} \int d^N x \int_0^\infty dk\ \rho(x,k) \ln\left(1 - e^{-\beta(\hbar\omega(k)-\mu)}\right). \tag{3.3}$$

where $\rho(x,k)$ is given by Eq. (3.16). By specializing to a massless field in 3 dimensions with zero chemical potential (to mimic the photon field), and substituting the optical approximation for the propagator Eq. (3.13), we obtain the sum over paths

$$\mathcal{F} \equiv \sum_{r=0} \mathcal{F}_r = \sum_r (-1)^r \frac{1}{2\pi^2\beta} \int_{\mathcal{D}_r} d^3x\ \Delta_r^{1/2} \int_0^\infty dk\ k \sin(k\ell_r) \ln\left(1 - e^{-\beta\hbar ck}\right). \tag{3.4}$$

Here the term $\mathcal{F}_0$, the direct path, gives the usual free energy for scalar black body radiation. Using the values for the direct path, we have $\Delta_0 = 1/\ell_0^2$ and $\ell_0 = |x' - x| \to 0$ when taking $x' \to x$. We get the familiar textbook expression

$$\mathcal{F}_0 = V \int_0^\infty dk\ \frac{k^2}{2\pi^2}\ \beta^{-1} \ln\left(1 - e^{-\beta\hbar ck}\right) = -\frac{\pi^2}{90} \frac{VT^4}{(\hbar c)^3}, \tag{3.5}$$

where V is the (possibly infinite) volume outside the bodies.

The general term $\mathcal{F}_r$ associated with the path r is calculated by performing the k integral in Eq. (3.4):

$$\mathcal{F}_r = (-1)^{r+1} \frac{\hbar c}{2\pi^2} \int_{\mathcal{D}_r} d^3x \Delta_r^{1/2} \frac{1}{2\ell_r^3} \left[-2 + \tilde{\ell}_r \left(\coth\tilde{\ell}_r + \tilde{\ell}_r \mathrm{csch}^2 \tilde{\ell}_r\right)\right] \tag{3.6}$$

where $\tilde{\ell}_r = \ell_r \pi T/\hbar c = \ell_r/\tilde{\beta}$ measures the path length relative to the thermal length scale.

Eq. (3.6) is the fundamental result of this section and gives a simple, approximate

description of thermal Casimir effects for geometries where diffraction is not too important. There are no divergences in any of the $\mathcal{F}_r$, ultraviolet or otherwise, even for the direct path (as we saw in eq. (3.5)) and the first reflection path. All the ultraviolet divergences are contained in the Casimir energy $\mathcal{E}$. Indeed, by expanding the integrand of equation (3.6) at short distances, *i.e.* $\tilde{\ell}_r \ll 1$, we obtain

$$\Delta_r^{1/2}\frac{1}{2\ell_r^3}\left[-2+\tilde{\ell}_r\left(\coth\tilde{\ell}_r+\tilde{\ell}_r\mathrm{csch}^2\tilde{\ell}_r\right)\right]\simeq\Delta_r^{1/2}\frac{1}{\tilde{\beta}^3}\left[\frac{1}{45\tilde{\beta}}\ell_r-\frac{4}{945\tilde{\beta}^3}\ell_r^3+...\right]. \quad (3.7)$$

Only the 1-reflection path length can go to zero to generate a divergence. For this contribution Δ_r diverges like $1/\ell_r^2$ as $\ell_r \to 0$, however this is compensated by the ℓ_r term in (3.7) so the expression is finite and then integrable.

To check for infrared divergences notice that at large distances, $\tilde{\ell}_r \gg 1$, the integrand of (3.6) goes to $\sim \Delta_r^{1/2}/\ell_r^2$. For an infinite flat plate the $\Delta_r \sim 1/z^2$, where z is the normal coordinate to the plate, and the integral is hence $\sim dz/z^3$ at large z. For finite plates the domain of integration is finite and for curved plates the enlargement factor falls even faster than $1/\ell^2$, and the integral remains convergent.

Since the integral converges in both the infrared and ultraviolet, it is safe to estimate the important regions of integration by naive dimensional analysis. This leads to the conclusion that *The paths that dominate the temperature dependence of the Casimir force have lengths of order the thermal length* $\tilde{\beta}$. High temperature implies short paths. Very low temperatures are sensitive to very long paths. Long paths involve both paths experiencing many reflections, which are sensitive to the actual dynamics at and inside the metallic surface, or paths making long excursions in an open geometry, which are sensitive to diffraction. Either way, low temperatures will present a challenge.

Parallel Plates

We know that in the limit of infinite, parallel plates the optical approximation to the propagator becomes exact. Hence our method gives another way to calculate the free energy of this configuration of conductors. It is convenient to study this example to

check against known results and to prepare the way for a study of the $T \to 0$ limit.

We recall that for this configuration the expression for the enlargement factor is $\Delta = 1/\ell^2$ and the lengths are given by $\ell_{2n} = 2na$ (where a is the distance between the plates) and $\ell_{2n+1,\,u} = 2(a-z) + 2na$, $\ell_{2n+1,\,d} = 2z + 2na$, the notation being the same as in Section 3.5.1, should at this point be familiar to the reader.

As in the zero temperature case it is useful consider even and odd reflection contributions separately and as for the zero temperature case, the sum over odd reflections turns into an integral over z from 0 to ∞

$$\mathcal{F}_{\text{odd}} = \sum_{n=0}^{\infty} \mathcal{F}_{2n+1,d} + \mathcal{F}_{2n+1,u} = \frac{\hbar c}{2\pi^2 \tilde{\beta}^3} S \int_0^{\infty} dx \frac{1}{2x^4} \left[-2 + x(\coth x + x\ \text{csch}^2 x)\right], \tag{3.8}$$

where $x = 2z/\tilde{\beta}$ and S is the area of the plate. The definite integral can be easily performed numerically and its value is $\nu = 0.06089...$,

$$\mathcal{F}_{\text{odd}} = 2\frac{\hbar c}{4\pi^2 \tilde{\beta}^3} S\nu = \frac{\pi T^3}{2(\hbar c)^2} S\nu \tag{3.9}$$

which is independent of the separation, a, and therefore does not contribute to the force.

Let us turn now to the even reflection paths. They have constant length $2na$, so the volume integral simply yields the volume between the surfaces $v = Sa$. We already calculated the zero-reflection term $\mathcal{F}_0$ in Eq. (3.5). The remaining even reflection contributions (2,4,6,... reflections) $\mathcal{F}_{\text{even},r\geq 2}$ can be written as an infinite sum

$$\mathcal{F}_{\text{even},r\geq 2} = -2\frac{\hbar c}{2\pi^2} Sa \frac{1}{\tilde{\beta}^4} \sum_{n=1}^{\infty} \frac{1}{2x_n^4} \left[-2 + x_n \left(\coth x_n + x_n \text{csch}^2 x_n\right)\right] \tag{3.10}$$

where $x_n = 2na/\tilde{\beta} \equiv n\tau$ (this defines the dimensionless temperature τ) and we have introduced an overall factor of two to take into account the multiplicity of the paths. Thus the total free energy for parallel plates is the sum of $\mathcal{F}_0$ (eq. (3.5) and the results

of eqs. (3.9) and (3.10)),

$$\mathcal{F}_{\|} = -\frac{\pi^4}{90}\frac{VT^4}{(\hbar c)^3} + \frac{\pi T^3}{2(\hbar c)^2}S\nu - \frac{\hbar c}{\pi^2\tilde{\beta}^4}Sa\sum_{n=1}^{\infty}\frac{1}{2x_n^4}\left[-2 + x_n\left(\coth x_n + x_n \mathrm{csch}^2 x_n\right)\right] \tag{3.11}$$

It is not possible to rewrite $\mathcal{F}_{\|}$ in a closed form, but the sum is easy to compute numerically and the high and low temperature expansions are easy to obtain analytically. At high temperatures (and fixed a) $\tau \to \infty$, and the summand $g(n)$ in eq. (3.11) falls rapidly enough with n

$$g(n) = \frac{1}{2(\tau n)^4}\left[-2 + (\tau n)\left(\coth(\tau n) + (\tau n)\mathrm{csch}^2(\tau n)\right)\right] = \frac{1}{2(\tau n)^4}\left[-2 + \tau n\right] + \mathcal{O}\left(e^{-\tau n}\right), \tag{3.12}$$

that the limit may be taken under the summation, with the result,

$$\mathcal{F}_{\mathrm{even},r\geq 2} \simeq -\frac{\hbar c}{\pi^2\tilde{\beta}^4}Sa\sum_{n=1}^{\infty}\left[\frac{1}{2n^3\tau^3} - \frac{1}{\tau^4 n^4}\right] = -\frac{\zeta(3)}{16\pi a^2}ST + \frac{\pi^2\hbar c}{1440a^3}S. \tag{3.13}$$

Notice that the second term cancels the even paths contribution to the Casimir energy. Hence the final expression for the high T expansion of the free energy is particularly simple,

$$\mathcal{F}_{\mathrm{tot}} = \mathcal{F} + \mathcal{E} = -\frac{\pi^2}{90\hbar c}VT^4 + \nu\frac{\pi}{2(\hbar c)^2}ST^3 - \frac{\zeta(3)}{16\pi a^2}ST + \mathcal{O}\left(e^{-\pi T a/\hbar c}\right). \tag{3.14}$$

The first term is usual black body contribution to the bulk free energy. It does not contribute to the force. The second term is also independent of a and does not give rise to any force. The third term instead gives the thermal Casimir force. Notice that $\hbar c$ has disappeared from this expression. Called the "classical limit", this high temperature behavior has been noted before and some early results are even due to Einstein (in [52] pg. 2; see also [45]). In the next section, after the thermal corrections to the pressure are calculated, we show how to extend this result to other geometries.

Note some interesting features of the $T \to \infty$ limit: First, the sum over paths converges like the sum of $(1/n)^3$ as indicated by the appearance of $\zeta(3)$. While slower

than the $T = 0$ convergence, it is still rapid enough to obtain a good approximation from low reflections. Second, note that the $T \to \infty$ problem in 3-dimensions corresponds exactly to a $T = 0$ problem in 2-dimensions. This is an example of the familiar dimensional reduction expected as $T \to \infty$. We can give a short proof of this result. Let us first write:

$$F = -\frac{1}{\beta} \log Z \tag{3.15}$$

where Z is the partition function. We need to evaluate Z to the lowest order in β when $\beta \to 0$. The thermal scalar field theory can be written as a free theory on the cylinder $\mathbf{R}^3 \times [0, \beta)$. For $\beta \to 0$ the dynamics along the thermal coordinate is frozen in the ground state, with energy $E_0 = 0$, where ϕ does not depend on the thermal coordinate. The partition function Z is now $Z = Z_3 + \mathcal{O}\left(e^{-\beta E_1}\right)$ where E_1 is the first excited state $E_1 \propto 1/\beta^2$ and Z_3 is the partition function of the remaining three-dimensional problem in $\mathbf{R}^3$. If the conductors geometry is symmetric along one spatial coordinate, say x (in the parallel plates problem we have two of these directions, x and y) this can now be interpreted as an Euclideanized time variable extending from 0 to L_x/c. So we will write $Z_3 = Z_{2+1} = e^{-\frac{1}{\hbar}\mathcal{E}_2 L_x/c}$ where $\mathcal{E}_2$ is the Casimir energy of the 2 dimensional problem of two lines of length L_y, distant a. The free energy F is then:

$$F = -\frac{1}{\beta} \log Z \simeq -\frac{1}{\beta} \log Z_{2+1} = T \frac{1}{\hbar} \frac{L_x}{c} \mathcal{E}_2 = -T L_x L_y \frac{\zeta(3)}{16\pi^2 a^2}. \tag{3.16}$$

Since $S = L_x L_y$ This is exactly the a-dependent term in eq. (3.14). If the geometry is not translational invariant then we can only say from eq. (3.16) that the free energy is linear in T (since Z_{2+1} is independent of β). Later, by using the optical approximation we will find an explicit analytic expression valid also for non-symmetric, smooth geometries.

For low temperatures, $\tau \to 0$, the terms in the n-sum in eq. (3.11) differ very little

from each other so we can use the Euler-McLaurin formula[51],

$$\sum_{n=1}^{\infty} g(n) = \int_0^{\infty} dx\; g(x) - \frac{1}{2}g(0) - \frac{1}{12}g'(0) + \ldots = \frac{\nu}{\tau} - \frac{1}{90} + \mathcal{O}(\tau). \tag{3.17}$$

Substituting into eq. (3.11) we find that the first term in eq. (3.17) cancels the sum over odd reflections (the second term in eq. (3.11)) and that the second term in eq. (3.17) combines with $\mathcal{F}_0$ to give a very simple result,

$$\mathcal{F}_{\text{tot}} = \mathcal{E} - \frac{(V - Sa)\pi^2 T^4}{90(\hbar c)^3}. \tag{3.18}$$

at low temperatures. This has a simple physical interpretation: the typical thermal excitations of the field at low temperature have very long wavelengths, it is hence energetically inconvenient for them to live between the two plates. As a result the only modification of the $T = 0$ result is to exclude from the standard black body free energy the contribution from the volume between the plates. One could imagine measuring this effect as a diminished heat capacity for a stack of conducting plates inside a cavity.

The low temperature result, eq. (3.18), is deceptively simple. Its simplicity obscures an underlying problem with the $T \to 0$ limit. We postpone further discussion until we have explored the temperature dependence of the pressure. Suffice it to say for the moment, that eq. (3.18) probably does not apply to realistic conductor with finite absorption, surface roughness, and other non-ideal characteristics.

3.6.2 Temperature dependence of the pressure

In this section we will obtain the temperature dependence of the pressure within our approximation and apply it to a preliminary study of the sphere and plate case. To begin, we calculate the thermal average of an operator $\mathcal{O}$ quadratic in the real scalar field ϕ. The average of a generic operator $\mathcal{O}$ is given by the trace over a complete set

of eigenstates $|\Psi_\alpha\rangle$ of the Hamiltonian weighted by a Boltzmann factor:

$$\langle \mathcal{O} \rangle_T = \sum_\alpha e^{-\beta \mathcal{E}_\alpha} \langle \Psi_\alpha | \mathcal{O} | \Psi_\alpha \rangle. \tag{3.19}$$

After some algebra we find

$$\begin{aligned} \langle \mathcal{O} \rangle_T &= \sum_j \mathcal{O}_j \langle 2n_j + 1 \rangle_T \\ &= \sum_j \mathcal{O}_j \frac{1 + e^{-\beta E_j}}{1 - e^{-\beta E_j}} \end{aligned} \tag{3.20}$$

where $\langle \rangle_T$ denotes the thermal average, j labels the normal modes ψ_j (cf. Section II), n_j is the occupation number of the mode j and E_j its energy. The quantities $\mathcal{O}_j$ are read from the decomposition of the diagonal part of the operator $\mathcal{O}$ written as $\mathcal{O}_{\text{diag}} = \sum_j \mathcal{O}_j (a_j^\dagger a_j + a_j a_j^\dagger)$ where a_j is the annihilation operator of the mode j.

The $\mathcal{O}_j$ for the pressure can be read easily from the analysis in Section 3.4:

$$P_j = \lim_{x' \to x \in \mathcal{S}} \frac{1}{4E_j} \partial'_{\vec{n}} \partial_{\vec{n}} \psi_j(x') \psi_j(x) \tag{3.21}$$

So we can write the pressure on the plate at non-zero temperature as

$$\begin{aligned} P(x \in \mathcal{S}) &= \lim_{x' \to x} \sum_j \frac{1}{4E_j} \partial'_n \partial_n \psi_j(x') \psi_j(x) \left(\frac{1 + e^{-\beta E_j}}{1 - e^{-\beta E_j}} \right) \\ &= \lim_{x' \to x} \partial'_{\vec{n}} \partial_{\vec{n}} \int_0^\infty dk e^{-k/\Lambda} \frac{k}{2\pi E(k)} \text{Im } G(x', x, k) \left(\frac{1 + e^{-\beta E(k)}}{1 - e^{-\beta E(k)}} \right) \\ &= \text{Im} \int_0^\infty dk e^{-k/\Lambda} \frac{k}{2\pi E(k)} \frac{1}{2} \partial^2_{\vec{n}} \, G(x, x, k) \left(\frac{1 + e^{-\beta E(k)}}{1 - e^{-\beta E(k)}} \right) \end{aligned} \tag{3.22}$$

where we have used Eq. (3.30).

Next we introduce the optical approximation for the propagator and limit ourselves to massless scalars $E(k) = \hbar c k$. The discussion of the divergences parallels that of Section 3.4 and needs not be repeated here. We remove P_0 and P_1 and leave all the finite contributions $r \in \mathcal{R}$. The optical approximation for the pressure exerted by a

massless scalar field reads

$$P(x) = \sum_{r\in\mathcal{R}}(-1)^{n_r}\partial_{\tilde{n}}^2\frac{\Delta_r^{1/2}}{16\pi^2}\left[\frac{1}{\tilde{\beta}}\coth\left(\ell_r/\tilde{\beta}\right)\right]. \tag{3.23}$$

where it is understood that the zeroth and first reflection terms, which contribute to the pressure on each surface individually, but not to the force between surfaces, have been dropped.

Before applying this to the sphere and plate problem, let us again look at the limiting behavior as $T \to \infty$ and $T \to 0$, and draw some conclusions independent of the detailed geometry. First consider $T \to \infty$. The shortest paths in the sum in eq. (3.23) are of order a, the intersurface separation. [Remember that the optical approximation is accurate as long as the important paths are short compared to R, a typical radius of curvature of the surfaces.] At high T we can take the $\tilde{\beta} \to 0$ limit under the sum over reflections since the resulting sum still converges. Therefore low reflections dominate, and we can see, retrospectively, that the high temperature approximation applies when $\tilde{\beta}/a \to 0$. So as $T \to \infty$,

$$P = \sum_{r}(-1)^{n_r}\partial_{\tilde{n}}^2\frac{\Delta_r^{1/2}}{16\pi^2}\left[\frac{1}{\tilde{\beta}} + \mathcal{O}\left(\frac{1}{\tilde{\beta}}e^{-\ell_r/\tilde{\beta}}\right)\right]. \tag{3.24}$$

This limit has been called (it has been previously found for the parallel plates case) the "classical limit" [52, 45, 16], since the final expression for high temperatures, reinserting $\hbar$ and c,

$$P \simeq \sum_{r}(-1)^{n_r}\partial_{\tilde{n}}^2\frac{\Delta_r^{1/2}}{16\pi}T \tag{3.25}$$

is independent of $\hbar$ and c apart from exponentially small terms. This expression amounts in neglecting the 1 in the expression $\langle 2n_j + 1\rangle_T$, corresponding to normal ordering or neglecting the contribution of the vacuum state.

At low temperatures, $\tilde{\beta} \to \infty$, it is not possible to interchange the limit with the

sum. The relevant quantity is $\frac{1}{\tilde{\beta}}\coth(\ell_r/\tilde{\beta})$, which goes like

$$\frac{1}{\tilde{\beta}}\coth\left(\frac{\ell_r}{\tilde{\beta}}\right) = \frac{1}{\ell_r} + \frac{\ell_r}{3\,\tilde{\beta}^2} - \frac{\ell_r^3}{45\,\tilde{\beta}^4} + \mathcal{O}\left(\frac{\ell_r^5}{\tilde{\beta}^4}\right) \tag{3.26}$$

as $\tilde{\beta} \to \infty$. The first term yields the familiar $T = 0$ expression. The others would give divergent contributions because of the factors of ℓ_r in the numerators (even after the inclusion of the enlargement factor Δ_r). Of course the sum over reflections of the *difference*, $\frac{1}{\tilde{\beta}}\coth(\ell_r/\tilde{\beta}) - \frac{1}{\ell_r}$, converges to zero as $\tilde{\beta} \to \infty$, so thermal corrections definitely vanish for any geometry as $T \to 0$ as expected. Once again we relegate more detailed consideration of the $T \to 0$ limit to a later subsection.

Sphere and plate

In this section we calculate the pressure and total force for the configuration of a sphere facing a plane at non-zero temperature within $5p$ reflections. The optical approximation should be accurate if the important paths are short compared to R, the radius of the sphere. On the other hand the thermal corrections to the force are sensitive to paths with lengths of order $\tilde{\beta}$. So we must have $R \gg \tilde{\beta}$ and $R \gg a$ in order to obtain reliable results from the optical approximation. Fortunately this is a region of experimental interest: present experiments use, for example, $a \approx 0.5\mu m$, $R \approx 100\mu m$, and at room temperature, $\tilde{\beta} \approx 2.5\mu m$. In this regime the optical approximation should give a good description of the thermal corrections to the force between perfectly reflective, perfectly smooth conductors.

The expression for the pressure is given by Eq. (3.23), the enlargement factors and lengths are the same as in the $T = 0$ case. By applying Eq. (3.23) to the $1s+3s$ paths we find the results in Figure 3-17. Notice that at high temperatures increasing the temperature essentially scales the whole plot proportionally to T. The force is then linearly dependent on the temperature (this is the 'classical limit' already discussed in Section 5.4.2). More details are given in the caption of Figure 3-17.

A dimensionless function $f(a/R, \tilde{\beta}/R)$ can again be defined by rescaling the total force F to extract the leading term as $a \to 0$. The limiting behavior $a \to 0$ is not

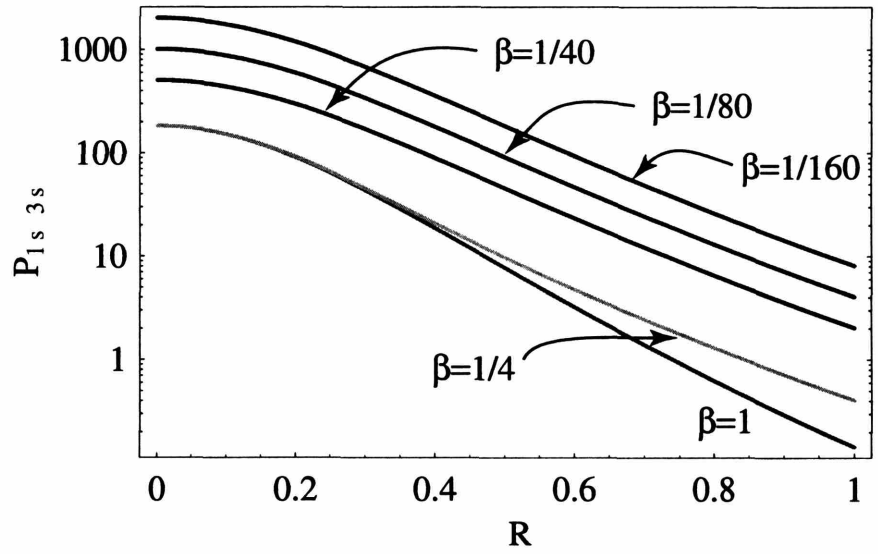

Figure 3-17: The ρ dependence of the $1s + 3s$ contribution to the pressure P_{1s+3s} for the sphere and the plate in units of $\hbar c/R^4$ for various temperatures. Two effects must be noticed. The top 3 curves (in blue) show the high-temperature region where the pressure is proportional to T (notice the logarithmic scale). The two lower curves (in orange and red) show the low-temperature region when increasing the temperature changes the asymptotic behavior of P for large ρ (*i.e.* $\rho > \tilde{\beta}$) while for small ρ the behavior reduces to the zero-temperature limit.

affected by temperature effects so we stick to the old definition for f:

$$F(a,\tilde{\beta},R) = -\frac{\hbar c\pi^3 R}{720a^3} f(a/R,\tilde{\beta}/R). \tag{3.27}$$

In Figure 3-18 we present f (up to 5 reflections) for 5 different values of $\tilde{\beta}/R$ (we choose 1, 1/2, 1/4, 1/8 and 1/16 recognizing that $\tilde{\beta} \sim 1$ strains the limits of our approximations) and varying a. Notice that in a neighborhood of $a/R = 0$, shrinking as $\tilde{\beta}/R$ increases, the function f is very well approximated by the $T = 0$ form, already discussed in Section 3.5.3, $f(a/R) \simeq 1 - 0.1a/R$. It is not useful to study the derivative $A(\tilde{\beta}/R) = \partial f(x,\tilde{\beta})/\partial x$ as $x = a/R \to 0$ since this will take the constant value predicted by the zero temperature analysis, or -0.1 in this approximation, for any value of the temperature we choose.

It is also clear from the previous discussions leading to equation (3.24) that in the opposite regime, for $a/\tilde{\beta} \gg 1$, we must have $F \propto R/a^2\tilde{\beta} = RT/a^2$ (the 'classical limit'). In fact, the first term in the high temperature expansion (3.24) integrated over ρ converges and gives a finite force linear in T. For this problem, the first term in the reflection expansion for high temperatures can even be calculated analytically:

$$F_{1s+3s} = -\hbar c\frac{R}{8\pi a^2\tilde{\beta}} + \mathcal{O}\left(e^{-R/\tilde{\beta}}\right) \simeq -\hbar c\frac{R}{8a^2}T. \tag{3.28}$$

Unfortunately there is no such simple closed expression for higher reflection terms (nor for this first term at arbitrary T). However, if one believes that the rank of contributions is similar to the parallel plates case one should feel safe to say that this truncation captures the optical approximation within a $\zeta(3) - 1 \simeq 20\%$. Hence our statements are at least *qualitatively* correct.

This expression for the force gives a prediction for the function f, defined in Eq. (3.27). At this level of accuracy ($1s + 3s$ reflection) and for $a/\tilde{\beta} > 1$, apart for exponentially small terms in the temperature expansion we have

$$f_{1s+3s} \simeq \frac{90}{\pi^4}\frac{a}{R}\frac{R}{\tilde{\beta}} \tag{3.29}$$

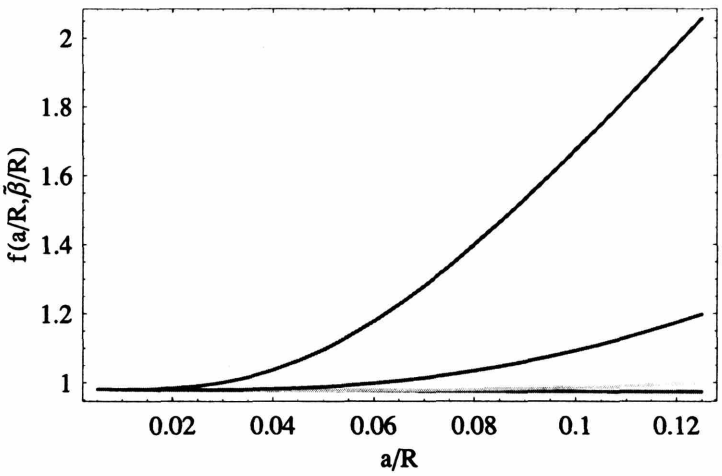

Figure 3-18: The function $f(a/R, \tilde{\beta}/R)$ as a function of a/R for $\tilde{\beta}/R$ (from red to violet or down up) $= 1, 1/2, 1/4, 1/8, 1/16$. $f(0) \simeq 0.98$ since we are summing only up to reflection $5p$. The two lowermost curves, red and orange ($\tilde{\beta} = 1, 1/2$) superpose almost exactly.

which grows linearly in a/R and is (interestingly enough) independent of R. This is evident in Fig. 3-18 for the curves with $\tilde{\beta} = 1/8,\ 1/16$. For higher $\tilde{\beta}$ the linear growth starts at higher values of a not shown in Fig. 3-18. Moreover the exponential accuracy manifests itself in the sudden change of behavior from $f \simeq 1 - 0.1a/R$ to $f \propto a/\tilde{\beta}$.

It is quite easy to extract a universal prediction from this data, whatever the definitive numbers are, after the sum over optical paths is carried to sufficiently high order: *for any non-zero temperature the function $f(a/R)$ will deviate from his zero-temperature behavior at $a > \tilde{\beta} \sim \hbar c/T$. The deviation will be in the upward direction, increasing the attractive force between the bodies.* Eventually, for sufficiently large distances, the high temperature behavior given by eq. (3.25) (or (3.29) for the sphere-plane problem) will be recovered.

3.6.3 Thermal corrections at low temperatures

The preceding examples have made it clear that in the language of the optical approximation, thermal corrections at low temperature arise from very long paths, $\ell_r \sim \tilde{\beta}$. This can be seen from the general form of the free energy, eq. (3.6), or in the attempt

to take the $\tilde{\beta} \to \infty$ limit under the summation in eq. (3.23), which fails because of the expansion, eq. (3.26). Here we examine this non-uniformity more carefully in general and in particular for the parallel plate case, where all the expressions are available. We then attempt to draw some conclusions about the magnitude of corrections at low temperature and the possibility of calculating them reliably in an model that idealizes the behavior of materials.

We return to eq. (3.22), which gives the exact expression for the pressure, and separate out the thermal contribution,

$$P(T) - P(0) \equiv \delta P = \mathrm{Im} \int_0^\infty dk \frac{1}{2\pi} \partial^2_{n'n} \mathcal{G}(x', x, k) 2 \frac{e^{-\beta\hbar ck}}{1 - e^{-\beta\hbar ck}}, \tag{3.30}$$

still exact. Expanding the denominator in a geometric series, we find

$$\delta P = \frac{1}{\pi} \mathrm{Im} \sum_{m=1}^{\infty} \int_0^\infty dk \partial^2_{n'n} \mathcal{G}(x', x, k) e^{-m\beta\hbar ck}. \tag{3.31}$$

Each term in the sum is a Laplace transform of the Greens function. Clearly, as $\beta \to \infty$ the frequencies that dominate this integral are $\propto 1/\beta \sim T$.

What are the low frequency contributions to $\mathcal{G}(x', x, k)$? In the ideal case of infinite, perfectly conducting, parallel plates, there is a gap in the spectrum at low k: $k \geq \frac{\pi}{a}$. However *in realistic situations* the plates are finite and/or curved, the geometry is open, and there is no gap in the spectrum. The low-k part of the spectrum is sensitive to the global geometry, including edges and curvature, and to the low frequency properties of the material. If the conditions are close to the ideal, the contributions to δP from small k may be small. However as $T \to 0$, they dominate. We conclude that the $T \to 0$ behavior of δP cannot be calculated for realistic situations.

The optical approximation does not take account of diffraction, and cannot accurately describe the $T \to 0$ limit. Nevertheless it is interesting to see how it fails, since this sheds light on the problem in general. Substituting the optical expansion for the

Greens function (replacing $\partial^2_{n'n} \to \frac{1}{2}\partial_z^2$ and setting $\hbar = c = 1$) we find

$$\begin{aligned}\delta P &= -\sum_{m=1}^{\infty}\sum_{r\geq 1}\frac{1}{8\pi^2}\partial_z^2\int_0^\infty dk\Delta_r^{1/2}\sin(k\ell_r)e^{-m\beta k} \\ &= -\sum_{m=1}^{\infty}\sum_{r\geq 1}\frac{1}{8\pi^2}\partial_z^2\Delta_r^{1/2}\frac{\ell_r}{m^2\beta^2+\ell_r^2}.\end{aligned} \tag{3.32}$$

The problems with $T \to 0$ are quite apparent: as $\beta \to \infty$ all paths become important.

Next we specialize to parallel plates where $\ell_r = (2ar \pm 2z)$. The derivative can be carried out explicitly. For simplicity we focus on $m = 1$ ($\delta P = \sum_{m=1}^{\infty}\delta P_m$),

$$\delta P_1 = -\frac{2}{\pi^2}\sum_{r=1}^{\infty}\frac{12(ar)^2-\beta^2}{\left(4(ar)^2+\beta^2\right)^3}, \tag{3.33}$$

which can be rewritten using the variable $\tau = 2\pi a/\beta$ introduced earlier,

$$\delta P_1 = -\frac{2\pi^2}{\beta^4}\sum_{r=1}^{\infty}\frac{3\tau^2r^2-\pi^2}{(\tau^2r^2+\pi^2)^3}. \tag{3.34}$$

The sum can be performed, giving

$$\delta P_1 = -\frac{1}{\pi^2}\left(\frac{1}{\beta^4}-\frac{\pi^3}{8a^3\beta}\coth\left(\frac{\pi\beta}{2a}\right)\operatorname{csch}^2\left(\frac{\pi\beta}{2a}\right)\right). \tag{3.35}$$

The second term in brackets is exponentially small as $\beta \to \infty$. If we ignore it, restore the m-dependence, and sum over m, we obtain

$$\delta P = -\frac{\pi^2}{90\beta^4}. \tag{3.36}$$

which agrees with our earlier calculation, as it must.

However eq. (3.34) allows us to study the convergence of the sum over reflections as $\beta \to \infty$. Instead of performing the sum analytically, we sum up to some $r_{\max} \equiv X$. Since $\tau \to 0$, we can once again use Euler-Maclaurin, to rewrite the sum over r as

$$\delta P_1 = -\frac{2}{\pi^2}\frac{1}{\beta^4}\left[\frac{1}{2}-\frac{X}{(1+\tau^2X^2/\pi^2)^2}+\frac{1}{2}\frac{3\tau^2X^2/\pi^2-1}{(1+\tau^2X^2/\pi^2)^3}+\ldots\right]. \tag{3.37}$$

where the omitted terms are higher Euler-Maclaurin contributions that are unimportant as $\beta \to \infty$ (*i.e.* $\tau \to 0$).

If the upper limit on the sum, X, is taken to ∞, only the first term, 1/2, survives and gives the expected result. The question is: How large must X be before the limiting behavior set in? Dropping the third term in eq. (3.37), which is subdominant, we can rewrite δP_1 as

$$\delta P_1 = -\frac{2}{\pi^2\beta^4}\left[\frac{1}{2} - \frac{X}{(1+X^2\tau^2/\pi^2)^2}\right] = -\frac{2}{\pi^2\beta^4}\left[\frac{1}{2} + \frac{1}{\tau}f(\tau X)\right]. \tag{3.38}$$

The function $f(z)$ is negative definite and has a minimum at $z = 1/2\sqrt{3} \simeq 0.29$ where it takes the value $-3^{3/2}/32 \simeq -0.16$. So in order the result Eq. (3.36) to be valid we must include $X \gg X_c = \pi/\sqrt{3}\tau$ terms in the sum. For example in a typical experimental situation we have $a = 0.5\mu m$ and $T = 300K$ so $\beta = 8\mu m$, $\tau = 8/\pi$ and $X_c = 8/\sqrt{3} = 4.6$. In this case it is necessary to go to $X \sim 20$ before the contribution of $|f(\tau X)/\tau|$ is smaller than 1/2. This means paths with ~ 40 reflections and path lengths of order $20\mu m$. With 40 chances to sample the surface dynamics of the material and paths of $20\mu m$ available to wander away from the parallel plate regime, the idealizations behind the standard parallel plates calculation must be called into question.

It must be said however that in the modern experiments the temperature corrections are at most of the order of a few percent at $a \sim 1\mu m$ and vanish when $a \to 0$. Nonetheless we want to point out that there is a conceptual difference between formulations based on the infinite parallel plates approximation, extended to curved geometries by means of the PFA, and a derivation (like ours) in which the curvature is inserted *ab initio*. The thermal and curvature scales interplay in a way that the usual derivations [16, 24] could not possibly capture, giving rise to different power law corrections in a/β. It is worth reminding the reader that the usual numerical estimates of thermal corrections are based on the infinite parallel plates power law $(a/\beta)^4$. A smaller power like $(a/\beta)^2$ would give a much bigger upper bound.

To summarize: temperature corrections are small at small T, but the existing

methods of calculating them, including both our optical approximation and the traditional parallel plates idealization, cannot be trusted to give a reliable estimate of the T-dependence at small T.

3.7 Preliminary Conclusions

In the first part of the chapter (sections 3.1-3.4) we have proposed a new method for calculating approximately Casimir energies between conductors in generic geometries. We use a stationary phase approximation imported from studies of wave optics that we have therefore named the "optical approximation". In this chapter we have outlined the derivation and applied it to three examples: the canonical example of parallel plates; the experimentally relevant situation of a sphere facing a plane; and the "Casimir pendulum", *i.e.* a conducting plate free to oscillate above an infinite plate, where the calculations can be performed analytically. In all of the above examples (except for parallel plates, where our result coincides with Casimir solution) the agreement with the Proximity Force Approximation is only to the leading order in the small distances expansion. The first order correction is found to be different. This is of particular importance in the example of the sphere and the plane because the first order correction in a/R (a is the distance sphere-plate and R is the radius of the sphere) will soon be measured by new precision experiments [25]. The optical approximation turns the Casimir sum over modes into a sum over topologically different paths, and from this point of view can be compared with the Poisson summation formula, which has proved useful to derive semiclassical uniform expansions for very diverse problems [20, 36]. In the case of the Casimir energy, replacing the usual highly divergent sum over modes by a sum over topologically distinct optical paths has two, very significant advantages: first, we have been able to show that the divergences in the Casimir energy are contained in contributions of very simple, one-reflection paths and can be easily and unequivocally regulated and discarded; and second, the convergence of the sum over paths is very rapid. Instead of requiring an infinite number of eigenvalues with exquisite precision one needs but a few path contributions, calcu-

lated with little numerical effort, to give a very good approximation to the Casimir energy for important geometries. "Semiclassical" methods have been used previously in the study of Casimir effects and the connection between the oscillating part of the density of states and the finite part of the Casimir energy has been pointed out before (see for example [15]). Our analysis shares with those the idea of shifting attention to approximations and to properties of the Helmholtz propagator. We have shown however that in order to obtain a correct low curvature approximation one has to use a uniform approximation of the kind we proposed here. There is plenty of room to improve the approximation presented here, especially when the connection with Balian and Bloch's multiple reflection expansion is made explicit. In particular it is intriguing that the Casimir energy for the sphere-plane problem is such a well-defined problem in a single variable, namely $x = a/R$ whose limiting values for $x \ll 1$ and $x \gg 1$ are famous [1, 29]. One can hope that an analytic solution or an approximation good for the entire range of x-values should be relatively easy to find. On the contrary it is an incredibly difficult problem and nobody has succeeded in finding such an exact solution or a valid approximation. In this work we have discussed the case of perfectly reflecting bodies (but for the need of a cutoff in regulating divergent terms). One can think of making a semiclassical analysis for arbitrary background fields or boundary conditions mimicking real dielectrics[39]. Such an analysis, not so relevant for the case of a scalar field, follows naturally after the discussion of the electromagnetic field and hence will be presented elsewhere.

In the second part of this chapter (sections 3.5 and following) we have shown how to adapt the optical approximation to the study of local observables. We have illustrated the method by studying the pressure, but the method applies as well to other components of the stress tensor, to charge densities, or any quantity that can be written in terms of the single particle Greens function. The advantage of the optical approximation is to extend the study of these local observables to novel geometries. In particular we developed an expression for the Casimir pressure on the bodies and applied our main result Eq. (3.31) to the study of three important examples: parallel plates, the Casimir pendulum and a sphere opposite a plate.

We have also shown how to calculate within this approximation scheme, thermodynamic quantities and thermal corrections to the pressure in the general case and applied our results to the example of parallel plates (retrieving the known results) and to the case of a sphere opposite a plate. Along the way we have given a proof of the "classical limit" of Casimir force for any geometry (within our approximation), *i.e.* the fact that Casimir forces at high temperatures are proportional to the temperature and independent of $\hbar$, a fact that previously was known only for parallel plates.

Finally, we argued that all known methods of computing the temperature dependence of the Casimir effect are suspect as $T \longrightarrow 0$.

Chapter 4

Casimir Effect for small scatterers

In this chapter I will show how to calculate Casimir forces between perfectly reflecting small bodies. The result is obtained by a proper mathematical definition of what a infinitely small scatterer is. This turns out to coincide with retaining only the only the lowest order term in the expansion of the scattering matrix in partial waves.

Since in this work we will be concerned only with scalar fields the problem is in some respects different from the electromagnetic field one. An electromagnetic field impinging on a metallic body can induce only dipole (or p-wave) scattering while the scalar field does induce monopole (or s-wave) scattering as well, since the coupling to matter is quite different. This affects the force sensibly and our results cannot be applied straightforwardly to the case of real atoms.

However the problem is interesting in itself and worth studying, despite the absence of massless scalar fields in nature. One of the surprises that spun from this analysis is that the theory has a tachionic mode when the scatterers are placed at a sufficiently short distance from each other. This feature is not present in the electromagnetic theory.

4.1 Introduction

Point-like interactions have provided a remarkably useful idealization for many situations in physics. In the context of scattering theory the concept of a point-like

scatterer was introduced in 1934 by Bethe and Peierls [54]. Fermi [55] used and refined their results to describe the motion of neutrons in hydrogenated substances (such as paraffin) by introducing what is now known as the 'Fermi pseudopotential'. The idea is that when the scattering potential is concentrated on a very small scale r_0 (in the case studied by Fermi the range was that of nuclear interactions compared to the distances between the atoms) but nonetheless its influence on the motion cannot be neglected, one can characterize the scattering in a simple and efficient way by means of a few quantities like the scattering length, finite in the $r_0 \to 0$ limit. The problem of 'how to separate the scales' in the Schrödinger equation triggered by those 1930's papers was addressed and elegantly solved over the years at different levels of formalism [58, 59, 57, 60, 56]. The key to the solution relies in a proper definition of a 'delta-function interaction' in dimensions greater than 1.

Of course this chapter will not be dealing with quantum mechanical scattering within matter, which is from many points of view a solved problem. The problem of 'separation of scales' however arises urgently in modern quantum field theory if stated as: "What is the quantum field theory response on length-scales L to a disturbance concentrated on a length scale $r_0 \ll L$?" How does quantum field theory respond to topological defects and singularities, in particular of the metric? Once formalized in proper mathematical terms the two problems look much closer than one would think.

The Casimir effect falls in this class of problems. The penetration length (r_0) of the electromagnetic field inside conductors is much smaller than the distance (L) between the conductors, which sets the scale of the experimentally measured force. We are interested in studying the dynamics of the conductors on the larger scale L by integrating out the electromagnetic field. This motivates the nomenclature 'Casimir effect' for a much wider set of problems than Casimir's original one.

Another example: in any candidate theory of the quantum geometry of space-time the problem of dealing with point-like singularities will inevitably arise. Remember for example that the Ricci scalar for a point-like particle (like Schwartzschild's solution) is a delta-function centered on the position of the particle. Quadratic fluctuations of a non minimally-coupled scalar (or of the metric) have hence a delta-function term

in their Lagrangian. The effect of such a term must be considered together with the other known effects of the black hole metric. It is then of paramount importance to analyze the problem of how one or more concentrated singularities influence the spectrum and low-energy behavior of the fluctuations of the field.

Analogous problems arise in condensed matter, quantum field theory and string theory since localized disturbances appear in all these theories, essentially only the names given to them being different (defects, domain walls, concentrated Aharonov-Bohm fluxes and branes to name some). With this in mind we will set-up the problem in very general terms and even though not all the details map one-to-one on specific examples the main results will apply to a wide class of examples.

The main results of this chapter are two. First, I will show that quantum fluctuations of a scalar field ϕ generate attractive forces between localized defects in the very same way Casimir forces act between metallic bodies. I calculate this force for an arbitrary number of defects with co-dimension[1] 1, 2 and 3 (see Table I). Note that previously the Casimir effect has been analyzed only for co-dimension 1. The main result of this chapter is Eq. (4.22), which gives the interaction energy as a function of the scattering lengths of the defects and their relative separations. For co-dimension $d \geq 4$ the force disappears, as required by the properties of the self-adjoint extensions of the Laplace operator on the punctured $\mathbf{R}^d$ (see [61], Chap. X).

Second, in the presence of two or more of these defects (of co-dimension > 1) the vacuum $\phi = 0$ is hopelessly unstable and a localized tachyon mode is formed when the defects approach closer than a critical distance. At this critical distance the attractive force diverges. I calculate the wave function of the tachyon and show that it leads to condensation of the bulk field ϕ to a vacuum expectation value $\overline{\phi}(x) \neq 0$ —but only in a limited region of space.

The consequences of these observations for some models will be discussed in Section 4.6.

[1]Co-dimension is the number of dimensions transverse to a manifold. For example a point in 2 dimensions, a line in 3 dimensions and a surface in 4 dimensions all have co-dimension 2.

Codim \ Dim	$\mathbb{R}^1$	$\mathbb{R}^2$	$\mathbb{R}^3$	$\mathbb{R}^4$
Casimir: 1	point	line	plane	hyperplane
2		**point**	**line**	**plane**
3			**point**	**line**
↓ Trivial: 4				point

Table 4.1: Flat manifolds divided according to dimension and co-dimension. The first line is the well-known Casimir problem, from the fourth line down the perturbation is 'invisible' to fluctuations. In this chapter we will be dealing with manifolds in lines 2 and 3.

4.2 The interaction energy

In this Section we will calculate the effective action [47] of a scalar field coupled quadratically to a static configuration of defects. The effective action S_{eff} and Casimir energy $\mathcal{E}$ are proportional to each other

$$S_{\text{eff}} = -T\mathcal{E}, \tag{4.1}$$

where T is the interaction time. In the following we will be interested in the Casimir energy of the problem.

We will see that the part of the Casimir energy responsible for the interaction between the defects is a cutoff-independent quantity, meaning that the separation of scales can be performed effectively in this quantum field theory.

We will consider the following action for the scalar field in $d+1$ dimensions ($\hbar = c = 1$):

$$S_\phi = \int d^d x dt \, \frac{1}{2}(\partial\phi)^2 - \frac{1}{2}\left(m^2 + \sum_i^N \mu_i \delta(x - a_i)\right)\phi^2. \tag{4.2}$$

Here δ is the $d-$dimensional Dirac's delta-function, mimicking the concentrated disturbance on the field, μ_i are constants, meaning that they do not depend on the field ϕ, but in general they can depend functionally on other fields living on the

defect.[2] The methods of [57] will be used in order to define these δ's correctly. In this section, in order to keep things simple we restrict our attention to points in 1, 2 and 3 dimensions. We will add an arbitrary number of flat directions in Section 4.5, hence fulfilling our promise of studying co-dimensions 1, 2 and 3.

Actions like Eq. (4.2) arise in different contexts. For example consider the case of a scalar bulk field ϕ coupled with N branes in curved or flat space (curvature can be easily included in Eq. (4.2)); or the case of a cosmic string (again the curvature outside the string must be considered); or the case of electrons coupled with Aharonov-Bohm fluxes (in this case one has fermions rather than bosons but, after squaring the Dirac equation, the analysis is analogous [60]). All these examples can be studied with the formalism introduced in this chapter, so in full generality we will study the quantum fluctuations of the action Eq. (4.2).

Some features of the Eq. (4.2) with only one delta function and constant m have been studied before, for example in connection with cosmic strings scenarios [56, 62, 63]. The action (4.2) in one dimension with a single delta and a space-dependent mass term $m^2 = m^2(x)$ has been studied in [50].[3] In this chapter we will consider the situation where a generic number of defects are present in $d \geq 1$ and m^2 is a constant. We will see that the situation will be different from that depicted in Ref.s [56, 62, 50] and unexpected physics is found. Moreover the generalization to x-dependent m^2 can be easily achieved by means of the techniques of Ref. [50] and we will not comment on it in this chapter. The inclusion of any other term in the action (4.2) describing the dynamics of the surface itself would not affect our calculations. We consider the positions of the defects a_i fixed and obtain an effective action. In the usual way this action can be used to describe adiabatically moving $a_i(t)$ (i.e. if the velocities $|\dot{a}_{ij}| \ll c$).

The forces between the defects can be calculated by taking the derivatives of the Casimir energy $\mathcal{E}$ with respect to its arguments $\{a_i\}$. It will turn out that in general

[2]The μ_i's are also called 'brane tensions'.

[3]The scale of variation of m^2 should be of the order of the 'long scale' L. The purpose of this chapter is to integrate out the physics at momenta $> 1/r_0$ which is symbolized by the delta functions in Eq. (4.2).

the forces are not additive, i.e. $\mathcal{E}$ is not a superposition of terms depending only on the relative distances $a_{ij} \equiv |a_i - a_j|$.

We use the following integral representation of the zero-point energy of the scalar field ϕ,

$$\mathcal{E} = \frac{1}{2}\int_0^\Lambda dE\rho(E)\sqrt{E}, \tag{4.3}$$

where Λ is a cutoff and ρ is the spectral density of the Hamiltonian operator H

$$H = -\nabla^2 + m^2 + \sum_{i=1}^{N}\mu_i\delta(x - a_i). \tag{4.4}$$

Define also the *unperturbed* hamiltonian H_0 as

$$H_0 = -\nabla^2 + m^2. \tag{4.5}$$

Equation (4.3) will look more familiar if the replacement $E \to \omega^2$ is done, and $\hbar$'s are restored. One can obtain the spectral density $\rho(E)$ as a functional of the propagator $G(E) = 1/(H - E)$ as

$$\rho(E) = \frac{1}{\pi}\lim_{\epsilon\to 0^+}\mathrm{Im}\,\mathrm{Tr}G(E + i\epsilon). \tag{4.6}$$

In the following we will often write $E + i0^+$ for $E + i\epsilon$ when $\epsilon \to 0^+$.

The propagator, $\mathcal{G}(x', x; E) \equiv \langle x'|G(E)|x\rangle$ satisfies the Schrödinger equation

$$(-\nabla'^2 + m^2 + \sum_{i=1}^{N}\mu_i\delta(x' - a_i) - E)\mathcal{G}(x', x; E) = \delta(x' - x), \tag{4.7}$$

and $\mathcal{G}_0 \equiv \langle x'|G_0(E)|x\rangle$ satisfies the analogous equation without δ's on the left-hand side. For m constant (which we will assume unless explicitly stated) and $\mathrm{Im}E > 0$

we have[4]

$$\mathcal{G}_0(x',x;E) = \begin{cases} \frac{i}{2\sqrt{E-m^2}} e^{i\sqrt{E-m^2}|x'-x|} & \text{if } d=1 \\ \frac{i}{4} H_0^{(1)}(\sqrt{E-m^2}|x'-x|) & \text{if } d=2 \\ \frac{e^{i\sqrt{E-m^2}|x'-x|}}{4\pi|x'-x|} & \text{if } d=3, \end{cases} \tag{4.8}$$

where $H_0^{(1)}$ is Hankel's function of first kind of order 0.

For $d = 1$ the problem is that of a scalar field on the line $\mathbb{R}$ in the background of a stack of δ-functions centered on $x = \{a_i\}$ [64]. If we assume $\mu_i > 0$ they will attract each other, like metallic plates do via the Casimir effect. These forces are not confining and no new physics is obtained with the generalization obtained by adding n transverse directions. This is the usual Casimir problem. We will see how the situation changes dramatically when $d > 1$.

To see how the solution for $\mathcal{G}$ is obtained, consider first the case with a single delta function with strength $\mu_1 = \mu$, placed at $x = a$. By solving the Lippman-Schwinger equation [58, 50, 57] one finds

$$\mathcal{G}(x',x;E) = \mathcal{G}_0(x',x;E) + \frac{1}{\alpha - \mathcal{G}_0(a,a;E)} \mathcal{G}_0(x',a;E)\mathcal{G}_0(a,x;E), \tag{4.9}$$

where $\alpha = -1/\mu$. This solution is perfectly good in $d = 1$ and was the basis of the analysis in [50] for non-constant m^2. For $d > 1$ it however suffers from a serious problem since $\mathcal{G}(a, a + r; E) \to \infty$ when the point splitting regulator $r \equiv |r| \to 0$. One can reabsorb this divergence [58] in a redefinition of α to obtain a finite result

$$\mathcal{G}(x',x;E) = \mathcal{G}_0(x',x;E) + \frac{1}{\alpha_r - B^{(d)}(E)} \mathcal{G}_0(x',a;E)\mathcal{G}_0(a,x;E), \tag{4.10}$$

where

$$B^{(d)} = \begin{cases} \frac{i}{2\sqrt{E-m^2}} & \text{if } d=1 \\ -\frac{1}{2\pi} \ln\left(\frac{\sqrt{E-m^2}}{iM}\right) & \text{if } d=2 \\ \frac{i\sqrt{E-m^2}}{4\pi} & \text{if } d=3, \end{cases} \tag{4.11}$$

[4]In the following we will not use any special notation for vectors and we will indicate with $|x|$ the norm of a vector in 1,2 and 3 dimensions.

where for $d = 2$ it has been necessary to introduce an arbitrary mass scale M which stays finite when the point splitting regulator $r \to 0$. So α must be redefined such that when $r \to 0$

$$\alpha_r = \begin{cases} \alpha & \text{if } d = 1 \\ \alpha + \frac{1}{2\pi} \ln Mr & \text{if } d = 2 \\ \alpha - \frac{1}{4\pi r} & \text{if } d = 3, \end{cases} \tag{4.12}$$

so the 'renormalized' α_r stays finite. It is clear from this equation that one needs a *positive* divergent α to reabsorb the negative divergencies when $r \to 0$. Large positive α mean *negative* very small μ (since $\alpha = -1/\mu$). A small negative μ corresponds to a weakly attractive potential. Hence the point-like scatterer limit can be thought of as the limit of a concentrated attractive potential, zero outside a sphere of radius r_0, with at most one bound state whose energy stays finite when $r_0 \to 0$ [58, 59]. For $d = 2$ any attractive potential has at least a bound state and so we always find a bound state also for $r_0 \to 0$ (for $d = 2$ the dependence of α on M is reminiscent of a renormalization group flow [60, 62, 65]); for $d = 3$ the bound state can be real or 'virtual' (i.e. a pole of the propagator $G(E)$ located on the second Riemann sheet) its energy being finite in the limit $r_0 \to 0$. The scattering length is (both for $d = 2$ and 3) a function of α and is hence finite in the $r_0 \to 0$ limit.

Another interpretation of this results comes from the theory of self-adjoint extensions of symmetric operators [59, 57]. Here the 'renormalized' α_r corresponds to a choice of self-adjoint extension for the Laplacian operator $-\Delta$ on the punctured $\mathbb{R}^d$ [59]. In $\mathbb{R}^2$ the self-adjoint extensions are not positive definite, meaning that they all have at least one (but it turns out there is only one) negative eigenvalue. This corresponds to the bound state described in the paragraph above. In the punctured $\mathbb{R}^3$ the self-adjoint extensions of $-\Delta$ can be either positive semi-definite (with a virtual state on the second Riemann sheet) or not (due to the existence of a single real and negative eigenvalue).

The propagator with N deltas at positions $\{a_i\}$, $i = 1, ..., N$, and $1 \leq d \leq 3$ can

be found [57]:

$$\mathcal{G}(x', x; E) = \mathcal{G}_0(x', x; E) + \sum_{i,j=1}^{N} (\Gamma^{-1})_{ij} \mathcal{G}_0(x', a_i; E) \mathcal{G}_0(a_j, x; E). \tag{4.13}$$

The matrix Γ is defined as (from now on we drop the subscript r on the α_r's)

$$\Gamma_{ij} = \left(\alpha_i - B^{(d)}(E)\right) \delta_{ij} - \widetilde{\mathcal{G}}_0(a_i, a_j; E), \tag{4.14}$$

where

$$\widetilde{\mathcal{G}}_0(a_i, a_j; E) \;=\; \begin{cases} 0 & \text{if } i = j \\ \mathcal{G}_0(a_i, a_j; E) & \text{if } i \neq j. \end{cases} \tag{4.15}$$

It is now possible to explain why we limited our discussion to $d \leq 3$. The reason is that looking at the Laplacian Δ on the punctured $\mathbb{R}^4$ one realizes that this operator is essentially self-adjoint [57, 61], meaning that it has a unique self-adjoint extension: the trivial one. The 4-dimensional delta function is 'too small' a perturbation to be seen by the Laplacian. What does go wrong in the renormalization procedure? The propagator in $d = 4$ is ($|x' - x| \equiv r$)

$$\mathcal{G}_0(x', x; E) \;=\; \frac{i\sqrt{E - m^2}}{8\pi r} H_1^{(1)}(\sqrt{E - m^2}\, r) \tag{4.16}$$

$$\sim\; \frac{i}{8\pi} \left(\frac{1}{r^2} + \sqrt{E - m^2} \ln r + \mathcal{O}(1) \right) \quad \text{if } r \sim 0 \tag{4.17}$$

so we cannot choose α in an E-independent way (because of the $\sqrt{E - m^2} \ln r$ term) to remove completely the divergences as we did before. The low-energy limit of a 4−dimensional concentrated potential is hence trivial and we will not discuss this problem anymore.

Having solved for the propagator we can find the density of states ρ simply by

taking the trace and the imaginary part. The result[5] is [50]

$$\rho(E) = \rho_0(E) - \frac{1}{\pi}\mathrm{Im}\frac{\partial}{\partial E}\ln\det\Gamma(E+i0^+,\{a\}), \tag{4.19}$$

where $\rho_0 = \pi^{-1}\mathrm{Im}\mathrm{Tr}G_0$ and the determinant of Γ is simply the determinant over the matrix indices ij.

The term ρ_0 in (4.19) is independent of the presence, strengths α_i and relative positions of the delta functions and we will neglect it in the following. The second term on the right-hand side of Eq. (4.19), can be used to calculate the Casimir energy as a function of the positions and strengths α of the scatterers:

$$\mathcal{E} = -\frac{1}{2\pi}\mathrm{Im}\int_0^\Lambda dE\sqrt{E}\frac{\partial}{\partial E}\ln\det\Gamma(E+i0^+,\{a\}). \tag{4.20}$$

The interaction part of this energy is obtained by subtracting from Eq. (4.20) the same quantity calculated with all the $L_{ij} = |a_i - a_j| \to \infty$. In this limit Γ becomes diagonal (considering that $\mathrm{Im}E > 0$) and the energy (4.20) becomes a sum of self-energies of isolated objects.

After performing the subtraction of the self-energies, the interaction energy can be written as

$$\mathcal{E} = -\frac{1}{2\pi}\mathrm{Im}\int_0^\Lambda dE\sqrt{E}\frac{\partial}{\partial E}\ln\frac{\det\Gamma(E+i0^+,\{a\})}{\det\Gamma(E+i0^+,\infty)}. \tag{4.21}$$

We keep using $\mathcal{E}$ to indicate the interaction energy, confident that this will not generate any confusion, since we will no longer be interested in the total energy.

The integrand in Eq. (4.21) falls exponentially fast on the semicircle $|E| \to \infty$ of the complex E plane[6] which allows us to integrate by parts, Wick-rotate to the

[5]The only algebraic identity worth of notice is the fact that

$$\sum_{ij}(\Gamma)^{-1}_{ij}\frac{\partial}{\partial E}\mathcal{G}_0(a_i,a_j;E) = -\frac{\partial}{\partial E}\mathrm{Tr}\ln\Gamma. \tag{4.18}$$

[6]In particular it goes to zero like $e^{-2\sin(\frac{\theta}{2})\sqrt{|E|}L}$ on the ray $E = |E|e^{i\theta}$, $\pi > \theta > 0$, where $L = \min|a_i - a_j|$ for any d.

negative E axis[7] and send the cutoff $\Lambda \to \infty$. We can moreover remove the Im because all the quantities are real and positive on the negative real E axis (since the propagator $\mathcal{G}_0$ is real and positive for E real and below the spectrum) except for $\sqrt{-E+i0^+} = i\sqrt{E}$.

This leads us to a final, compact expression for $\mathcal{E}$

$$\mathcal{E} = \frac{1}{4\pi}\int_0^\infty \frac{dE}{\sqrt{E}} \ln \frac{\det \Gamma(-E,\{a\})}{\det \Gamma(-E,\infty)}. \tag{4.22}$$

This is the main result of this chapter and together with the definition of Γ, Eq. (4.14), can be used to calculate the interaction energy of point-like scatterers due to fluctuations of the field ϕ. In the rest of this chapter we present several examples of the applications of this formula.

4.3 Examples

As a first example and a check for our result, Eq. (4.22), let us calculate the well-known interaction energy between two delta functions at distance L, in 1 dimension (we assume $\alpha_1 = \alpha_2 \equiv \alpha < 0$):

$$\mathcal{E} = \frac{1}{4\pi}\int_0^\infty \frac{dE}{\sqrt{E}} \ln\left(1 - \frac{e^{-2L\sqrt{E+m^2}}}{(1-2\alpha\sqrt{E+m^2})^2}\right). \tag{4.23}$$

This formula reproduces the usual results for the Casimir energy of two penetrable plates in 1 dimension [66].

As another example in $d = 1$ consider the case of three repulsive delta functions ($\alpha_i = -1$ for $i = 1,2,3$). The interaction energy can be calculated with the ease with which one can take a determinant of a 3x3 matrix. The result is plotted in Fig. 4-1 as a function of the position x of one of the three deltas while the other two are held fixed at $x = 0$ and $x = 5$. The interaction energy is not additive: the interaction energy of N semi-penetrable plates does not split into a sum of $N(N-1)/2$ terms due

[7] During the Wick rotation we do not pick any pole contribution on the positive imaginary semi-plane of the first Riemann sheet because the total Hamiltonian Eq. (4.4) is self-adjoint.

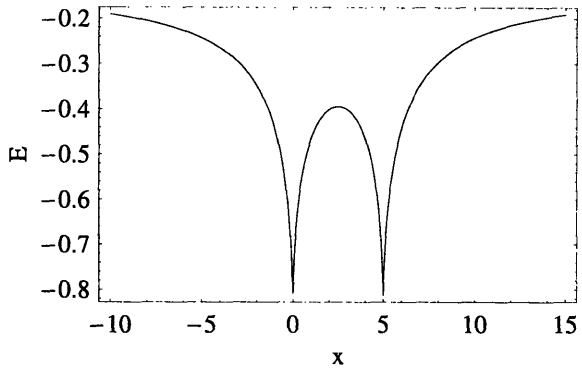

Figure 4-1: Interaction energy, in arbitrary units, for three delta functions on the line as a function of the position x of one of them and $m = 0$. $\alpha = -1$ for all three deltas, one delta is held fixed at $x = 0$, another at $x = 5$.

to pairwise interactions. Rather, by expanding the logarithm a *reflection expansion* is obtained in the spirit of Ref. [4].

Before calculating the interaction energy for 2 or more deltas in $d > 1$ it is instructive to look at the case of a single delta function centered in $x = 0$, to introduce some properties of the bound state of a single delta.

Consider $d = 3$. The propagator is (for Im $E > 0$)

$$\mathcal{G}(x', x; E) = \frac{e^{i|x'-x|\sqrt{E-m^2}}}{4\pi|x'-x|} + \frac{1}{\alpha - \frac{i\sqrt{E-m^2}}{4\pi}} \frac{e^{i(|x'|+|x|)\sqrt{E-m^2}}}{16\pi^2|x'||x|}. \tag{4.24}$$

There is evidently a pole at $E = E_0$ such that $\sqrt{E_0 - m^2} = -i4\pi\alpha$. For $\alpha < 0$ this is a real bound state at $E_0 = m^2 - 16\pi^2\alpha^2$ and the wave function ψ_0 of this bound state is obtained by noticing that

$$\mathcal{G} \sim \frac{1}{E_0 - E}\psi_0^*(x')\psi_0(x), \tag{4.25}$$

for E near the pole E_0. We hence expand (4.24) about E_0 to find

$$\psi_0(x) = \frac{\sqrt{2(-\alpha)}}{|x|}e^{-4\pi(-\alpha)|x|}. \tag{4.26}$$

For $\alpha > 0$, on the contrary, the pole is on the 2^{nd} Riemann sheet and hence is a

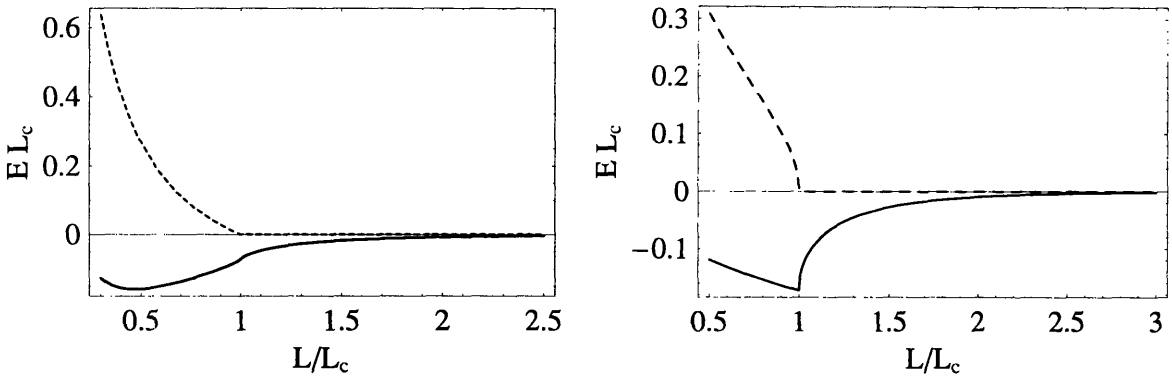

Figure 4-2: Interaction energy $\mathcal{E}$ (the continuous line is $\Re\mathcal{E}$ and the dashed line is $-\mathrm{Im}\mathcal{E}$) in units of $1/L_c$, for two delta functions as a function of their distance L. a) The $\mathbb{R}^3$ case with $m = 0$. b) The $\mathbb{R}^2$ case with $m/M = 2$.

virtual state and does not belong to the spectrum of H. Whether this pole is real or virtual, physically it represents the s-wave scattering over a concentrated attractive potential. $1/\alpha$ is indeed proportional to the scattering length in the s-wave channel [58]. The s-wave is the only contribution surviving in the limit when the scatterer is small compared to the wavelength $1/\sqrt{E-m^2}$.

We have to require the spectrum of H to be contained in the positive real axis for the vacuum, $\phi = 0$, of our field theory to be stable. So if $\alpha < 0$ we have to choose $m > 4\pi(-\alpha)$. If $\alpha > 0$ any choice of m, in particular $m = 0$, is enough to ensure the stability of the $\phi = 0$ vacuum.[8]

considering $d = 3$ further, let us now calculate the interaction energy between two identical delta functions with $\alpha_1 = \alpha_2 = \alpha > 0$ (so, according to the previous paragraph no bound state exists for isolated scatterers) at a distance $|a_1 - a_2| = L$. After the Wick rotation and defining $k \equiv \sqrt{E}$ we obtain

$$\mathcal{E} = \frac{1}{2\pi}\int_0^\infty dk \ln\left(1 - \frac{e^{-2L\sqrt{k^2+m^2}}}{L^2\left(4\pi\alpha + \sqrt{k^2+m^2}\right)^2}\right). \tag{4.27}$$

It is not difficult to see that it exists a critical distance L_c, being the positive

[8]It is worth noting that the opposite choice for the sign of α is needed to avoid a bound state in the $d = 1$ case.

solution of the equation

$$L_c e^{mL_c} = \frac{1}{4\pi\alpha + m}, \tag{4.28}$$

such that if $L < L_c$ the argument of the logarithm in Eq. (4.27) becomes negative for sufficiently small k and we get a negative imaginary part in the Casimir energy. A negative imaginary part of $\mathcal{E}$ means, as usual, an instability of the $\phi = 0$ vacuum in the presence of the two δ's. In fact, by studying the eigenvalues of the matrix Γ one can see that for $L < L_c$ the spectrum of H has a bound state with negative E, and since $E = \omega^2$ this is a clear indication for the existence of a tachyon. We will return on the implications of this instability for the low-energy physics.

The force $\mathcal{F} \equiv -\partial\mathcal{E}/\partial L$, always attractive and central, diverges logarithmically at the critical length L_c. For $m = 0$ and $(L - L_c)/L_c \ll 1$ one finds:

$$\mathcal{F} \simeq -\frac{1}{4\pi L^2} \ln\left(\frac{L_c}{L - L_c}\right). \tag{4.29}$$

The long-distance behavior, $L \gg L_c$, of the force depends on the mass of the boson ϕ. For $m > 0$ the potential between the two δ's decreases exponentially. For $m = 0$, instead, a power-law tail is obtained:

$$\mathcal{E} \simeq -\frac{L_c^4}{4\pi L^5}. \tag{4.30}$$

This $1/L^5$ law is stronger than the Casimir-Polder law (induced polarization interaction [1]) which falls like $1/L^7$. This means that we should not think of these delta functions as mimicking polarizable molecules or metallic particles. Indeed, to correctly describe a metallic sphere of radius R, surface Σ and penetration depth r_0 one should rather assume that $r_0 \ll R$ adding hence to H_0 in Eq. (4.5) a potential $V(x) = \int_\Sigma d^2y \mu\delta^{(3)}(x - y) = \mu\delta(r - R)$ and send $\mu \to \infty$ *before* sending $R \to 0$. This clearly is a different limit than the one we are describing here.

Now that we have discussed the divergences associated with Γ, its renormalization and we know about the existence of vacuum instabilities related to negative E bound states of the hamiltonian H we are ready to tackle the two dimensional case where

all these complications arise at the same time.

The free propagator is $\mathcal{G}_0(x', x; E) = \frac{i}{4} H_0^{(1)}(\sqrt{E - m^2}|x' - x|)$ if $\mathrm{Im}E > 0$. Notice that even for a single delta no choice of α eliminates the bound state. There will always be at least one bound state with energy $E_0 = m^2 - M^2 e^{-4\pi\alpha}$. This is due to the fact that any attractive potential in 2 dimensions has a bound state. We must choose our mass such that $E_0 > 0$ and the instability is not present (it suffices that $m > Me^{-2\pi\alpha}$). However we will see that in $d = 2$, exactly as in the $d = 3$ case discussed above, in the presence of two or more δ's there exists a critical distance such that for closer approach a bound state has $E < 0$, generating a tachyon again.

Take N point-like scatterers, each with renormalized strength α_i and a renormalization mass M. It is convenient to define $M_i \equiv Me^{-2\pi\alpha_i}$ so Γ in (4.13) is

$$\Gamma_{ij} = \left(\frac{1}{2\pi} \ln \frac{\sqrt{E - m^2}}{iM_i} \right) \delta_{ij} - \widetilde{\mathcal{G}}_0(a_i, a_j; E). \tag{4.31}$$

The interaction energy for two identical deltas ($M_1 = M_2 = \mathcal{M}$, and $m > \mathcal{M}$ as required for the stability of isolated scatterers) separated by a distance L is ($k \equiv \sqrt{E}$)

$$\mathcal{E} = \frac{1}{2\pi} \int_0^\infty dk \ln \left(1 - \frac{K_0^2(L\sqrt{k^2 + m^2})}{\ln^2 \left(\sqrt{k^2 + m^2}/\mathcal{M} \right)} \right), \tag{4.32}$$

where K_0 is a Bessel function K of order 0, and the critical length is the solution of the equation $K_0(mL_c) = \ln m/\mathcal{M}$. The force diverges as $L \to L_c$ in $d = 2$ as well but the explicit expression is more difficult to recover. For $L \gg L_c$ the force is exponentially small, since we had to assume a mass $m > 0$ for the field ϕ.

4.4 Localized Vacuum Instability

Let us calculate the shape of the tachyon in 3 dimension found in the discussion after Eq. (4.27) (take $m = 0$). Let us first notice that (for any number of scatterers) the Wick-rotated matrix $\Gamma(-E)$ is real and symmetric and can hence be put in diagonal form. In the case at hand we have only two delta functions with equal strength α

and one can show that the spectral decomposition of Γ^{-1} is

$$(\Gamma^{-1})_{ij}(-E,\{a_1,a_2\}) = \frac{1}{\gamma_1} v_i^{(1)} v_j^{(1)} + \frac{1}{\gamma_2}\, v_i^{(2)} v_j^{(2)} \tag{4.33}$$

where

$$\gamma_1 = -\frac{e^{-L\sqrt{E}}}{4\pi L} + \frac{\sqrt{E}}{4\,\pi} + \alpha, \tag{4.34}$$

$$\gamma_2 = \frac{e^{-L\sqrt{E}}}{4\pi L} + \frac{\sqrt{E}}{4\,\pi} + \alpha, \tag{4.35}$$

and

$$v^{(1)} = \{\frac{1}{\sqrt{2}}, \frac{1}{\sqrt{2}}\} \tag{4.36}$$

$$v^{(2)} = \{\frac{1}{\sqrt{2}}, -\frac{1}{\sqrt{2}}\}. \tag{4.37}$$

The bound state pole is generated by a zero E^* in the γ_1 eigenvalue. For $L < L_c = 1/4\pi\alpha$ we have E^* as the real positive solution of the equation $\gamma_1(E) = 0$ (remember: the integration variable E appears as $-E$ in Γ so positive E here are real, negative eigenvalues of H)

$$\sqrt{E} + \frac{1}{L_c} = \frac{e^{-L\sqrt{E}}}{L}. \tag{4.38}$$

Comparing the behavior of the propagator for E close to a pole E^*

$$\mathcal{G}(x',x;E) \simeq \frac{\psi_0^*(x')\psi_0(x)}{E^* - E} \tag{4.39}$$

with

$$\mathcal{G}(x',x;E) \simeq \frac{1}{\gamma_1} \sum_{i,j} v_i^{(1)} v_j^{(1)} \mathcal{G}_0(x',a_i;E)\mathcal{G}_0(a_j,x;E) \tag{4.40}$$

we find the wave function of the (not normalized) bound state as

$$\psi_0(x) = \frac{e^{-\sqrt{E^*}|x-a_1|}}{|x-a_1|} + \frac{e^{-\sqrt{E^*}|x-a_2|}}{|x-a_2|}. \tag{4.41}$$

Something can be said also in the case in which we have many identical defects (and assume all the a_{ij}'s are of the same order of magnitude), without necessarily having to solve the equations explicitly. Instructed by the previous analysis we can state that the ground state will be a highly symmetric state $v \sim \{1/\sqrt{N}, ..., 1/\sqrt{N}\}$ which will then give a symmetric wave function $\psi_0(x) \propto \sum_i v_i \mathcal{G}(x, a_i; E^*)$ delocalized over the entire array of defects. The positivity of the v_i's coincide with the constraint that the ground state must not have any node.

Hence for $L < L_c$ a free field theory coupled to these defects does not make any sense. Its vacuum state $\phi = 0$ is unstable. The imaginary part of the energy (as an analytic continuation to $L < L_c$) is related to the 'decay time' of the vacuum state, due to particle creation.

Let us for a moment speculate on the consequences of this instability. Adding higher order terms in ϕ to the Lagrangian —one can for example think of adding a $\lambda\phi^4$ term— should eventually stabilize the field with a vacuum expectation value (vev) $\overline{\phi}(x) \neq 0$ in a somewhat large region around the two scatterers. However the actual value of the vev $\overline{\phi}(x)$ and the size and shape of the condensation region cannot be easily constructed and will be subject of future work.

This scenario of a local condensation and creation of localized vacuum instabilities due to defects could be interesting in inflation cosmology as well (the field ϕ being the inflaton). It must be also remarked that a similar scenario occurs in brane cosmology when an open string has its ends attached to two D-branes [67, 68]. When the branes are pushed closer than a critical length one of the modes of the string becomes a tachyon.

4.5 Extension to $n-1$ transverse dimensions

Now that we know the density of states $\rho(E)$ for the 'basic' problem of points in 1, 2 and 3 dimensions, we can move along the lines of Table I to generate solutions for manifolds with co-dimensions 1, 2 and 3. We shall then add $n-1$ transverse, flat dimensions. The total dimension of the space is now $d+n-1$. The calculations

in the preceding part of this chapter can be recovered by putting $n = 1$ in all the formulas. We will use the methods of [69] and [50] where one solves for the density of states $\rho(E)$ of the basic problem on a $d-$dimensional section and insert the result in the equation for the energy per unit $n-1$-dimensional 'area' S [69]

$$\mathcal{E}^{(n)} = \int_{\mathbb{R}^{n-1}} \frac{d^{n-1}p}{(2\pi)^{n-1}} \int_0^\infty dE \frac{1}{2} \left(\sqrt{p^2 + E} - \sqrt{p^2} \right) \rho(E). \tag{4.42}$$

The subtraction $-\sqrt{p^2}$ removes a divergent but $a-$independent term, since the integral $\int dE\rho(E)$ is a-independent. We will also remove the a-independent 'self-energy' terms by subtracting from $\rho(E)$ the density $\rho(E, \infty)$ with all $a_{ij} \to \infty$. We can then perform the (dimensionally regularized) integral over p, Wick-rotate and perform an integration by parts on E to obtain

$$\mathcal{E}^{(n)} = \frac{1}{2\pi} \frac{\Gamma(1 - \frac{n}{2}) \sin \frac{n\pi}{2}}{(4\pi)^{n/2}} \int_0^\infty dE E^{\frac{n}{2}-1} \ln \frac{\det \Gamma(-E; \{a\})}{\det \Gamma(-E; \infty)}. \tag{4.43}$$

For example the interaction energy (per unit length) of two straight, infinite strings in 3 dimensions ($d = 2, n = 2$ so $d + n - 1 = 3$) put at a distance L is

$$\mathcal{E}^{(2)} = \frac{1}{8\pi} \int_0^\infty dE \ln \left(1 - \frac{K_0^2(L\sqrt{E + m^2})}{\ln^2 \left(\sqrt{E + m^2}/M \right)} \right). \tag{4.44}$$

One can hence calculate the interaction energy of any two flat manifolds due to the quantum fluctuations of a bulk field ϕ. As an example in co-dimension 1 consider the Randall-Sundrum scenario [70] with two branes at a distance r_c from each other. The fluctuations of a given component of the metric G or of a bulk field ϕ (see [71] and references therein), have a space-dependent mass with two delta functions singularities on the two branes. The attractive force due to the quantum fluctuations of this field has a Casimir-like behavior. The curvature in the 5^{th} direction does not change the physics.[9] If however the branes have co-dimension 2 or 3 (and are defined as the limit of an attractive potential) is in the class of problems that we have studied

[9] If the brane is inside an horizon for the 5d metric most probably this assertion is not true, however. But this is not the case for the Randall-Sundrum model.

in this chapter and a perturbation would eventually condense, if $r_c < L_c$. Following the same arguments above we can also say that if the branes have co-dimension > 4 the fluctuations in the bulk will not see the brane. The cosmological implications of such a scenario will be subject of future work.

4.6 Omissions and Applications

The propagator, Eq. (4.13), comes directly from scattering theory. In that context it was natural to assume that the interaction between the particle and the scatterer (consider Fermi [55] and Zel'dovich [58] examples) is attractive. One considers an attractive center whose attraction grows when $r_0 \to 0$ such that at most one bound state is present and its energy remains finite (i.e. of $\mathcal{O}(1)$). Even thought we assumed that only one bound state is present at energies of $\mathcal{O}(1)$ this is the most generic situation that can occur in scattering theory. In fact if a second bound state is present, it will be an energy $\mathcal{O}(1/r_0^2)$ below our bound state. In the limit $r_0 \to 0$ its influence on low-energy scattering disappears. It goes out of the spectrum. In scattering theory however such a negative energy state is harmless. This is not the case for a bosonic field, for which it represents a tachyon. However for fermions this objection is irrelevant since we just have to fill this state and pretend that it belongs to the Dirac sea. It is then possible to see that this state with energy $\sim -1/r_0^2 \to -\infty$ does not influence the scattering matrix, nor the Casimir energy, at low energies. For $r_0 \to 0$ then the Casimir energy for bulk fermions is influenced only by lightly bound states.

One may wonder: what happens if the potential is *repulsive* and concentrated? The answer is that for $d > 1$ its influence on the scattering matrix (and hence on the spectrum) disappears when $r_0 \to 0$. Obviously this is not true in 1 dimension because we cannot 'go around' the scatterer. For a repulsive potential in $d > 1$ the renormalization procedure leading to (4.13) cannot be performed since μ has the wrong sign and sending $r_0 \to 0$ just kills the correction to $\mathcal{G}_0$ in (4.13).

More precisely, if in the Lagrangian we include a term $V_0\theta(r_0 - |x|)\phi^2(x)$ with

$V_0 > 0$ and then we take the limit $V_0 \to \infty$ and $r_0 \to 0$ with $V_0 r_0^2$ finite, the spectrum we obtain is just the free one: the scatterer disappears. In a sense, the only smile the Cheshire cat can leave behind is the lightly (i.e. $\mathcal{O}(1)$ instead of $\mathcal{O}(1/r_0^2)$) bound (or virtual) state. If this is not present then the scatterer is invisible to the fluctuations.[10] If the purpose of calculating the effective action was to calculate quantum corrections to a classical solution (as often occurs) then we deduce that for a repulsive potential or for $d \geq 4$ the classical solutions are unchanged by quantum fluctuations.

Let us now comment on two possible applications of the formalism we have developed: cosmic strings and concentrated Aharonov-Bohm fluxes. We anticipate that further work is required in both cases. In the literature on cosmic strings the difficulty generated by a bound state tied to a *single* cosmic string has been recognized a long time ago [62, 63]. In that context the bound state arising from Eq. (4.10) is rightly considered fictitious, because the smoothed potential is always positive ($\mu > 0$). Nonetheless, in [62] after projecting out this bound state at $E_0 < 0$, the propagator (4.13) is trusted and shown to be in good agreement with the numerical solution of the smoothed problem. It is not clear if projecting out a state from the propagator by hand has non-trivial (wrong) consequences on the density of states and the Casimir energy so we preferred not to follow this path even if it gives correct results for other quantities. We hence required the field to have a non-zero mass so that this bound state is stable. In the end it is not clear if the Casimir attraction and the birth of the tachyon could arise in cosmic strings coupled with bulk fields.

Another example to which the above techniques and results should be relevant is the case of a fermion around a concentrated tube of flux (Aharonov-Bohm case[11]). The spectrum of Dirac's equation can be inferred from that of a Klein-Gordon equation after squaring the former. The fact that we are dealing with fermions rather than bosons, is not a difficulty. Another difficulty however arises: for Aharonov-

[10]We have already remarked on the impossibility to consider the Casimir-Polder interaction between small metallic spheres as the interaction of point-like scatterers the way we construct them here. Small metallic particles of radius r still have a penetration depth $r_0 \ll r$ so effectively are co-dimension 1 surfaces.

[11]The one loop energy of QED flux tubes has been calculated in [64] using a combination of analytical and numerical methods. Our method could be used to calculate the interaction energy of two such tubes in the limit where their radius is small compared to their relative distance.

Bohm fluxes and the more general case of cosmic strings charged under some U(1) symmetry, it has been shown [72] that the contribution to the scattering cross section given by the non-zero external vector potential is asymptotically larger in the low energy regime than the contribution of the singularity in the core. Since we believe that cross sections and Casimir forces are tightly bounded quantities we would not apply any of the above arguments without treating the propagation in the external space properly. This will be done elsewhere.

Renormalization of branes coupling for a single brane (or δ-function in our case) with co-dimension 2 (and dimension 5) in a conical space has been studied in [65]. Arising from local divergences, the renormalization flow is not affected by the presence of other branes and the results in [65] apply also to our situation. Their renormalization of the brane coupling μ (λ_2 in their notation) corresponds to our renormalization $\alpha \to \alpha_r$. Their renormalization of the effective action corresponds to our subtraction of the a-independent terms in the Casimir energy. These two are the only subtractions needed (if ϕ^4 terms are not present) and it is heartening to see that our results coincide with those of [65]. Moreover one can make an amusing observation if one compares the two approaches to the delta function, the one in terms of scattering (that we used here) and the one in [65] in terms of renormalization group. Notice that the renormalization group flow for μ is IR free and has a Landau pole: the location of the Landau pole coincides with the location of the bound state in our approach.

4.7 Conclusions

We have calculated the force between an arbitrary number of surfaces (branes) with co-dimension > 1 due to the quadratic fluctuations of a boson ϕ living in the bulk. The force turns out to be attractive and it diverges when the distance between the branes approaches a critical value L_c is approached. This phenomenon has no analogues in the widely studied co-dimension 1 case.

The divergence of the force is accompanied by the birth of a vacuum instability,

a mode with negative mass squared localized around the scatterer. In 3 dimensions, the long-range properties of this force (decreasing like $1/L^6$) are shown to be different from the Casimir-Polder $1/L^8$ law, the explanation relying in the proper mathematical definition of the point-like limit.

Some implications of these effects have been pointed out.

Chapter 5

Casimir Force on a Single Plate or Casimir Buoyancy

In this chapter I will study the force on a single plate due to inhomogeneities of the background. An example could be the case of a plate in the vacuum of the electromagnetic field near a gravitating body. The shift of the proper frequencies of the virtual photons from point to point induces a force on the plate.

We will be able to prove that if the background is sufficiently smooth then the force is always a 'buoyancy force' in the sense that it pushes the plate toward regions of higher potential. This rather surprising result (which is robust to the introduction of a temperature) can be thought of as an Archimedes effect in the sea of virtual photons. However the quantum nature of the problem manifests itself as soon as the background is made less smooth. The interference between the photons scattered from the bumps in the background invalidates the general result.

5.1 Introduction

The interaction of a quantum field with a material medium sometimes can be idealized by placing a boundary condition on the field at the interface with the medium. Then the effects of the medium can be interpreted as modifications of the zero point energy of the field due to the boundary condition on the surface. The classic example

is the force between two parallel, grounded conducting plates due to zero point fluctuations of the electromagnetic field first discovered by Casimir[1]. Hence problems of this nature are known in general as Casimir problems. If the surface $\mathcal{S}$ is embedded in an inhomogeneous medium, then the quantum fluctuations of ϕ sense the inhomogeneities and give rise to a force per unit area on the surface even in the absence of a second surface. We will refer to this force as *Casimir buoyancy.* As "buoyancy" implies, the force is opposite to the force that acts on the quanta of the fluctuating field, at least in the cases we have been able to study.

In this paper we examine the problem of Casimir buoyancy. We formulate and study the problem for the simplest possible cases. We consider a scalar quantum field, ϕ, obeying the boundary conditions imposed by a sharply peaked background on an $n-1$ dimensional hyperplane embedded in n-dimensional Euclidean space. We assume that the mass of the scalar field varies in the direction normal to the surface, *i.e.* we introduce an interaction $\frac{1}{2}V(x_\perp)\phi^2$ into the Lagrangian,

$$\mathcal{L} = \frac{1}{2}\partial_\mu\phi\partial^\mu\phi - \frac{1}{2}m^2\phi^2 - \frac{1}{2}V(x_\perp)\phi^2 - \frac{1}{2}\lambda\Delta(x_\perp - a)\phi^2 \tag{5.1}$$

The function Δ, normalized to $\int dx\Delta(x) = 1$, is assumed to be sharply peaked at $x_\perp = a$. Usually a Dirac δ-function will do. We are particularly interested in the "Dirichlet limit", where the coupling λ goes to infinity and the field obeys the Dirichlet condition, $\phi = 0$, on the hyperplane. It is easy to imagine problems to which such a formulation applies, where a quantum field is subject to forces on two different scales, forces at a high energy scale that can be idealized as a boundary condition, and forces of order the mass of ϕ that can be regarded as a smoothly varying background.[1] We believe that similar considerations apply to a gauge vector (*e.g.* electromagnetic) field in an inhomogeneous medium and to fermion fields. The generic problem of a quantum field constrained on a surface and modulated by other forces in the bulk also arises in brane world scenarios, where similar effects should also be expected.

[1]In the *real* Casimir effect the idealization of the influence of the metal or dielectric on the electromagnetic field as a static background must be taken with some care. In particular some divergencies arising from this idealization could be absent if a dynamic description of the material is adopted [73].

We have not considered buoyancy in a curved space-time where the effect could arise from an inhomogeneous curvature [74].

As usual in Casimir physics, there is little intuition to guide us *a priori*. For example, there is no reason to expect the buoyancy force at a point x to depend only on V at the point x. In general we find that the buoyancy depends non-locally on V. However when the background field is smooth enough to admit a WKB approximation we find that the buoyancy reduces to a local function of the background field. Likewise we know of no argument to give the sign of the Casimir buoyancy. Should it be parallel to the force on the quanta of ϕ, or antiparallel? In all the examples we have been able to study we find that the force is opposite to the force on the quanta, hence a buoyancy.

Casimir problems can suffer from divergences of two different kinds[75]. The first are the familiar divergences that afflict any quantum field theory. The Casimir energy for a fluctuating field ϕ in a time-independent background[2] $\sigma(x)$ is the full one-loop effective energy, $E[\sigma]$, the sum over all one loop Feynman diagrams with arbitrary insertions of σ, as shown in the first line of Fig. 5-1[76]. The low order Feynman diagrams diverge: the 1-point function diverges for $n \geq 1$, the two point function for $n \geq 3$, *etc.* As usual, these divergences are cancelled by counterterms that are polynomials in σ, $\mathcal{L}_{\rm CT} = c_1\sigma + \frac{1}{2}c_2\sigma^2 + \ldots$ (some are shown in Fig. 5-1). The Casimir energy becomes dependent on the renormalized parameters of the σ-field dynamics. For example the need for the counterterm $\frac{1}{2}c_2\sigma^2$ in three dimensions generates a dependence on the renormalized σ-mass.

The second type of divergence is more interesting and more challenging. A realistic material medium cannot be idealized by a boundary condition at all energy scales. When the frequency of the fluctuating field is high compared to the natural scale of the interactions that characterize the material, its effects fade away. A background that constrains *all* modes of a fluctuating field is unphysical, and can introduce divergences into physical observables that cannot be removed by standard renormalization methods[77]. The origin of these divergences is quite clear from the Feynman dia-

[2]For us $\sigma(x) = \lambda\delta(x-a) + V(x)$.

grams. Each diagram involves integrals over the momenta carried by the external lines. $\sigma(x) = \int dp e^{-ipx}\hat{\sigma}(p)$. If the background has a discontinuity in some derivative, say the k-th, then at large p, $\hat{\sigma}(p) \sim p^{-k}$ and the integrals diverge for sufficiently large number of dimensions. There are no renormalization counter terms available to cancel these divergences. They signify that the quantity under consideration, even a directly measurable one like the Casimir force, is sensitive to the high energy cutoffs, Ω, above which the material no longer affects the field (say $\hat{\sigma}(p) = 0$ for $p > \Omega$).

In a given model there may be some quantities which admit a Casimir (*i.e.* boundary condition) description and others that do not. The boundary condition idealization shares with the effective field theory the notion of a separation of scales. The material structure is characterized by a high energy scale, the cutoff Ω. Modes with energies below this scale obey a boundary condition, modes with energies at or above Ω do not. If the boundary condition method is applicable, then physics at energies much lower than Ω can be described by the boundary condition without reference to Ω at all. For Casimir's original problem, parallel conducting plates, the plasma frequency $\omega_{\rm plasma}$ sets the high energy scale $\Omega \sim \hbar\omega_{\rm plasma}$, and the plate separation, d, or rather $\hbar c/d$, is the energy scale of physical interest. When $\omega_{\rm plasma} \gg c/d$ the force between parallel plates is well described by the boundary condition calculation. It can be shown that the Casimir idealization works for Casimir forces between rigid bodies in vacuum and for local observables like the energy density outside the material (at distances greater than $\hbar c/\Omega$), two examples of immense practical importance. Other observables are not so fortunate. It was shown in Ref. [77] that the Casimir *pressure* on a sphere of radius R, for example, depends on the cutoff, so it is not possible to study the pressure, even when $\hbar c/R \ll \Omega$, without characterizing the material in detail.

It is important to learn the circumstances under which there is an effective low energy description of buoyancy independent of the material cutoffs. We find that the answer to this question depends on the number of dimensions, n. In one dimension, where the surface is a point, there are no divergences of any kind and the Casimir buoyancy is independent of the cutoffs. Thus, for example, it goes to a finite limit

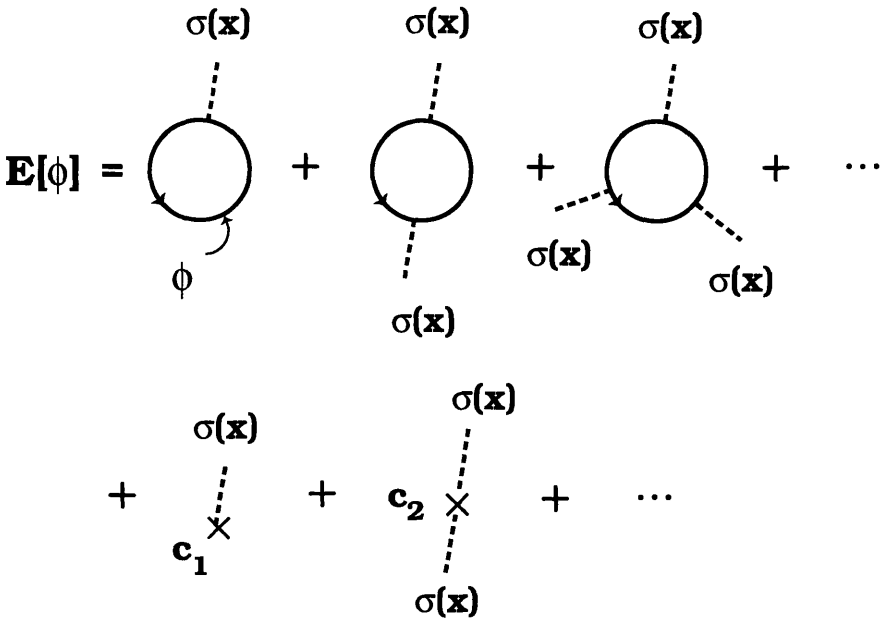

Figure 5-1: *The Casimir energy of a fluctuating field, ϕ, coupled to a time independent background field, σ, via $\mathcal{L}_I = \frac{1}{2}\sigma(x)\phi^2$ is proportional to the sum of all one loop diagrams. The sum must include the contributions of counter terms, polynomials in σ, required to cancel the loop divergences. The structure of the counter terms depends on the number of dimensions, n. The second line in the figure shows the counter terms required in three dimensions where the 1- and 2- point functions are primitively divergent.*

as $\lambda \to \infty$. Higher dimensions can be studied relatively easily using the formalism developed in Refs. [78]. For $n < 2$ the situation is the same as for $n = 1$. For $2 \leq n < 3$, the Casimir buoyancy remains independent of the details of the surface, but the limit $\lambda \to \infty$ cannot be taken (it diverges like λ^{n-2}). For $n \geq 3$ there is no separation of scales. The buoyancy depends on the details of the structure of the material.

In the next section we describe the formulation of the Casimir buoyancy problem in one dimension. We recast it in terms of the Schrödinger equation Greens function with potential $V(x)$, and express the buoyancy in terms of the bound and scattering states of V. We study both fixed λ and the limit $\lambda \to \infty$. In Section III we describe some important approximations and special cases: For deep and smooth $V(x)$ we derive a WKB approximation; we study the case where $V(x) + m^2 = 0$ (a turning

point) which cannot be analyzed by means of WKB, proving buoyancy in this case as well. We study the Casimir buoyancy force in a thermal state finding the buoyancy is qualitatively not affected by a non-zero temperature. For a reflectionless potential we show that only the bound states matter. We study the buoyancy outside the range of $V(x)$ and construct the first Born approximation as an example of non-local but simple result. In Section IV we go through some explicit, solvable examples. Then in Section V we generalize from $n = 1$ to higher dimensions.

5.2 Formulation of the problem

The situation of interest is summarized by eq. (5.1). It might arise if a quantum field is coupled to one field characterized by a high mass scale that lives on the hyperplane $x_\perp = 0$, and to another field V characterized by a lower energy scale. As usual we take V to be time independent and externally determined; we ignore the back reaction of ϕ on V. The principal dynamical effects occur in the one non-trivial direction along which V varies, so we begin by studying the one-dimensional problem.

5.2.1 General considerations

In one dimension the Lagrangian for ϕ reads

$$\mathcal{L} = \frac{1}{2}\dot{\phi}^2 - \frac{1}{2}\phi'^2 - \frac{1}{2}\left(m^2 + \lambda\Delta(z-a) + V(z)\right)\phi^2 \tag{5.2}$$

We are interested in the vacuum energy of the ϕ-field as a functional of Δ and V,

$$\mathcal{E} = \frac{1}{2}\hbar \sum\!\!\!\!\!\!\int \omega = \frac{1}{2}\hbar \int_0^\infty dE\sqrt{E}\frac{dN}{dE}, \tag{5.3}$$

a sum over the discrete spectrum, if any, and integral over the continuum, where the $\{\omega^2\}$ are the eigenfrequencies of the Schrödinger Hamiltonian,

$$\mathcal{H} = -d^2/dx^2 + m^2 + \lambda\Delta(x-a) + V(x), \tag{5.4}$$

which will, in general, range over both discrete and continues values.[3] So the problem can be recast in the form of a Schrödinger equation, $\mathcal{H}\phi = E\phi$, with $E = \omega^2 \equiv k^2 + m^2$. If we define $\mathcal{G}(x, x', E) = \langle x'|\frac{1}{\mathcal{H}-E}|x\rangle$ to be the equivalent Schrödinger Greens function, then we can write the density of states, dN/dE, as

$$\frac{dN}{dE} = \frac{1}{\pi}\,\mathrm{Im}\int d^{\,n}x\,\mathcal{G}(x, x, E + i\epsilon) \tag{5.5}$$

where n is the number of spatial dimensions. The $i\epsilon$ displaces the poles in $\mathcal{G}$ into the lower half E-plane, and insures that the propagator, $\mathcal{G}(x, x', t) = \int dE e^{-iEt}\mathcal{G}(x, x', E + i\epsilon)$, is causal. Substituting for the density of states into eq. (5.3), the Casimir energy can be written

$$\mathcal{E} = \frac{1}{2\pi}\mathrm{Im}\int_0^\Omega dE\sqrt{E}\int d^{\,n}x\mathcal{G}(x, x, E + i\epsilon), \tag{5.6}$$

where we have assumed that the spectrum is positive definite[4] and we have introduced a cutoff Ω above which the boundary must be characterized in greater detail. We already discussed in the Introduction the conditions (on n and $\sigma = \lambda\Delta + V$) under which we can take $\Omega \to \infty$ without affecting the low energy physics. We will go over some these arguments again in Section 5.5. At the moment we assume all these conditions to be fulfilled so we can take the limit $\Omega \to \infty$ without placing further restrictions on $\sigma(x)$.

5.2.2 Force on a sharp surface

We are interested in the case where $\Delta(x - a)$ is a Dirac δ-function, $\Delta(x) = \delta(x)$, and $\lambda > 0$ since this repels the field ϕ from the "surface" $x = a$. If we restrict the analysis to 1 spatial dimension (the extension to $n > 1$ with translational symmetry in $n - 1$ dimensions will be performed in Section 5.5) it is possible to express the Greens function $\mathcal{G}$ in terms of the (simpler) Greens function, $\mathcal{G}_0(x', x, E) \equiv \langle x'|\frac{1}{\mathcal{H}_0-E}|x\rangle$ in

[3] We set $\hbar = c = 1$ until further notice.

[4] Negative energy single particle states in an external field correspond to vacuum instabilities that we do not consider here.

the presence of $V(x)$ alone,

$$\mathcal{H}_0 = -\frac{d^2}{dx^2} + m^2 + V(x). \tag{5.7}$$

First, we write the Lippmann-Schwinger equation[5] for $\mathcal{G}$ in terms of $\mathcal{G}_0$ and $\Delta(x)$,

$$\mathcal{G}(x,x',E) = \mathcal{G}_0(x,x',E) - \lambda \int dy \mathcal{G}_0(x,y,E)\Delta(y-a)\mathcal{G}(y,x',E) \tag{5.8}$$

When $\Delta(x-a) \to \delta(x-a)$ it is easy to solve for $\mathcal{G}$,[6]

$$\mathcal{G}(x,x',E) = \mathcal{G}_0(x,x',E) - \lambda \frac{\mathcal{G}_0(x,a,E)\mathcal{G}_0(a,x',E)}{1+\lambda \mathcal{G}_0(a,a,E)} \tag{5.9}$$

For the density of states, we require the integral over x of $\mathcal{G}(x,x,E)$. Using the identity

$$\begin{aligned} \int dx \mathcal{G}_0(x,a,E)\mathcal{G}_0(a,x,E) &= \int dx \langle x| \frac{1}{\mathcal{H}_0 - E}|a\rangle \ \langle a|\frac{1}{\mathcal{H}_0 - E}|x\rangle \\ &= \langle a| \frac{1}{(\mathcal{H}_0 - E)^2}|a\rangle, \\ &= \frac{\partial}{\partial E}\mathcal{G}_0(a,a,E) \end{aligned} \tag{5.10}$$

we obtain

$$\begin{aligned} \int dx \mathcal{G}(x,x,E) &= \int dx \mathcal{G}_0(x,x,E) - \frac{\lambda}{1+\lambda \mathcal{G}_0(a,a,E)} \frac{\partial}{\partial E}\mathcal{G}_0(a,a,E) \\ &= \int dx \mathcal{G}_0(x,x,E) - \frac{\partial}{\partial E} \ln\left(1+\lambda \mathcal{G}_0(a,a,E)\right) \end{aligned} \tag{5.11}$$

Substituting into eq. (5.6), we find

$$\mathcal{E} = -\frac{1}{2\pi} \mathrm{Im} \int_0^\Omega dE \sqrt{E} \frac{\partial}{\partial E} \ln\left(1+\lambda \mathcal{G}_0(a,a,E+i\epsilon)\right) \tag{5.12}$$

[5]Here we are considering a fully renormalized Hamiltonian $\mathcal{H}$, a function of renormalized masses and couplings.

[6]After this paper was completed Brian Winn, in a conversation with one of us (AS), pointed out that singularly perturbed Hamiltonians like (5.4) have been studied in chaotic billiards theory where they are called *Šeba billiards* and generalizations of Eq. (5.9) can be found in the literature on this subject [79].

where we have dropped a term of the form $\mathcal{E}_0 = \frac{1}{2\pi}\mathrm{Im}\int_0^\Omega dE\sqrt{E}\int dx\mathcal{G}_0(x,x,E+i\epsilon)$, which does not depend on a and therefore does not contribute to the Casimir force, $-d\mathcal{E}/da$. Since we are only interested in the force, not the energy, we differentiate with respect to a, $\mathcal{F} = -\partial\mathcal{E}/\partial a$,

$$\mathcal{F} = \frac{1}{2\pi}\mathrm{Im}\int_0^\infty dE\sqrt{E}\frac{\partial^2}{\partial E\partial a}\ln\left(1+\lambda\mathcal{G}_0(a,a,E+i\epsilon)\right) \tag{5.13}$$

where we have taken $\Omega \to \infty$ since according to our previous discussions the limit exists and is finite.

The analytic structure of the integrand of eq. (5.13) is important for our analysis (see Figure 5-2) because only the imaginary part contributes to $\mathcal{F}$, and the integrand is real for real E except at its singularities. The $\sqrt{E}$ gives a branch cut running from $E = 0$ to ∞, which we place along the negative real axis. For real, positive E there are two regions of interest. Above threshold for scattering, $E > m^2$, $\mathcal{G}_0$ is complex, so the integrand has a cut with branch point at $E = m^2$. For E real and below threshold $\mathcal{G}_0(a,a,E)$ is real, so the only singularities occur when the argument of the logarithm, $1+\lambda\mathcal{G}_0(a,a,E+i\epsilon)$, vanishes, where the integrand has poles. When E is below the spectrum of $\mathcal{H}_0$, $\mathcal{G}_0(a,a,E)$ is positive and $1+\lambda\mathcal{G}_0(a,a,E)$ cannot vanish. So there are no singularities in the domain $0 < E < m^2$ unless $\mathcal{H}_0$ has bound states. Suppose, then, that $\mathcal{H}_0$ has bound states at E_1, E_2, E_3, ... E_M. Because $\mathcal{G}_0 \sim 1/(E_j - E)$ near the j^{th} bound state, is easy to see that $1+\lambda\mathcal{G}_0(a,a,E)$ must vanish at a value of E between the j^{th} and $j+1^{\text{th}}$ bound states of $\mathcal{H}_0$. At each of these energies there is a contribution to the imaginary part from the $i\epsilon$ in the argument of $\mathcal{G}_0$. Therefore at least $M-1$ poles contribute to $\mathcal{F}$. If the pole just above E_M occurs at an energy below m^2 then there is one more. These contributions have a simple physical interpretation: They are the contributions to the Casimir force from the bound states in $V(x)$ subject to the boundary condition $\Delta\psi'(a) = \lambda\psi(a)$. The analytic structure of the integrand of eq. (5.13) in the complex E-plane is summarized in Fig. (5-2).

From these considerations it is clear that the problem is simplified if we rotate the integration contour to the negative imaginary axis. Making the obvious analogy

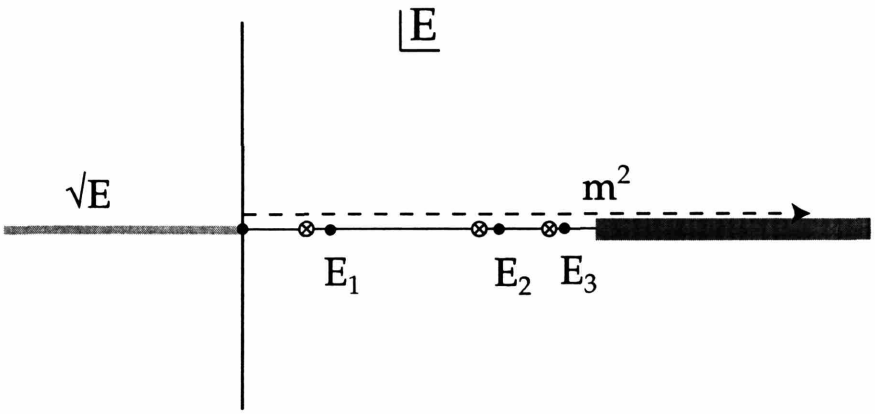

Figure 5-2: *Analytic structure of the integrand of eq. (5.13) in the complex E-plane. The left hand cut comes from the $\sqrt{E}$, the right hand cut beginning at $E = m^2$ comes from scattering states. The pole contributions are marked by solid circles. They lie just above the bound states of $V(x)$, marked with $\otimes$.*

to Feynman diagram methods, we refer to this as "Wick rotation" to the "Euclidean form" of the Casimir buoyancy. There is no contribution to the force from the semi-circle at large $|E|$, because for $E \gg V$ we have $\mathcal{G}_0(a, a, E) \sim \frac{i}{2\sqrt{E}}$. Although this yields a contribution to $\mathcal{E}$ (logarithmically divergent in the cutoff Ω), it is independent of a, and therefore does not affect the force.

The result,

$$\mathcal{F} = \frac{1}{2\pi} \int_0^\infty dE \sqrt{E} \frac{\partial^2}{\partial E \partial a} \ln\left(1 + \lambda \mathcal{G}_0(a, a, -E)\right) \ , \tag{5.14}$$

is particularly useful because the argument of the logarithm is positive definite. Eq. (5.14) can be integrated by parts without contributions at the limits because the surface term at $E \to \infty$ is independent of a and the surface term at $E = 0$ vanishes:

$$\mathcal{F}(a, \lambda, V) = -\frac{1}{4\pi} \int_0^\infty dE \frac{1}{\sqrt{E}} \frac{\partial}{\partial a} \ln\left(1 + \lambda \mathcal{G}_0(a, a, -E)\right) . \tag{5.15}$$

Here we have restored some of the arguments on the function $\mathcal{F}$ as a reminder of its important variation with position, λ, and background field, V. It will be sometimes convenient to introduce the imaginary momentum $\kappa = \sqrt{E + m^2}$ (here E is the

dummy variable in (5.15)) in the Euclidean domain,

$$\mathcal{F}(a,\lambda,V) = -\frac{1}{2\pi}\int_m^\infty d\kappa\kappa \frac{1}{\sqrt{\kappa^2-m^2}}\frac{\partial}{\partial a}\ln\left(1+\lambda\mathcal{G}_0(a,a,-\sqrt{\kappa^2-m^2})\right) \ , \quad (5.16)$$

This result can be rewritten usefully by introducing the Jost solutions to the Schrödinger equation, $\mathcal{H}\psi = -E\psi$ (notice the minus sign in front of E, due to the Wick rotation), which are defined by their behavior as $x \to \pm\infty$[80],

$$\begin{aligned} \lim_{x\to\infty} \psi^+(\kappa,x)e^{\kappa x} &= 1 \\ \lim_{x\to-\infty} \psi^-(\kappa,x)e^{-\kappa x} &= 1 \end{aligned} \quad (5.17)$$

The boundary conditions of eqs. (5.17) render the functions $\psi^\pm$ analytic for Re $\kappa > 0$. On the contour $-\infty < E < 0$ needed in eq. (5.16) the Jost solutions are real and fall exponentially in the limits given in eq. (5.17). The Greens function can be written in terms of the Jost solutions,

$$\mathcal{G}_0(x,y,-\sqrt{\kappa^2-m^2}) = \frac{T(\kappa)}{2\kappa}\psi^+(\kappa,x_>)\psi^-(\kappa,x_<) \quad (5.18)$$

where $x_>$ ($x_<$) is the greater (lesser) of x or y, and $T(\kappa)$ is the transmission coefficient. Upon substituting for $\mathcal{G}_0$ in eq. (5.16), we obtain

$$\mathcal{F}(a,\lambda,V) = -\frac{\hbar c}{2\pi}\int_0^\infty d\kappa\kappa \frac{1}{\sqrt{\kappa^2-m^2}}\frac{\partial}{\partial a}\ln\left(1+\frac{\lambda T(\kappa)}{2\kappa}\psi^+(\kappa,a)\psi^-(\kappa,a)\right)$$

In the last equation we have restored the factors of $\hbar$ and c ($E = \kappa^2 - m^2$ has units of 1/length^2 in these units).

5.2.3 $\lambda \to \infty$: the Dirichlet case

When the strength, λ, of the sharp background field becomes large compared to the eigenvalue, ω, the mode of the field with frequency ω vanishes at $x = a$. If all the modes that contribute to the buoyancy have eigenvalues below λ, then effectively the field itself obeys the boundary condition $\phi(a,t) = 0$. As discussed in Ref. [77],

this description is acceptable if the physical observable of interest remains becomes independent of λ in the limit. In the case of buoyancy force in one dimension the limit $\lambda \to \infty$ exists.

$$\lim_{\lambda\to\infty} \mathcal{F}(a,\lambda,V) \equiv \mathcal{F}_\infty(a,V) \;=\; -\frac{1}{2\pi}\int_0^\infty \frac{dE}{\sqrt{E}}\frac{\partial}{\partial a}\ln \mathcal{G}_0(a,a,-E) \qquad (5.19)$$

which can be also written as

$$\mathcal{F}_\infty(a,V) \;=\; -\frac{1}{4\pi}\int_m^\infty d\kappa\kappa\frac{1}{\sqrt{\kappa^2-m^2}}\left(\frac{1}{\psi^+(\kappa,a)}\frac{\partial\psi^+(\kappa,a)}{\partial a}+\frac{1}{\psi^-(\kappa,a)}\frac{\partial\psi^-(\kappa,a)}{\partial a}\right) \qquad (5.20)$$

It is instructive to study the contribution to the Casimir force of the bound states in the $\lambda \to \infty$ limit.[7] Returning to the non-rotated formula eq. (5.13), taking $\lambda \to \infty$ and substituting the Jost solutions representation for the Greens function, we have

$$\mathcal{F}_\infty(a,V) = -\frac{1}{2\pi}\mathrm{Im}\int_0^\infty dE\frac{1}{\sqrt{E}}\frac{\partial}{\partial a}\ln\left(\psi^+(E,a)\psi^-(E,a)\right). \qquad (5.21)$$

Remembering that Jost solutions are real for $E < m^2$, it is clear that the only contributions in this range come from possible zeros in $\psi^\pm(E,a)$, where the integrand picks up an imaginary part because the integration contour goes above the pole on the Re E axis. The locations of these zeros depends on a, so we label them as $E_{j^\pm}(a)$. Near the j^{th} zero in $\psi^\pm$,

$$\psi^\pm(E,a) = (E - E_{j^\pm}(a) + i\epsilon)\left.\frac{\partial\psi^\pm(E,a)}{\partial E}\right|_{E=E_{j^\pm}(a)} + \ldots \qquad (5.22)$$

where we have restored the $i\epsilon$ to make the nature of the singularity clear. Substituting into eq. (5.21) and extracting the imaginary part, we obtain a very simple expression

[7]The analysis for finite λ is similar, but technically more complicated. In practice, following the discussion in the previous section, one has to find the poles of $1 + \lambda\, \mathcal{G}_0(a,a,E)$ say $E(a)$, which are also eigenvalues of $\mathcal{H}$, and proceed as before.

for the bound state contribution to $\mathcal{F}_\infty$.

$$\mathcal{F}_\infty(a,V)|_{\text{bound states}} = -\frac{\hbar c}{4}\sum_{j^\pm}\frac{1}{\sqrt{E_{j^\pm}(a)}}\frac{\partial E_{j^\pm}(a)}{\partial a} = -\frac{\partial}{\partial a}\left[\frac{\hbar c}{2}\sum_{j^\pm}\sqrt{E_{j^\pm}(a)}\right] \tag{5.23}$$

Here we have used the fact that the various partial derivatives are related by

$$d\psi = \frac{\partial\psi}{\partial E}dE + \frac{\partial\psi}{\partial a}da = 0 \tag{5.24}$$

along the contour $\psi^\pm(E_{j^\pm}(a),a) = 0$ in the E,a plane.

The simple form of eq. (5.23) has a simple origin: the $\{\sqrt{E_{j^\pm}(a)}\}$ are the eigenenergies of ϕ in $V(x)$ constrained to vanish at $x = a$, so the quantity in brackets is the bound state contribution to the Casimir energy for a scalar field in the potential $V(x)$ *forced to vanish at* $x = a$. This is an equivalent formulation of the Casimir buoyancy in the Dirichlet ($\lambda \to \infty$) limit. From this interpretation it is clear that the number of terms in the sum in eq. (5.23) lies between $N-1$ and N, where N is the number of bound states in $V(x)$.

To complete this parametrization of the Casimir buoyancy we write the continuum contribution as an integral over the scattering momentum k, so another expression for the total buoyancy in the $\lambda \to \infty$ limit, equivalent to eq. (5.20) is

$$\mathcal{F}_\infty(a,V) = -\frac{\partial}{\partial a}\left[\frac{\hbar c}{2}\sum_{j^\pm}\sqrt{E_{j^\pm}(a)} - \frac{\hbar c}{2\pi}\mathrm{Im}\int_0^\infty dk\frac{k}{\sqrt{k^2+m^2}}\ln\left(\psi^+(E,a)\psi^-(E,a)\right)\right] \tag{5.25}$$

If the k-integration were rotated to the positive imaginary axis, $k \to i\kappa$, two kinds of contributions would arise: a) from the cut from $\frac{1}{\sqrt{k^2+m^2}}$ and b) from poles in $\psi^+\psi^-$ corresponding to the same states counted in the sum over j. The pole contribution would exactly cancel the sum and the integral over κ would yield eq. (5.20) as it must.

5.3 Approximations and Special Cases

Casimir buoyancy is an unfamiliar phenomenon. Its properties are not readily apparent from the general expressions, eqs. (5.20) and (5.25). In this section we study the buoyancy in special situations where it simplifies. First we look at smooth, deep potentials where the WKB approximation applies. Next we look at reflectionless potentials, where we show that only the bound states contribute to the buoyancy. Third, we look at the buoyancy in the domain beyond the range of $V(x)$, and finally we study the first Born approximation, where the buoyancy is simple, but not local.

5.3.1 WKB approximation

If the potential is smooth and strong, a WKB expansion can be made for the Casimir buoyancy. We work with the Wick rotated form, eq. (5.20). To apply WKB [81] we introduce a fictitious "$\tilde{\hbar}$" into the Hamiltonian, $\mathcal{H} \to -\tilde{\hbar}^2 \frac{d^2}{dx^2} + W(x)$ (henceforth we will write $W(x)$ for $m^2 + V(x)$) and write

$$\psi^{\pm}(E,x) = \exp\left(-\frac{1}{\tilde{\hbar}} s_0(x,E) + s_1(x,E) + ...\right). \tag{5.26}$$

and find

$$\begin{aligned} s_0(x,E) &= \pm \int_0^x dy \sqrt{-E + W(y)} \\ s_1(x,E) &= -\frac{1}{4} \ln(-E + W(x)) \end{aligned} \tag{5.27}$$

so the domain $E < 0$ corresponds to the WKB forbidden region (since $W(x) > 0$, which we have assumed from the outset) and gives real $s_{0,1,...}$, $\psi_{\pm}$ and $\mathcal{G}_0$.

The criterion for the validity of the WKB expansion (with $\tilde{\hbar}$ set to unity), $s_1' \ll s_0'$, reduces to

$$\frac{d}{dx} \frac{1}{\sqrt{W(x)}} \ll 1, \tag{5.28}$$

from which we conclude that $W'(x)/W^{3/2}$ should be small and in particular where

$W = m^2 + V(x)$ should not vanish[8] (*i.e.* at turning points). Hence the WKB approximation applies to potentials which are "deep" in the sense that $\int dy\sqrt{W(y)} \gg 1$ and far from turning points where $W(x) = 0$.

It is straightforward to construct the Greens function, in the WKB approximation,

$$\mathcal{G}_{0\ \mathrm{WKB}}(a, a, -E) = \frac{1}{2\sqrt{E + W(a)}} \tag{5.29}$$

and, upon substituting into eq. (5.15), and performing the integral over E, we find

$$\begin{aligned}\mathcal{F}(\lambda, a)_{\mathrm{WKB}} &= \frac{\partial}{\partial a}\frac{\hbar c}{4\pi}\left(\pi\sqrt{W(a)} + \lambda\ln(W(a)) - \sqrt{\lambda^2 - 4W(a)}\ln\frac{\lambda - \sqrt{\lambda^2 - 4W(a)}}{\lambda + \sqrt{\lambda^2 - 4W(a)}}\right) \\ &\equiv -\frac{\partial}{\partial a}\Omega(a, \lambda)_{\mathrm{WKB}}. \end{aligned} \tag{5.30}$$

is a local function of the potential, $V(a)$. We call this function the *quantum potential* $\Omega(a, \lambda)$.

Equation (5.30) simplifies considerably in the Dirichlet limit,

$$\mathcal{F}_{\infty\ \mathrm{WKB}}(a) = \frac{\partial}{\partial a}\frac{\hbar c}{4}\sqrt{m^2 + V(a)} \equiv -\frac{\partial}{\partial a}\Omega(a)_{\mathrm{WKB}}. \tag{5.31}$$

A remarkably simple result for such a complex phenomenon. One general feature can be easily deduced from this form of the quantum potential Ω: it decreases when the potential $V(x)$ increases and hence the force felt by the plate is a *buoyancy* force. We will encounter this phenomenon throughout the rest of this paper in extensions (to regions where the simple WKB form is not valid, to non-zero temperature and to higher number of dimensions) and several examples.

5.3.2 Points at which $V(x) + m^2 = 0$

When the potential is smooth (with a definite length-scale $b \sim [\frac{1}{W}\frac{dW}{dx}]^{-1}$) but there exists an x_0 such that $V(x_0)+m^2 = 0$ (or in general an interval where $(V(x)+m^2)b^2 \ll 1$) then WKB cannot be applied. The simple formula eq. (5.31) breaks down. For

[8] If $W \sim x^{2n}$ then $W'/W^{3/2} \sim x^{-n-1}$ becomes arbitrarily large as $x \to 0$.

example in the case of symmetric potential $m^2 + V(x) = x^2$ the force must vanish at $x = 0$ for symmetry, while eq. (5.31) predicts $\mathcal{F} \to$ constant.

To understand what really happens when the delta function reaches the point x_0 one needs a more clever guess than WKB. Moreover, adding more terms of the WKB series cannot help since the asymptotic nature of WKB means that adding terms improves the result for *larger* values of $b^2(V + m^2)$, so certainly not close to x_0. The formally correct procedure would be to find a differential equation 'similar' to the one we are studying but solvable and a smooth map from one to the other [82]. In this way we would obtain a *uniform* approximation near the turning point x_0. However such an analysis goes beyond the goal of this paper, so to clarify the situation we will assume that close to $x_0 = 0$ we have (remember that $W(x) \geq 0$)

$$W(x) = V(x) + m^2 \simeq \omega^2 x^2 + \mathcal{O}\left(x^3\right). \tag{5.32}$$

If we have $0 \neq W(0) \equiv W_0 \ll 1/b^2$, this constant could be reabsorbed by a shift of E and the range of integration in eq. (5.24), we will consider this case at the end of this section.

We then study the propagator in the neighborhood of $x_0 = 0$ *i.e.* the propagator $\mathcal{G}_0$ of the equation

$$-\phi''(x) + \omega^2 x^2 \phi(x) = E\phi(x) \tag{5.33}$$

which is the usual harmonic oscillator problem. We now set $\omega = 1$ and we will reintroduce it only at the end of the calculation to have dimensionally correct results.

From the two independent Jost solutions of this equation it is straightforward to write the the propagator for the harmonic oscillator as

$$\mathcal{G}_0(a, a, E) = \frac{2^{-(E+1)/2}}{\sqrt{\pi}} \Gamma\left(\frac{1-E}{2}\right) e^{-a^2} H_{\frac{E-1}{2}}(a) H_{\frac{E-1}{2}}(-a) \tag{5.34}$$

where H is the Hermite function, a generalization of the Hermite polynomials related to the parabolic cylinder function [83]. Notice that the poles of the gamma function give the correct spectrum of the bound states.

One can then calculate the buoyancy force for any λ, by inserting eq. (5.34) into eq. (5.15) and performing the integral numerically. In the Dirichlet case $\lambda \to \infty$ however the results simplifies using eq. (5.19) to

$$\mathcal{F}_{\infty \text{ h.o.}} = -\frac{1}{4\pi}\int_0^\infty \frac{dE}{\sqrt{E}}\left((1+E)\left(\frac{H_{-(3+E)/2}(-a)}{H_{-(1+E)/2}(-a)} - \frac{H_{-(3+E)/2}(a)}{H_{-(1+E)/2}(a)}\right) - 2a\right). \quad (5.35)$$

In this case the expression for small a can be recovered by expanding the integrand in powers of a and integrating term by term (the expansion can be carried on to any order of a because the integrals over E converge):

$$\begin{aligned}\mathcal{F}_{\infty \text{ h.o.}} &\simeq \frac{1}{4\pi}\left(a\left(\int_0^\infty dE \frac{1}{\sqrt{E}}\left(\frac{8\,\Gamma(\frac{3+E}{4})^2}{\Gamma(\frac{1+E}{4})^2} - 2E\right)\right) + \mathcal{O}\left(a^3\right)\right) \\ &\simeq \frac{1}{4\pi}\omega^{3/2}a(3.24...) + \mathcal{O}\left(\omega^{5/2}a^3\right) \end{aligned} \quad (5.36)$$

which again exhibits the buoyancy phenomenon, *ie.* the Casimir force pushes the plate toward points at higher potential. Notice that the force vanishes as $a \to x_0 = 0$ as it should from symmetry arguments.[9]

If $V(x_0) + m^2 = W_0$ and $W_0 \ll 1/b^2$ ($b^2 = 1/\omega$ in this case) one can repeat the preceding derivation, change the lower limit of integration over E from 0 to $W_0 b^2$ (W_0/ω in the case at hand) and write

$$\mathcal{F}_{\infty \text{ h.o.}} \simeq \frac{1}{4\pi}\omega^{3/2}a f(W_0/\omega), \quad (5.37)$$

where we have defined

$$f(x) = \int_x^\infty dy \frac{1}{\sqrt{y-x}}\left(\frac{8\,\Gamma(\frac{3+y}{4})^2}{\Gamma(\frac{1+y}{4})^2} - 2y\right), \quad (5.38)$$

and $f(0) = 3.24...$. Although we do not have an analytic expression for f it can

[9]If we want to compare this result with an exact one we can choose $n = 4$ Poschl-Teller (see Section 5.4.2) with $m = \sqrt{20}$ for which $V(x) + m^2 \sim 20x^2$ near $x = 0$. In this case $\mathcal{F}_{\text{exact}}/\mathcal{F}_{\text{approx}} = 0.94$ as $a \ll 1$. Such an agreement must be considered impressive, since the propagator is not a local function of the potential V and a local approximation to V does not guarantee at all a local approximation to G. Evidently, for sufficiently smooth potentials this turns out to be the case.

be studied numerically with ease and to a great accuracy. In the opposite limit $W_0/\omega \gg 1$ one can still shift the range of integration and then, by working out the asymptotic limit of the propagator eq. (5.34) as $E/\omega \gg 1$, one finds the now familiar WKB result eq. (5.31). We will apply eq. (5.37) to the case of Pöschl-Teller potential in Section 5.4.2.

One can also study higher order zeros (or minima) of W, *i.e.* points where $W(x) \sim x^{2n}$ in a similar fashion. The Jost solutions of such a problem should be found, possibly in a series for small x, and by means of them the propagator can be written explicitly in the neighborhood of the minimum $x = 0$. Here we will not extend our analysis to those cases since no qualitatively new phenomenon arises.

5.3.3 Temperature dependence in the WKB approximation

One can also study the case where the field is in a non-zero temperature thermal state rather than a vacuum state. The Casimir energy is then the integral of the energy momentum tensor component T_{00} evaluated on the thermal state. The result is [4]

$$\mathcal{E}_\lambda = -\frac{1}{2\pi}\mathrm{Im}\int_0^\Omega dE\sqrt{E}\coth\left(\beta\frac{\sqrt{E}}{2}\right)\frac{\partial}{\partial E}\log\left(1+\lambda\mathcal{G}_0(a,a,E)\right). \tag{5.39}$$

One can Wick-rotate this expression as well, since the Matsubara poles are on the negative real E axis. After the rotation the Greens function becomes real (the i from $\sqrt{E}$ cancels with an i from coth) and one has an imaginary part from the cot function. Dropping a term $\propto \lambda \log\Omega$ arising from the semicircle at $|E| = \Omega$ one has

$$\mathcal{E}_\lambda = -\frac{1}{2\pi}\int_0^\Omega dE\sqrt{E}\ \mathrm{Im}\Big\{\cot\left(\beta\frac{\sqrt{E}}{2}-i\epsilon\right)\Big\}\frac{\partial}{\partial E}\log\left(1+\lambda\mathcal{G}_0(a,a,-E)\right). \tag{5.40}$$

In the limit $\epsilon \to 0$ one has $\mathrm{Im}\cot(x-i\epsilon) = \pi\sum_n \delta(x-n\pi)$. The final expression is then a sum over Matsubara frequencies.

$$\mathcal{E}_\lambda = -\frac{1}{2}\int_0^\Omega dE\sqrt{E}\sum_n \delta\left(\beta\frac{\sqrt{E}}{2}-n\pi\right)\frac{\partial}{\partial E}\log\left(1+\lambda\mathcal{G}_0(a,a,-E)\right). \tag{5.41}$$

The study of this expression would require a paper on its own. Here we will limit our analysis of the WKB case, since a closed exact expression can be easily obtained in this case. To obtain it however, we have to go back to the original, non Wick-rotated WKB expression eq. (5.39) (we again use the notation $W(x) = V(x) + m^2 > 0$)

$$\mathcal{E}_\lambda \simeq -\frac{1}{2\pi}\mathrm{Im}\int_0^\Omega dE\sqrt{E}\coth\left(\beta\frac{\sqrt{E}}{2}\right)\frac{\partial}{\partial E}\log\left(1+\frac{i\lambda}{2\sqrt{E+i\epsilon-W(a)}}\right). \quad (5.42)$$

The force in the Dirichlet limit (the cutoff Ω can again be sent to ∞ without problems) is

$$\mathcal{F}_\infty \simeq \frac{1}{4\pi}\frac{dV}{da}\mathrm{Im}\int_0^\infty dE\sqrt{E}\coth\left(\beta\frac{\sqrt{E}}{2}\right)\frac{\partial}{\partial E}\left(\frac{1}{E-W(a)+i\epsilon}\right), \quad (5.43)$$

and by trading the E derivative with a $W(a)$ derivative inside the integral, taking the imaginary part and the limit $\epsilon \to 0$ we find

$$\begin{aligned}\mathcal{F}_\infty(a,\beta) &\simeq -\frac{1}{4\pi}\frac{dW}{da}\frac{\partial}{\partial W}\int_0^\infty dE\sqrt{E}\coth\left(\beta\frac{\sqrt{E}}{2}\right)(-\pi\delta(E-W)) \\ &= \frac{1}{4}\frac{d}{da}\left(\sqrt{W}\coth(\beta\sqrt{W}/2)\right) \equiv -\frac{d}{da}\Omega(a,\beta), \end{aligned} \quad (5.44)$$

where the last expression defines again a local *thermal quantum potential*

$$\Omega(a,\beta) = -\frac{1}{4}\sqrt{W}\coth(\beta\sqrt{W}/2). \quad (5.45)$$

In the low temperature limit $T \to 0$ we have $\Omega \to -\sqrt{W}/4$ as it should (compare with eq. (5.31)). In the high temperature limit $T \to \infty$, $\beta \to 0$ one finds $\mathcal{F}_\infty \propto T^{-1}dW/da$. Contrary to what one could expect from the known 'classical limit' $\mathcal{F} \propto T/a$ of Casimir force between rigid bodies [84, 4], the force goes to zero when the temperature grows indefinitely. However here we are in a totally different limit, where the background potential is slowly varying and we are considering only the zero reflection term for $\mathcal{G}_0$. The rigid bodies expansion of $\mathcal{G}$ that gives rise to the well-known Casimir force actually is made up of non-local reflection contributions [4].

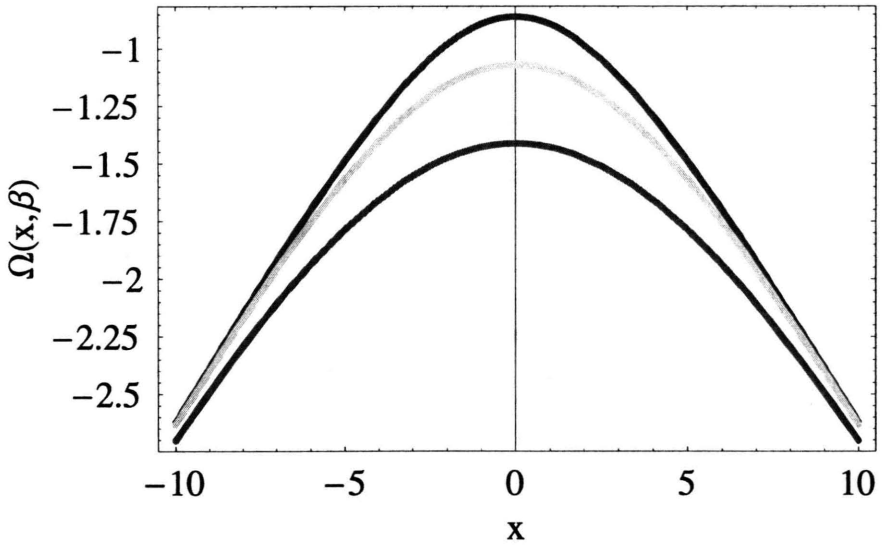

Figure 5-3: *Turning on the temperature does not affect the Casimir buoyancy qualitatively. Here we plot* Ω *for the potential* $W(x) = 10 + x^2$ *and* $\beta = 1, 0.6, 0.4$ *from up down respectively. The minimum of* W *at* $x = 0$ *is always a maximum of* Ω_{WKB}.

This expression is valid whenever WKB is valid, hence when the length-scale of the potential b is such that $Wb^2 \gg 1$. We have already discussed the buoyancy effect, *i.e.* the quantum potential has a maximum where V has a minimum. A non-zero temperature does not modify this prediction qualitatively as can be seen from Figure 5-3.

5.3.4 Reflectionless potentials

The continuum contribution to the Casimir buoyancy vanishes in the Dirichlet limit if a potential is reflectionless. For a reflectionless potential, $\psi^+(k,x) \to \frac{1}{T(k)} e^{ikx}$ as $x \to -\infty$, so $\psi^-(k,x) = \frac{1}{T^*(k)} \psi^{+*}(k,x)$. In this case $\psi^+(k,a)\psi^-(k,a) = |\psi^+(k,a)|^2 / T^*(k)$. Looking back to eq. (5.25), we see that the imaginary part of the logarithm is independent of a so the force vanishes. Thus the Casimir buoyancy in a reflectionless potential is entirely determined by the bound states.

5.3.5 Beyond the range of the potential

Here we consider a background potential which vanishes identically for $|x| > b$. The same results apply to a short range potential ($V(x) \propto e^{-\mu|x|}$) in the limit $x \to \infty$. For $x < -b$ in the Euclidean domain,

$$\begin{aligned} \psi^-(\kappa, x) &= e^{\kappa x} \\ \psi^+(\kappa, x) &= \frac{1}{T(\kappa)} e^{-\kappa x} + \frac{R(\kappa)}{T(\kappa)} e^{\kappa x} \end{aligned} \tag{5.46}$$

The Greens function becomes

$$\mathcal{G}_0(a, a, -\sqrt{\kappa^2 - m^2}) = \frac{1}{2\kappa} \left(1 + R(\kappa) e^{2\kappa a}\right) \tag{5.47}$$

so the buoyancy can be written,

$$\mathcal{F}(\lambda, a) = -\frac{\hbar c}{2\pi} \int_m^\infty \frac{\kappa d\kappa}{\sqrt{\kappa^2 - m^2}} \frac{\partial}{\partial a} \ln \left(1 + \frac{\lambda}{2\kappa} \left(1 + R(\kappa) e^{2\kappa a}\right)\right) \quad \text{for } a < -b. \tag{5.48}$$

For $x > b$ a similar expression holds with $R \to \overline{R}$, the reflection coefficient on the right. If the potential is symmetric, then $\overline{R} = R$. If the mass, m, of the fluctuating field is non-zero, then $\mathcal{F}$ falls like e^{-2ma} when $a > b$. The explicit form depends on the reflection coefficient in the Euclidean domain. In Section IV the explicit example of a δ-function background is studied.

5.3.6 First Born approximation

When the background potential is weak the Casimir buoyancy can be expanded in powers of V. The first term is simple when $m = 0$ and $\lambda \to \infty$. A straightforward calculation gives the Greens function to $\mathcal{O}(V)$,

$$\mathcal{G}_0(a, a, E) = \frac{i}{2k} + \frac{1}{4k^2} \left(e^{2ika} \int_{-\infty}^a dy e^{-2iky} V(y) + e^{-2ika} \int_a^\infty dy e^{2iky} V(y)\right) + \mathcal{O}(V^2). \tag{5.49}$$

$\mathcal{G}_0$ has no bound states at this order, so only the continuum contribution in eq. (5.25) need be calculated. Straightforward evaluation leads to

$$\mathcal{F}_1 = -\frac{\hbar c}{2\pi} \int_{-\infty}^{\infty} \frac{dz}{2z} V(z+a) = -\frac{\hbar c}{4} \mathbf{H}[V,a] \tag{5.50}$$

(where the integral is intended as the Cauchy principal value) which is a non-local functional of V known to mathematicians as the *Hilbert transform* $\mathbf{H}$ of V [85] at the point a.

5.4 Examples

In this section we report the Casimir buoyancy in three explicit sample background potentials and use them to study the domains of application of the approximations in the previous section. First we treat the potential $\ell(\ell+1)/x^2$ on the half-line $x > 0$. Second we explore the family of Pöschl-Teller potentials, $-n(n+1)\mathrm{sech}^2 x$. Finally we study the δ-function, $\beta\delta(x)$, which has been studied in other contexts[64].

5.4.1 $V(x) = \ell(\ell+1)/x^2$

The potential V_0/x^2 leads to a well defined problem on the half-line $x > 0$ when V_0 is positive. It is convenient to parameterize V_0 by $\ell(\ell+1)$, so we can use results familiar from the study of three dimensional central potentials. Note, however, that ℓ need not be integer. Since $V(x)$ is positive definite there is no obstruction to taking $m = 0$, which we adopt to simplify the calculation. The formalism of Section II has to be modified slightly on account of the boundary at $x = 0$. In particular, the Jost solution $\psi^-(x,E)$ has to be replaced by the solution, $\phi(x,E) \propto j_\ell(kx)$, *regular at* $x = 0$. The other Jost solution is given by $h_\ell^{(1)}(kr)$. With this adaptation, and noting that the potential has no bound states, we can compute the Casimir buoyancy as an integral over scattering states, rotated to imaginary momentum,

$$\mathcal{F}(\lambda,\ell,a) = -\frac{\hbar c}{2\pi a^2} \int_0^\infty d\xi \left(-\ln\left(1 + \lambda a I_{\tilde{\ell}}(\xi) K_{\tilde{\ell}}(\xi)\right) + \frac{\lambda a I_{\tilde{\ell}}(\xi) K_{\tilde{\ell}}(\xi)}{1 + \lambda a I_{\tilde{\ell}}(\xi) K_{\tilde{\ell}}(\xi)} \right) \tag{5.51}$$

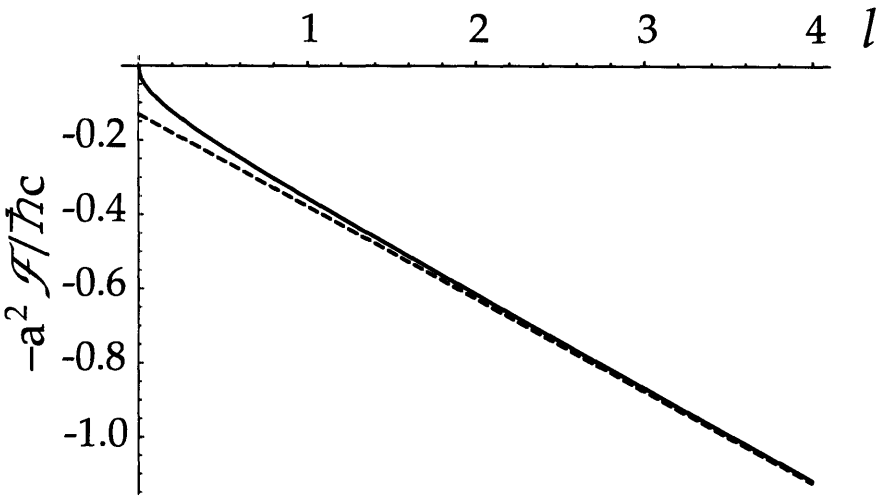

Figure 5-4: *Casimir buoyancy, $-a^2\mathcal{F}/\hbar c$, for $V(x) = \ell(\ell+1)/x^2$ in the Dirichlet limit. The dashed curve is the exact result of eq. (5.52). The solid curve is the WKB approximation, eq. (5.53).*

where $\tilde{\ell} = \ell + 1/2$, and I_ν and K_ν are modified Bessel functions. It is easy to verify that the ξ integral is convergent. In the Dirichlet limit the buoyancy is simply proportional to $1/a^2$ (for dimensional reasons it could not be different),

$$\lim_{\lambda\to\infty} \mathcal{F}(\lambda,\ell,a) = \mathcal{F}_\infty(\ell,a) = -\frac{\hbar c}{2\pi a^2}\int_0^\infty d\xi \left(1 + \xi\frac{I'_{\tilde{\ell}}(\xi)}{I_{\tilde{\ell}}(\xi)} + \xi\frac{K'_{\tilde{\ell}}(\xi)}{K_{\tilde{\ell}}(\xi)}\right) \tag{5.52}$$

The potential $\ell(\ell+1)/x^2$ is neither weak nor reflectionless. It is however smooth and deep, so the WKB approximation should be accurate. $\mathcal{F}_{\rm WKB}(\lambda,\ell,a)$ can be calculated easily from eq. (5.31), and the limit $\lambda \to \infty$ is particularly simple,

$$\mathcal{F}_{{\rm WKB}\ \infty}(\ell,a) = -\frac{\hbar c\sqrt{\ell(\ell+1)}}{4a^2} \tag{5.53}$$

The exact result and the WKB approximation are compared in the $\lambda \to \infty$ limit in Fig.5-4. The difference is very small once $\ell > 1$. In fact WKB does even better: if we make the standard Langer replacement, $\sqrt{\ell(\ell+1)} \to (\ell + \frac{1}{2})$[81, 82], then the WKB and exact results coincide within the widths of the lines in Fig. 5-4.

In Fig. 5-5 we compare the exact result with the WKB approximation for finite

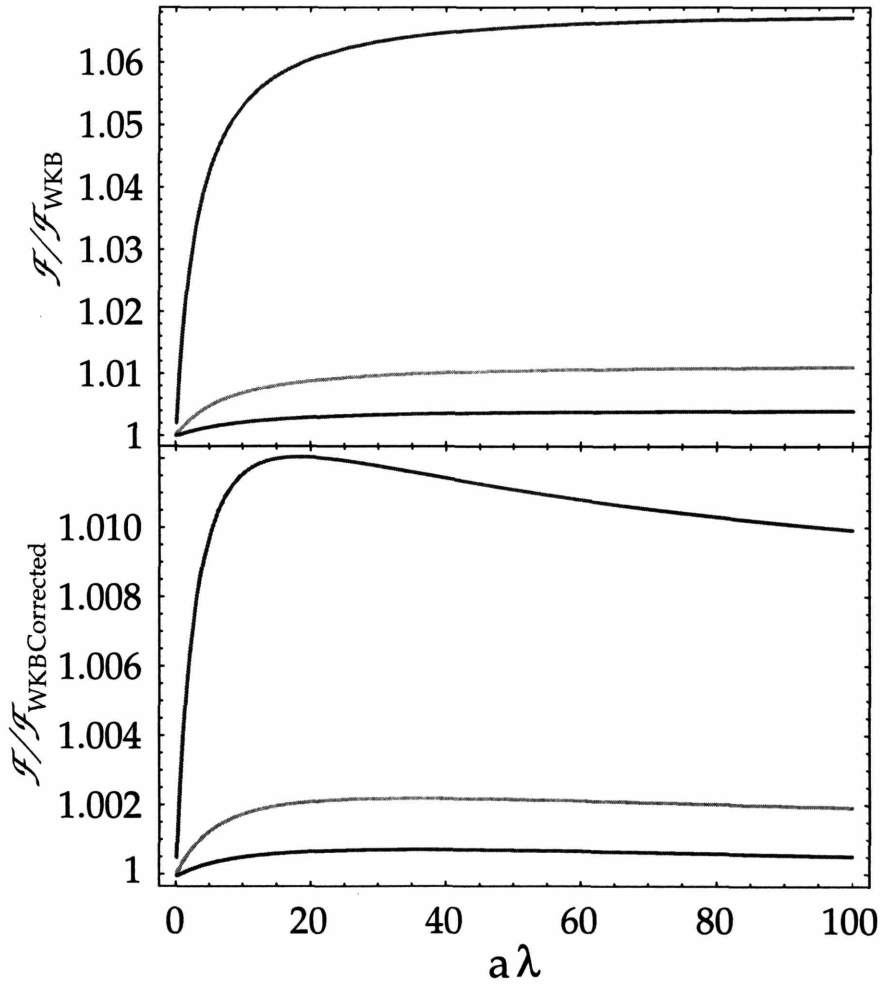

Figure 5-5: *(a) Ratio of Casimir buoyancy to the WKB approximation for* $V(x) = \ell(\ell+1)/x^2$. *Up to down (red to blue)* $\ell = 1, 3, 5$; *(b) Same as (a) with the "correction",* $\ell(\ell+1) \to (\ell+\frac{1}{2})^2$.

λ. Clearly WKB is an excellent approximation in this case.

5.4.2 Pöschl-Teller potentials

The potentials $V_n^{\rm PT}(x) = -n(n+1)\mathrm{sech}^2(x)$, $n = 1, 2, 3, ...$, are reflectionless and the associated solutions to the Schrödinger equation can be expressed in terms of elementary functions.[10] The Casimir buoyancy can be computed from the bound states alone. For simplicity we restrict ourselves to the $\lambda \to \infty$ limit in this case. In practice, it is easier to compute the integrals in the Euclidean region using eq. (5.20) since the scattering wavefunctions, $\psi^{\pm}(E, a)$ are easy to construct but the roots of $\psi^{\pm}(E_{j^{\pm}}(a), a) = 0$ are hard to find for $n > 2$. The necessary Jost solutions for imaginary momentum are given by

$$\psi_n^{\pm}(\kappa, x) = \left(\frac{d}{dx} - \tanh x\right)\left(\frac{d}{dx} - 2\tanh x\right) ... \left(\frac{d}{dx} - n\tanh x\right) e^{ikx}\Big|_{k=\pm i\kappa} \tag{5.54}$$

up to an inessential normalization. The necessary product of Jost solutions is given by

$$\begin{aligned} \psi_1^+(\kappa, a)\psi_1^-(\kappa, a) &= \tanh^2 a - \kappa^2 \\ \psi_2^+(\kappa, a)\psi_2^-(\kappa, a) &= (1 - \kappa^2 - 3\kappa\tanh a - 3\tanh^2 a)(1 - \kappa^2 + 3\kappa\tanh a - 3\tanh^2 a) \end{aligned} \tag{5.55}$$

for example for $n = 1$ and $n = 2$. The required integrals can be performed explicitly for $n = 1$ and numerically for larger n.

The case $n = 1$ is particularly simple and instructive:

$$\mathcal{F}_1^{\rm PT}(m, a) = \hbar c \frac{\tanh a\ \mathrm{sech}^2 a}{2\sqrt{m^2 - \tanh^2 a}} \tag{5.56}$$

As usual the Casimir force is in the direction opposite to the gradient of $V(x)$. The

[10] The apparent dimensional inconsistency in $V_n^{\rm PT}$ needs a word of explanation. If we begin with a dimensionally correct Hamiltonian, $-d^2/dx^2 + m^2 - V_0\mathrm{sech}^2(x/b)$ and define a dimensionless unit of distance, $z = x/b$, then $V_0 b^2$ is the dimensionless potential which equals $n(n+1)$ in the Pöschl-Teller problem.

WKB approximation to the Pöschl-Teller potentials is

$$\mathcal{F}^{\rm PT}_{n\ {\rm WKB}}(m,a) = \hbar c n(n+1)\frac{\tanh a\ \mathrm{sech}^2 a}{4\sqrt{m^2 - n(n+1)\mathrm{sech}^2 a}} \tag{5.57}$$

In order to understand how well the WKB result approximates the exact results we have plotted the force $\mathcal{F}$ divided by $\sqrt{n(n+1)}$ for fixed $\mu \equiv m/\sqrt{n(n+1)} = \sqrt{2}$. In these variables, the WKB result eq. (5.57) is independent of n and the the exact curves tend to the WKB curve as n is increased. This is no surprise since for large n the Poschl-Teller potential becomes more and more semiclassical.

Even for large n, however, if $\mu \simeq 1$ we cannot use WKB since the minimum of the potential at $x = 0$ is *almost* a turning point, *i.e.* $(V(0)+m^2)b^2 \ll 1$ (remember we set $b = 1$). In this case however we can resort to the harmonic oscillator approximation of Section 5.3.2 which, for $a \to 0$ and specializing to the Poschl-Teller potential, takes the form (the notation is the same as in Section 5.3.2)

$$\mathcal{F}^{\rm PT}_{n\ {\rm h.o.}} \simeq \frac{1}{4\pi}(n(n+1))^{3/4} a f\left(\frac{m^2 - n(n+1)}{\sqrt{n(n+1)}}\right). \tag{5.58}$$

The results are plotted in Figure 5-7. As in the comparison with WKB the agreement is better the higher n, *i.e.* the more 'semiclassical' is the potential.

5.4.3 δ-function background

The case of a localized background potential reaches the extreme limit when $V(x) \to \beta\delta(x)$. The Casimir force here is a non-local effect, as can be understood from the fact that the potential vanishes (almost) everywhere, and the overall sign of the force cannot be predicted *a priori*. The WKB approximation as developed in the previous section includes only the local semiclassical modification of the Green's function, which vanishes in this case. There is a semi-classical method for this case (*e.g.* as $\beta, \lambda \to \infty$) which sums over classical paths that reflect from one surface to the other[9, 4] and accounts successfully for both the sign and the magnitude of the Casimir force. By applying the analysis of Section III.C with $R(k) = \overline{R}(k) = \beta/(2ik-$

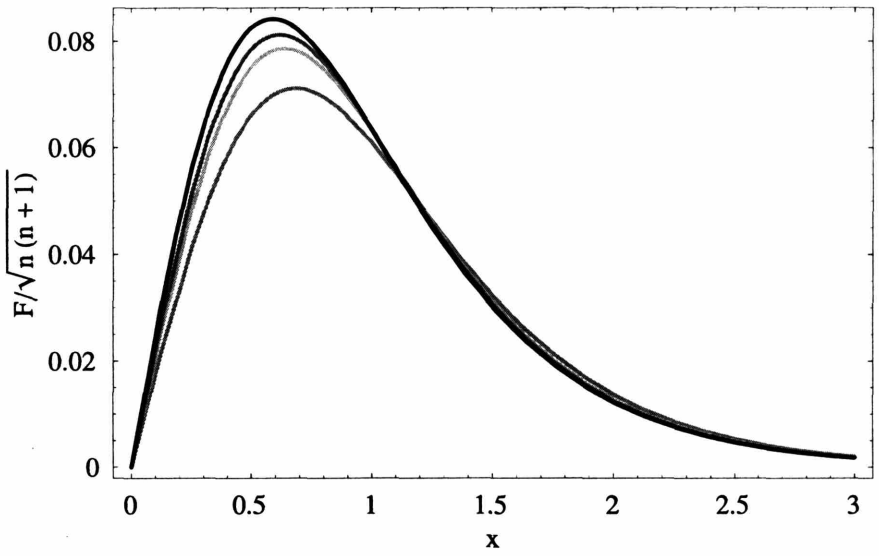

Figure 5-6: *Casimir force for Poschl-Teller potential in the Dirichlet limit. Exact vs. WKB results. From down up (red, green and blue) we have the exact results for* $n = 1, 2, 3$ *and in on the top, in black, the WKB approximation.* $\mu^2 \equiv m^2/n(n+1) = 2$ *for all the curves.*

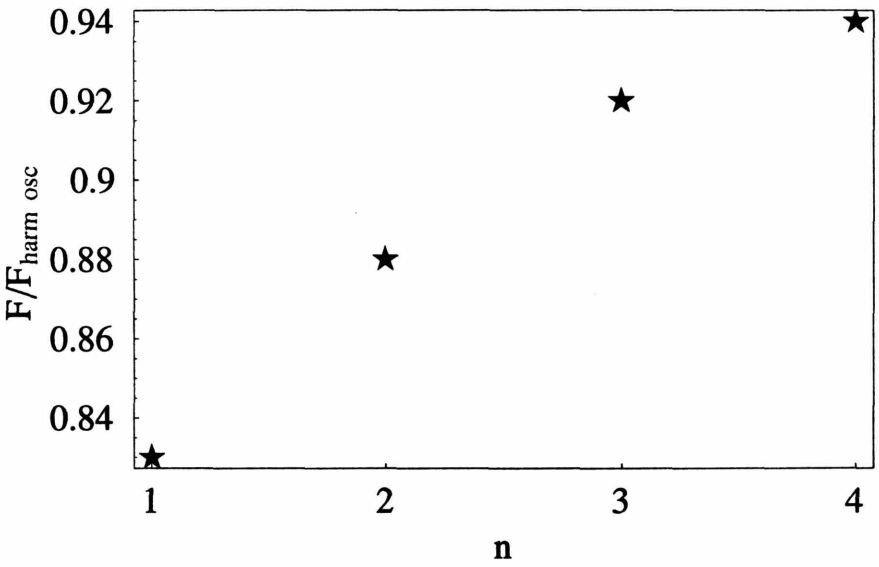

Figure 5-7: *Casimir force for Poschl-Teller potential in the Dirichlet limit. Exact vs. the harmonic oscillator approximation, eq. (5.58). On the vertical axis we plotted the ratio of the Casimir force and the harmonic oscillator approximation* $a \to 0$ *for* $n = 1, 2, 3, 4$. *For all the points we chose* m^2 *such that* $V(0) + m^2 = 0$, *so* $x = 0$ *is a turning point.*

β), we obtain

$$\mathcal{F}(\lambda,\beta,m,a) = -\frac{\hbar c}{2\pi}\int_m^\infty \frac{\kappa d\kappa}{\sqrt{\kappa^2-m^2}}\frac{\partial}{\partial a}\ln\left(1+\frac{\lambda}{2\kappa}\left(1-\frac{\beta}{2\kappa+\beta}e^{-2\kappa a}\right)\right) \tag{5.59}$$

The special case $\beta = \lambda$ has been studied in other contexts (see eq. (70) of Ref. [86]), and our result agrees for that special case. For $\lambda \neq \beta$ however no new physics arises and we will not study that case here. More interesting is the limit $\lambda, \beta \to \infty$ with $m = 0$ in which case the integral can be performed yielding

$$\mathcal{F} = -\frac{\hbar c\pi}{24a^2}, \tag{5.60}$$

the correct Casimir force for two impenetrable walls in one dimension at distance a from each other.

Another interesting limit is $\lambda \to \infty$, $\beta \to 0$ for $m = 0$ which makes contact with the Born approximation of Section III.D,

$$\mathcal{F}(\lambda,\beta,m,a)|_{m=0,\lambda\to\infty} = -\frac{\hbar c\beta}{4\pi a} + \mathcal{O}(\beta^2) \tag{5.61}$$

which agrees with the result obtained from eq. (5.50). Here we have a non-local force which is still a buoyancy force.

5.5 Beyond one dimension

Field theories become more divergent in higher dimensions. Casimir effects are no exception, indeed they are more problematic because both the loop divergences and the sharp background divergences become worse. Methods for renormalizing the loop divergences, at least in dimensions where the interaction with the background field is, in fact, renormalizable, have been worked out in Refs. [77, 86, 64]. Divergences arising from the sharp background can be avoided by smoothing out the δ-function as described in Ref. [77].

Once the buoyancy has been calculated in one dimension, the extension to higher

dimensions can be constructed by the methods of Ref. [78]. The core dynamics is the same in higher dimensions. The results can be summarized as follows: All the results for $n = 1$ generalize to any $n < 2$ without complication. For $2 \leq n < 3$ the generalization succeeds *except that the limit* $\lambda \to \infty$ *cannot be taken.* In that range of n the Casimir buoyancy depends on the cutoff, λ, on the strength of the boundary interaction. Thus there is no separation of scales, no "effective" low energy description of Casimir buoyancy. As $n \to 3$ two further complications arise: first, a new counterterm, $\mathcal{L}_{\rm CT} = c_2\sigma^2$, must be introduced to renormalize the two point (in the background field, σ) function. This means that the buoyancy depends on a renormalized coupling, actually the mass of the σ, that has to be specified. Second, as suggested by the appearance of an interaction proportional to $\sigma^2(x)$ induced by renormalization, the δ-function gives a divergent buoyancy. Instead it is necessary to smooth it out, replacing it for example, by a Gaussian, as described in detail in Ref. [77]. The buoyancy force then depends explicitly on the structure of the surface as well as the shape of the background. In the case of a real material one should make oneself sure of giving a proper description of the reaction of the material, using for example a plasma model for the metal with plasma frequency $\omega_{\rm plasma}$. In that case we expect that, if the $\lambda \to \infty$ and the $\omega_{\rm plasma} \to \infty$ limits exist then they coincide.

The problem of interest is an $n-1$ dimensional hyperplane immersed in a medium which is modulated in the $x_\perp$-direction. As shown in Ref. [78], the Casimir energy (per unit 'area' of the $n-1$ transverse directions) for such an interface can be written as,

$$\mathcal{E}^n = \frac{1}{2}\int \frac{d^{n-1}p}{(2\pi)^{n-1}} \int_0^\infty dE \left(\sqrt{p^2+E} - \sqrt{p^2+m^2}\right)\left(\frac{dN}{dE} - \sum_{k=1}^{M} \frac{dN^{(M)}}{dE}\right) + \mathcal{E}_{\rm FD}(M) \tag{5.62}$$

where $\sqrt{E} = \sqrt{k^2+m^2}$ is the contribution to the energy from momentum in the $x_\perp$ direction. dN/dE is the density of states for the one dimensional problem and $dN^{(M)}/dE$ is the contribution to the density of states to $M^{\rm th}$ order in the background field, $\sigma(x) = \lambda\Delta(x-a)+V(x)$.[11] $\mathcal{E}_{\rm FD}(M)$ is the contribution of the Feynman diagrams

[11]The "Levinson" subtraction discussed at length in Ref. [78], is unnecessary here since the first

through M^{th} order in the background field plus the contributions of counterterms necessary for renormalization.

The number of Born subtractions is determined by the degree of divergence of the field theory in σ with a $\sigma\phi^2$ coupling. For $n < 3$ only the tadpole diagram diverges, so only the first Born approximation must be subtracted. For the moment we set $N = 1$ and discuss the extension to $n = 3$ at the end of this section.

The p-integration in eq. (5.62) is to be understood in the sense of dimensional regularization, and can be performed,[12]

$$\mathcal{E}^n = -\frac{1}{2}\frac{\Gamma(-n/2)}{(4\pi)^{n/2}}\int_0^\infty dE\ E^{n/2}\left(\frac{dN}{dE} - \frac{dN^{(1)}}{dE}\right) + \mathcal{E}_{\text{FD}}(1) \tag{5.63}$$

The first Born approximation and the contribution of the tadpole diagram plus counterterm are linear in λ and linear in V. Therefore the V dependent term they generate is independent of a, so they do not contribute to the buoyancy and can be dropped,

$$\mathcal{F}^n = \frac{1}{2}\frac{\Gamma(-n/2)}{(4\pi)^{n/2}}\int_0^\infty dE\ E^{n/2}\frac{\partial^2 N}{\partial a \partial E} \tag{5.64}$$

This remarkably simple form is valid for $n < 3$, and, of course, agrees with Section II for $n = 1$.

As in one dimension, we take $\sigma(x) = \lambda\delta(x-a)+V$, construct the Greens function, rotate the integration to the negative E axis and integrate by parts,

$$\mathcal{F}^n = -\frac{1}{2\pi}\frac{\Gamma(1-\frac{n}{2})\sin\frac{n\pi}{2}}{(4\pi)^{n/2}}\int_0^\infty dE E^{\frac{n}{2}-1}\frac{\partial}{\partial a}\ln\left(1+\lambda G_0(a,a,-E)\right). \tag{5.65}$$

This should be compared with eq. (5.16), which is the specialization to $n = 1$.

Note that the poles in $\Gamma(1-n/2)$ are cancelled by the factor of $\sin n\pi/2$, which arose from the imaginary part of $(-E)^{n/2}$. Thus the only singularities in eq. (5.65)

Born subtraction does not contribute. To carry through the analysis for $n = 2$ a Levinson subtraction would be necessary.

[12]Formally, the integral is defined and performed for values of Re n small enough that it converges. It is then analytically continued to real, positive n, with careful treatment of singularities encountered along the way.

arise from divergences at the upper limit of the E integration. These get more serious as n increases because of the prefactor of $E^{n/2-1}$. It is easy to see that the E-integral in eq. (5.65) converges for $n < 3$: The high (negative) energy behavior of $G(a, a, -E)$ is dictated by the WKB approximation, eq. (5.29),

$$G(a, a, -E) \to \frac{1}{2\sqrt{E + W(a)}} + \mathcal{O}\left(E^{-1}\right) \tag{5.66}$$

(here again $W = m^2 + V$) and this behavior leads to a convergent integral for $n < 3$. However, if we attempt to take $\lambda \to \infty$ before doing the integral, we lose convergence already at $n = 2$.

Beyond eq. (5.65) the buoyancy depends on the specific form of $V(x)$. To get a feel for its variation, we evaluate the WKB approximation,

$$\mathcal{F}^n_{\text{WKB}} = \frac{\lambda}{2(4\pi)^{\frac{n}{2}+1}} W^{\frac{n-3}{2}} \frac{dV}{da} \Gamma\left(1 - \frac{n}{2}\right) \sin\left(n\frac{\pi}{2}\right) f\left(\frac{\lambda}{2\sqrt{W(a)}}\right), \tag{5.67}$$

where

$$f(x) = \int_0^\infty dy y^{n/2-1} \frac{1}{y+1} \frac{1}{\sqrt{y+1} + x}. \tag{5.68}$$

This function can be expressed by means of hypergeometric functions as

$$f(x) = -\frac{\pi}{x}\left(\left(1 - x^2\right)^{\frac{n}{2}-1} - 1\right) \csc\left(\frac{n\pi}{2}\right) + \frac{2}{\sqrt{\pi}} \Gamma\left(\frac{3}{2} - \frac{n}{2}\right) \Gamma\left(\frac{n}{2}\right) F\left(1; \frac{3}{2} - \frac{n}{2}, \frac{3}{2}; x^2\right) \tag{5.69}$$

however does not carry much more information than the original integral, in particular because the interesting limit $\lambda \to \infty$ translates in $x \to \infty$ where the hypergeometric function has both a real and an imaginary part. The imaginary part is cancelled by the first term and the real part is the one we are interested in but this is difficult to isolate. However, before carrying on an asymptotic analysis of this integral it is straightforward to evaluate the $n = 2$ result

$$\mathcal{F}^{n=2}_{\text{WKB}} = \frac{1}{16\pi} \frac{dV}{da} \log\left(1 + \frac{\lambda}{2\sqrt{W(a)}}\right) = -\frac{d}{da} \Omega^{n=2}_{\text{WKB}}, \tag{5.70}$$

where the quantum potential is

$$\Omega_{\rm WKB}^{n=2} = -\frac{1}{16\pi}\left(\frac{\sqrt{W}\,\lambda}{2} + \left(W - \frac{\lambda^2}{4}\right)\log(1 + \frac{2\sqrt{W}}{\lambda}) - W\,\log(\frac{2\sqrt{W}}{\lambda})\right). \quad (5.71)$$

Neither the quantum potential nor the force have a finite limit when $\lambda \to \infty$ in 2 dimensions. They diverge logarithmically in λ. The case $n = 1$ result coincides with the result of Section II.

Let us now return to the original integral representation to get an asymptotic expansion for large x (*i.e.* large λ). Writing it as

$$f(x) = \int_0^\infty dz e^{-zx} 2 \int_1^\infty dy e^{-yz} \frac{1}{y}(y^2 - 1)^{n/2-1}, \quad (5.72)$$

performing the integral over y, expanding in series for small z and integrating term by term in z one gets[13]

$$\begin{aligned} f(x) \;&\simeq\; 2\pi \frac{1}{x^{3-n}} \csc(n\pi) + \frac{1}{x}\pi \csc\left(\frac{n\pi}{2}\right) + (2-n)\pi \frac{1}{x^{5-n}} \csc(n\pi) - \\ &-\; \frac{\Gamma(\frac{1}{2} - \frac{n}{2})\Gamma(\frac{n}{2})}{\sqrt{\pi}x^2} + \mathcal{O}\left(x^{-3}\right) + \mathcal{O}\left(x^{n-7}\right). \end{aligned} \quad (5.73)$$

This expansion agrees very well with the exact expression eq. (5.69) already at $x \simeq 2$, as can be seen in Figure 5-8, except in the limit $n \to 1$. The expansion (5.73) has a pole in $n = 1$ that goes like x^{-4}. This is not present in the original function f and indeed adding more terms pushes the pole to higher and higher powers of x^{-1}. However in this case we know the exact result either from Section II (equation (5.30)) or by taking the limit $n \to 1$ of eq. (5.69) *before* expanding for $\lambda \to \infty$ (the two limits do not commute).

One thing to notice is that in passing from $n < 2$ to $n > 2$ the first term in eq. (5.73) becomes dominant over the second one. At exactly $n = 2$ they almost cancel each other leaving behind a term $\log(x)/x$ which reproduces the leading term

[13]Alternatively one could use the Mellin representation of the hypergeometric function [83] and move the contour of integration in order to pick the desired poles. This procedures is much more involved than the one described here and yields the same results.

in eq. eq. (5.70) (also the higher order terms agree with the expansion of eq. (5.70) for $\lambda \to \infty$). Another thing is that from this asymptotic expansion one can see that in the Dirichlet limit one has a finite force if and only if $n < 2$. For $n < 2$ the second term in eq. (5.73) is dominant over the first one and hence the force is independent of λ

$$\mathcal{F}_{\infty}^{n<2} \simeq \hbar c \frac{dV}{da} \frac{1}{4(4\pi)^{\frac{n}{2}}} W^{\frac{n-2}{2}} \Gamma\left(1 - \frac{n}{2}\right). \tag{5.74}$$

Having neglected the first term in eq. (5.73), however, this form cannot be used when $n \to 2$. Incidentally however notice that the limit $n \to 1$ now can be taken safely (and it gives the usual result eq. (5.31)) since we have not included the term $\propto \csc(n\pi)/x^{3-n}$ which generated pole in $n = 1$. This pole was a fiction of our procedure of taking the limit $\lambda \to \infty$ before $n \to 1$. It was signifying that for $n = 1$ the next term in the large x expansion of f decreases slower than $1/x^2$, indeed it is $\propto \log(x)/x^2$. As we said, including more and more terms in the asymptotic expansion pushes this pole further and further away.

As anticipated, for $n \geq 2$ the buoyancy force diverges when $\lambda \to \infty$. Keeping the first term in eq. (5.73) one obtains

$$\mathcal{F}_{\infty}^{n>2} \simeq \frac{\hbar c}{4^n \pi^{\frac{n}{2}}} \frac{dV}{da} \lambda^{n-2} \Gamma\left(1 - \frac{n}{2}\right) \sec\left(n\frac{\pi}{2}\right). \tag{5.75}$$

Notice that for $n \to 3$ we have a structure $\mathcal{F} \propto \frac{1}{n-3}\lambda dV/da$ which comes from a term $\propto \log \Lambda \int d^4x (V(x) + \lambda\delta(x-a))^2$ in the effective action (here Λ is the QFT cutoff). The pole $1/(n-3)$ from $\sec(n\pi/2)$ is the dimensional regularization way of seeing the logarithmic divergence $\log \Lambda$ in the two-legs graphs for $3+1$ dimensions.

The result eq. (5.67) (and its asymptotic expansions eq. (5.74) and eq. (5.75)) embodies all the behaviors we expect from the general analysis. It is a continuous function of n and finite for $n < 3$ and the Dirichlet limit, $\lambda \to \infty$, can only be taken for $n < 2$.

To go all the way to $n = 3$, the plane in three dimensional space, it would be necessary to invoke the full apparatus of the field theoretic approach to Casimir effects: the surface must be smoothed out and the second Born approximation to the

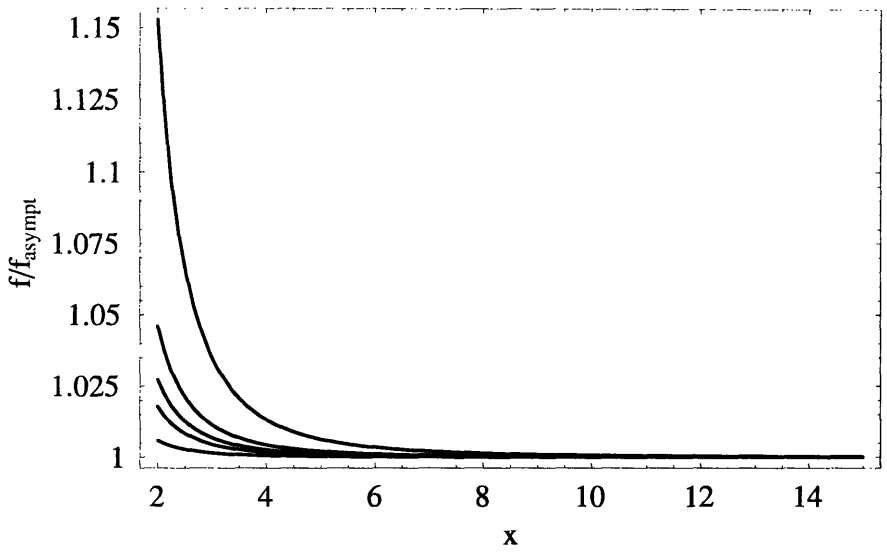

Figure 5-8: *Comparison of f in eq. (5.69) with its asymptotic expansion eq. (5.73) for various n from up to down $n = 1.4, 1.8, 2, 2.2, 2.6$.*

density of states must be subtracted from the E-integration and added back together with the counterterm as a Feynman diagram.

5.6 Is Casimir Buoyancy universal?

In the previous examples we have found Casimir buoyancy is ubiquitous. However all the previous examples share the fact that they can be very well described by the zero-order reflection term in the propagator. The WKB approximation was always an excellent approximation. There are obvious examples in which this is not true: Take for example the background V as made of a tall wall (a tall square wall will do the job) *plus* a shallow potential, decreasing toward the wall. If the shallow potential would not be present the delta function would be attracted toward the wall so for continuity this must be true for sufficiently small potentials *even if the total potential is decreasing toward the wall.* This is true because in the expression for the propagator $\mathcal{G}_0$ we cannot neglect the influence of the tall wall (that is why we called it 'tall') and this enters only through a non perturbative term in the form of the contribution from a closed path that goes from a to the wall and bounces back to a. More quantitatively by considering the background as made up of a wall and a smooth W, one can expand

the propagator as [22]

$$\mathcal{G}_0(a,a,E) = \frac{i}{2\sqrt{E-W(a)}} + \frac{ie^{-i\pi\mu/2}}{2\sqrt{E-W(a)}} e^{iS_1(a,a,E)} \tag{5.76}$$

where $S_1(a,a,E)$ is the action of the closed path that goes from a to a bouncing on the wall and μ is the Maslov index of this orbit ($\mu = 1$ is the wall is 'smooth' on frequencies $\sqrt{E}$ and $\mu = 2$ for otherwise 'hard' walls). Inserting into eq. (5.15) one finds a general formula including both local (e.g. W and its derivatives) and non-local (depending on integrals of W or independent of W) contributions. The two effects interplay and they are difficult to separate but it is easy to extract the two limits: 1) When $W \to 0$ one recovers the Casimir attraction between impenetrable plates (compare with eq. (5.59) with $\beta \to \infty$) 2) When the wall is far away ($S_1 \gg 1$) the second term is exponentially smaller than the first and we find buoyancy from the first term only.

In general then a more correct statement would be that *Casimir buoyancy will occur in the cases where non-local effects, like closed orbits contributions to the propagator, are negligible.* We believe we have presented enough examples here to convince the reader that this is not a too stringent request.

Chapter 6

A duality between the properties of nodal lines of random functions and the Casimir energy

In this chapter I will put forward a duality between the statistical properties of nodal lines in random waves and the Casimir energy.

Random waves are a good model for several problems in statistical physics and in problems of wave scattering. I will show that some of this properties, in particular the probability of having a given configuration of nodal lines is equal to the (exponential) of the Casimir energy of a corresponding configuration of conductors.

6.1 Introduction

Random waves (RW) have been an object of interest for their statistical properties both in wave mechanics and statistical mechanics. In wave mechanics they turned out to be an incredibly interesting and rich scenario for studying the statistics of topological properties, like phase singularities [88]. In optics they made a good statistical model for speckle patterns [89] in laser beams. In quantum mechanics they have been studied [90, 91] in connection with semiclassical wave functions in chaotic billiards. In statistical mechanics their properties have been put in connection with

the statistic of defects and vortices [92] and an interesting duality with a percolation problem has been put forward recently [93].

The purpose of this chapter is to exploit in a new direction the description of RW in terms of quantum field theory (QFT).[1] I will make a quantitative connection between the ground state energy (or Casimir energy) of a scalar field in a given configuration of semi-penetrable conductors in $d-1$ space dimensions and the probability of having a certain configuration of nodal lines in d dimensions.

This chapter is far from being exhaustive or self-contained. I will briefly introduce the concept of random wave referring the reader to the existing literature for their statistical properties, in particular the properties of their nodal lines. I will then rephrase the concept of Casimir energy for a scalar field in a static background (a toy model for QED where the static background models the conductors) in a language closer to that of random waves statistics. I will then point out the connection between Casimir energy in this background and probability of having a certain nodal line configuration. Finally I will draw some consequences on the nodal line probability and comment on the possible extensions on which further work is needed.

6.2 Random Waves

An isotropic random wave (RW) in d dimensions is the random function defined on a subset of $\mathbb{R}^d$ (we will not use any particular notation for vectors but there is little room for confusion) as

$$\phi(x) = \sum_{j=1}^{J} \sqrt{\frac{2}{J}} \epsilon(k_j) \cos(k_j x + \delta_j) \tag{6.1}$$

where the phases δ_j are uniformly distributed in $[0, 2\pi)$ and the vectors k_j are random variables as well. We will assume isotropy of ϵ, *i.e.* $\epsilon(k)$ is an even, analytic function of the length of the vector k.

[1] The statistical mechanics description of RW is related to this via the usual QFT-statistical mechanics duality (Wick rotation). In this sense this description is already contained in the work of B. Halperin in [89] who employed it to study the statistic of vortices and defects.

For any finite J the moments $\langle\phi(x_1)...\phi(x_n)\rangle$ are not factorizable, but in the limit $J \to \infty$ Wick theorem holds [88] (among other things one requires the existence and finiteness of at least the second moment, *i.e.* $\langle\phi^2(x)\rangle < \infty$):

$$\langle\phi(x_1)...\phi(x_{2n})\rangle = \sum_{\text{Contractions}} \langle\phi(x_i)\phi(x_j)\rangle ... \langle\phi(x_k)\phi(x_l)\rangle . \tag{6.2}$$

In the following we will hence always assume the limit $J \to \infty$ is taken.

Wick's theorem is equivalent to saying that the statistical properties of RW can be described by a Gaussian probability functional

$$P[\phi] = \frac{1}{Z} \exp\left(-\frac{1}{2}\int d^d x d^d x' \phi(x') h(x', x) \phi(x)\right), \tag{6.3}$$

where Z is a normalization constant and $h(x', x) = h(|x' - x|)$ for isotropic RW. From this probability functional the reader could already recognize the usual set-up of the statistical mechanics of a non-interacting real field ϕ. The function h is determined by the spectrum $\epsilon(k)$ (and vice versa). We will now determine their connection.

To this purpose is convenient to pass to the Fourier components of the field $\phi_k = \int d^d x e^{ikx}\phi(.x)$ and define $h(k)$ through

$$\int d^d x d^d x' e^{ikx - ik'x'} h(x', x) = (2\pi)^d \delta^{(d)}(k' - k) h(k). \tag{6.4}$$

In terms of ϕ_k the probability functional is

$$P[\phi] = \frac{1}{Z} \exp\left(-\frac{1}{2}\int \frac{d^d k}{(2\pi)^d} h(k) |\phi_k|^2\right). \tag{6.5}$$

The limiting Gaussian probability functional (6.3) or (6.5) can describes the statistical properties of (6.1) if we choose the spectrum $\epsilon(k)$ as

$$\lim_{J\to\infty} \frac{1}{J}\epsilon^2(k) = \frac{1}{h(k)} \frac{d^d k}{(2\pi)^d} \tag{6.6}$$

which means that in the limit $J \to \infty$ the sum over k_j must be substituted by the

integral in $d^d k$ whose measure is given by right-hand side of (6.6). This is the promised connection between $h(x)$ and $\epsilon(k)$. In this way when $J \to \infty$ the propagator G tends to

$$G(x,0) \equiv \langle \phi(x)\phi(0) \rangle = \lim_{J\to\infty} \sum_{j=1}^{J} \frac{1}{J} \epsilon^2(k_j) \cos(k_j x) = \int \frac{d^d k}{(2\pi)^d} \frac{1}{h(k)} e^{ikx}. \tag{6.7}$$

where we used the fact that ϵ is even in k to substitute e^{ikx} for $\cos(kx)$.

There are at least two 'natural' choices for the spectrum $h(k)$:

- The *scalar field* spectrum $1/h(k) = \theta(\Lambda - |k|)/(k^2 + m^2)$ where one has to introduce the cutoff Λ to ensure the finiteness of $G(x,x) = \langle \phi^2(x) \rangle$.

- The very singular *monochromatic* spectrum $h(k)$, such that $1/(2\pi h(k)) = \delta(|k| - K)$. This last choice gives $G(x,0) = J_0(Kx)$ which is a statistical model for the solutions of the Schrödinger equation $-\Delta\psi = K^2\psi$ in chaotic billiards.

6.3 Casimir Energy and Nodal Lines

We now turn to the main point of this chapter: the connection between nodal lines properties and Casimir energy. For simplicity at the moment we assume $d = 2$, the generalization to other d will be straightforward.

Following [91] we introduce the functional

$$X_\gamma[\phi] = \frac{1}{2} \int_\gamma ds \phi^2(x(s)). \tag{6.8}$$

where the integral is defined over the reference line $\gamma = \{x(s) | s \in [0, \ell]\}$ and parameterized with the length of the line itself, s. For any given reference curve γ, $X_\gamma[\phi]$ is a random variable whose generating function $S_\gamma(\lambda)$ is defined as

$$S_\gamma(\lambda) \equiv \left\langle e^{-\lambda X_\gamma[\phi]} \right\rangle = \int \mathcal{D}\phi \; P[\phi] \; e^{-\frac{1}{2}\lambda \int_\gamma ds \; \phi^2(x(s))}. \tag{6.9}$$

It has been shown in [91] that $S_\gamma(\lambda)$ can be interpreted approximately as the prob-

ability of having a nodal line in the tube of radius $r = (\langle(\nabla\phi)^2\rangle\,\lambda)^{-1/3}$ built around the reference curve γ (in d dimensions $1/3$ gets substitutes by $1/(d+1)$). Notice that the radius r of the tube goes to zero when $\lambda \to \infty$. The approximation allowing us to interpret S_γ as the probability of having a nodal line relies mainly on a mean-field approximation where $\phi^2/(\nabla\phi^2) \to \phi^2/\langle(\nabla\phi)^2\rangle$ as discussed in [91]. It is not easy to estabilish the limits of this approximation so we will adopt it as a working hypothesis and we will see later a situation in which it possibly fails. From now on we will simply say that S_γ is 'the probability to have a nodal curve γ' without referring to the tube radius r or the approximation within which this interpretation has been derived.

Let us write in (6.9) $P[\phi]$ explicitly inside the probability functional

$$S_\gamma(\lambda) = \int \mathcal{D}\phi \frac{1}{Z} \exp\left(-\frac{1}{2}\int d^2x d^2x'\ \phi(x')(h(x',x) + \delta^{(2)}(x'-x)V(x))\phi(x)\right), \tag{6.10}$$

where we have defined

$$V(x) = \lambda \int_\gamma ds\ \delta^{(2)}(x - x(s)). \tag{6.11}$$

Let us now specialize the problem in two ways:

- Choose $h(x',x)$ to mimic a scalar field, with a cutoff Λ intended in all the momentum integrals

$$h(x',x) = \delta^{(2)}(x'-x)(-\Delta + m^2). \tag{6.12}$$

- Consider a random wave in the strip $[0,T] \times \mathbb{R}$. Denote the two cartesian coordinates in the plane as x_0, x_1 so $0 \le x_0 \le T$ and $x_1 \in \mathbb{R}$. Choose the reference line γ as made of $n \ge 1$ disconnected lines parallel to the x_0 axis and intersecting the x_1 axis at the points $\{a_1, ..., a_n\}$

$$\gamma = \{a_1, ..., a_n\} \times [0,T]. \tag{6.13}$$

With this assumptions the final expression for the generating function $S_\gamma(\lambda)$ is

then

$$S_\gamma(\lambda) = \frac{1}{Z}\int \mathcal{D}\phi \exp\left(-\frac{1}{2}\int_{[0,T]\times\mathbb{R}} d^2x\ \phi(x)(-\Delta + m^2 + V(x))\phi(x)\right) \tag{6.14}$$

where $\Delta = \partial^2/\partial x_0^2 + \partial^2/\partial x_1^2$. This expression itself is reminiscent of two intertwined concepts in QFT and statistical field theory: the Casimir energy $\mathcal{E}$ in the first and the free energy F in the second. The connection with the latter is evident, without any need for formal manipulations, $F = -\log(S_\gamma(\lambda))$. The connection with the Casimir energy becomes evident as well if we perform a clockwise (inverse) Wick rotation in the x_0 coordinate, $x_0 \to it$. Then (6.14) becomes

$$\frac{1}{Z}\int \mathcal{D}\phi \exp\left(i\frac{1}{2}\int_{[0,T]\times\mathbb{R}} dtdx_1\ \phi(t,x_1)(-\partial^2 - m^2 - V(x_1))\phi(t,x_1)\right) = e^{-i\mathcal{E}_\gamma T}. \tag{6.15}$$

Here $\partial^2 = \partial^2/\partial t^2 - \partial^2/\partial x_1^2$ and $\mathcal{E}_\gamma$ the Casimir energy in the background V and

$$V(y) = \sum_{i=1}^{n} \delta(a_i - y). \tag{6.16}$$

We can now establish the promised connection between the generating functional $S_\gamma(\lambda)$ and the Casimir energy $\mathcal{E}_\gamma$ of the corresponding background as

$$S_\gamma(\lambda) = e^{-T\mathcal{E}_\gamma}. \tag{6.17}$$

In words: *The probability of having a (translationally symmetric) nodal line γ in a random wave ensemble is related to the Casimir energy of a configuration of conductors given by a constant-time section of γ.*

The generalization to d dimension is easily obtained (and is already understood in the previous paragraph). Since a nodal hypersurface has codimension 1 so does its constant-x_0 section. Hence the problem maps to the Casimir energy of codimension 1 surfaces. The dual Casimir problem then is the usual problem of penetrable, codimension 1 surfaces (see [94] for the case with arbitrary codimension). For example, the $d = 4$ case maps into the $\mathbb{R}^3$ Casimir problem with penetrable 2-dimensional sur-

faces. The limit $\lambda \to \infty$ is the limit of perfect conductors (or Dirichlet limit, because $\phi = 0$ on the conducting surfaces).

In the rest of the chapter we will use this duality to make statements on the nodal line statistic from the knowledge of the properties of Casimir energy.

6.4 Applications

Let us start with a well known problem of a Casimir energy calculation: the presence of various divergencies, when taking $\Lambda,\ \lambda \to \infty$. We will now discuss the interpretation of these divergencies for the nodal lines probability.

A volume divergence $\propto V\Lambda^{d+1}$ (divergent when $\Lambda \to \infty$) is removed by the factor of $1/Z$ in our definition of $P[\phi]$. This term is however independent of the presence and shape of γ. In QFT it would represent a cosmological constant term. For what concerns the divergencies arising when $\lambda \to \infty$ (the so-called Dirichlet limit) let us recall that the tube radius r built around the reference line γ, goes to 0 when $\lambda \to \infty$. It is then natural that the probability $S_\gamma(\lambda)$ of having a nodal line within a distance r from γ goes to zero when $\lambda \to \infty$. This reflects in the fact that $\mathcal{E} \to +\infty$ when $\lambda \to \infty$.

We also know that the interaction energy (the one that depends on the distance between the bodies) remains finite when $\Lambda, \lambda \to \infty$. This means that there are some properties of the nodal lines, connected with the interaction part of $\mathcal{E}$, which are well-defined also when the tube radius $r \to 0$ and the cutoff goes to infinity. In order to identify them we must define a quantity which stays finite in this limit. Led by the intuition about the Casimir energy of rigid conductors we recognize that this problem is related to the removal of the self-energy for rigid, disconnected bodies. Suppose then our curve γ is composed of two disconnected pieces $\gamma = \gamma_1 \cup \gamma_2$ (we always require them to be straight and both parallel in the x_0 direction). Their Casimir energy can be written as

$$\mathcal{E}_\gamma = \mathcal{E}_{\gamma_1} + \mathcal{E}_{\gamma_2} + \mathcal{E}_{\text{int}} \tag{6.18}$$

where the first two terms are independent on the distance between the nodal lines and

the last term goes to zero when the distance between the two curves goes to infinity (this can be taken as a definition of $\mathcal{E}_{\rm int}$). The terms $\mathcal{E}_{\gamma_{1,2}}$ are the energies of isolated plates.

Let us define the quantity $\mathcal{P}$ as the ratio of the probability of having $\gamma_1 \cup \gamma_2$ and the probability of having both γ_1 *and* γ_2 independently of each other:

$$\mathcal{P} = \frac{S_{\gamma_1+\gamma_2}(\lambda)}{S_{\gamma_1}(\lambda)S_{\gamma_2}(\lambda)} = e^{-T\mathcal{E}_{\rm int}}. \tag{6.19}$$

The interpretation of $\mathcal{P}$ is the following: if $\mathcal{P} > 1$ ($\mathcal{P} < 1$) then it is easier (more difficult) to find a nodal line γ_2 if another line γ_1 is present.

The interaction energy $\mathcal{E}_{\rm int}$ is always finite (even when $m \to 0$ and/or $\Lambda, \lambda \to \infty$) and hence so is $\mathcal{P}$. Moreover we know from quantum field theory that $\mathcal{E}_{\rm int} < 0$ and that it increases when the nodal lines are pulled apart. Hence we can say that the presence of a nodal line γ_1 makes it easier for another nodal line to be born. Hence in this case nodal lines *induce* other nodal lines in their vicinity.

The choice of the scalar field spectrum allows us to use all the machinery of QFT (including the Hamiltonian formulation) to calculate the Casimir energy $\mathcal{E}_{\rm int}$. Depending on the value of λ, Λ, m and the distance between the nodal lines a, we can use a weak or a strong coupling approximation for $\mathcal{E}_{\rm int}$. Since λ has dimension ℓ^{d-1} (ℓ is a length scale) the relevant dimensionless parameter is $\epsilon = a\lambda^{1/(d-1)}$. Moreover assuming $\Lambda \gg m$, $\langle(\nabla\phi)^2\rangle \sim \Lambda^2$ we have $\lambda \sim 1/r^{d+1}\Lambda^2$. By choosing a, r, Λ we have $\epsilon \ll 1$ for weak coupling and $\epsilon \gg 1$ for the strong coupling regime.

We will now make some explicit sample calculation in these two regimes.

In the *weak coupling* regime can use a Feynman diagram expansion [64] (one must use the Euclidean cutoff Λ on the k integrals) for the Casimir energy $\mathcal{E}$

$$\mathcal{E} = \lambda\mathcal{E}_1 + \lambda^2\mathcal{E}_2 + ... \tag{6.20}$$

where $\mathcal{E}_1$ is given by the tadpole diagram, $\mathcal{E}_2$ is given by the 2 legs diagram and so on. We will now calculate the first two terms of the series (6.20) showing that $\mathcal{E}_1$ drops between numerator and denominator in $\mathcal{P}$ and then calculating the first correction to

$\mathcal{P}$, i.e. $\mathcal{E}_2$. We will also show that $\mathcal{E}_2 < 0$, which implies $\mathcal{P} > 1$, in a region of order $1/m$ around any nodal line.

For the tadpole diagram we have

$$\mathcal{E}_1 = \int d^{d-1}x V(x) \left\langle \phi^2(x) \right\rangle = \left\langle \phi^2(0) \right\rangle \int d^{d-1}x V(x) \tag{6.21}$$

or in Fourier space

$$\mathcal{E}_1 = \int \frac{d^{d-1}k}{(2\pi)^{d-1}} V(k) \int \frac{d^d q}{(2\pi)^d} \frac{1}{q^2 + m^2}, \tag{6.22}$$

where $V(k)$ is the Fourier transform with respect to the $d-1$ spatial dimensions

$$V(k) \equiv \int d^{d-1}x V(x) e^{ikx} \tag{6.23}$$

so that in $d = 2$ and with $V(x) = \delta(x) + \delta(x - a)$ we have

$$V(k) = 1 + e^{ika}. \tag{6.24}$$

Since $\int dx V(x)$ does not depend on a, the tadpole diagram does not contribute to the interaction energy $\mathcal{E}_{\text{int}}$ and hence does not contribute to $\mathcal{P}$. We must then go to the next diagram, the one with two legs to find the first non zero correction to $\mathcal{E}_{\text{int}}$. The two-legs diagram contribution can be written as

$$\mathcal{E}_2 = -\int \frac{d^{d-1}k}{(2\pi)^{d-1}} V(k) V(-k) \int \frac{d^d q}{(2\pi)^d} \frac{1}{(q+k)^2 + m^2} \frac{1}{q^2 + m^2}. \tag{6.25}$$

It contains an a-dependent interaction term. To calculate this a-dependent term we can send $\Lambda \to \infty$ (for $d = 2$ we can take this limit safely) and by means of the usual technology for handling Feynman diagrams we find

$$\mathcal{E}_2 = -\frac{1}{2\pi} \int_0^1 dx \int_{-\infty}^{\infty} \frac{dk}{2\pi} e^{ika} \frac{1}{m^2 + x(1-x)k^2}. \tag{6.26}$$

Performing the integrals gives

$$\mathcal{E}_2 = -\frac{1}{2m}\left(1 - \Phi(2\sqrt{ma})\right), \tag{6.27}$$

where Φ is the error function. Then $\mathcal{P}$ can be written, to this order in λ, as

$$\mathcal{P} = e^{T\frac{\lambda^2}{2m}(1-\Phi(2\sqrt{ma}))}. \tag{6.28}$$

As we said before $\mathcal{P}$ decreases when a increases. Moreover for $a \gg 1/m$ we can do an asymptotic expansion for Φ finding

$$\mathcal{P} \simeq \exp\left(T\frac{\lambda^2}{4m\sqrt{am}}e^{-4am}\right), \tag{6.29}$$

so $\mathcal{P} \simeq 1$ effectively for $a \gg 1/m$.

The strong coupling limit has to be tackled with different, non-perturbative techniques.

The $d = 2$ case can also be solved exactly for any number n of parallel nodal lines by using the techniques in [94]. The resulting exact expression for $n \geq 3$ is too cumbersome to be presented here and we refer the reader to [94] for details.

Two parallel nodal lines separated by a distance a in the limit $\Lambda \to \infty$ are dual to the problem of two points in 1 space dimension at a distance a. The Casimir energy for this configuration is:

$$\mathcal{E}_{\text{int}} = \frac{1}{4\pi}\int_0^\infty \frac{dE}{\sqrt{E}} \ln\left(1 - \frac{e^{-2a\sqrt{E+m^2}}}{(1+\frac{2}{\lambda}\sqrt{E+m^2})^2}\right). \tag{6.30}$$

We can use this formula to make some predictions about $\mathcal{P}$. To begin we know that $\mathcal{E}_{\text{int}} < 0$ and that it has a minimum at $a = 0$ as $\mathcal{E}_{\text{int}}(a = 0, \Lambda \gg \lambda) \simeq -\lambda \log(2)/2\pi$ (here we put for simplicity $m = 0$). It can be proved that this is also equal to $\mathcal{E}_{\text{single}}(2\lambda) - 2\mathcal{E}_{\text{single}}(\lambda)$ (where $\mathcal{E}_{\text{single}}$ is the energy of a single delta function when $\Lambda \to \infty$), which appeals to intuition since at $a = 0$ we are just superposing two delta functions to create a delta function with double strength. If $m > 0$ it can be proved

that $\mathcal{E} \propto \exp(-2ma)$ and hence again $\mathcal{P} \simeq 1$ when $a \gg 1/m$. In any case we can say that $\mathcal{P}$ decreases when a increases.

A difficulty must be noticed here, concerning how far one can push the interpretation of S_γ as the probability of having a nodal line γ. Reasoning like in [95], assuming Dirichlet boundary conditions on a line γ intersecting the x_1 axis at say $x_1 = 0$ we have then to expand our RW in series of $\sin(k_j x_1)$ (with random coefficients). Reasonably the subset of RW that has a nodal line on γ should be expandible in this basis as well. If moreover our spectrum is cut off at Λ then one expects that for $a \ll \pi/\Lambda$ one should find much fewer nodal lines (the first zero of $\sin z$ is at $z = \pi$). In fact a similar phenomenon is found in [95] for the monochromatic spectrum. The nodal line length density normalized to its asymptotic value goes to ~ 0.5 for $x_1 = 0$. However increasing x_1 the nodal line length density suddenly increases to a value higher than the asymptotic value and then relaxes, oscillating, to 1. In analogy our quantity $\mathcal{P}$ should then start from a value < 1 at $a = 0$, increase in a region $1/\Lambda$ to a value $\mathcal{P} > 1$ and then relax to $\mathcal{P} = 1$. Evidently the first, $\mathcal{O}(1/\Lambda)$ region is not captured by our analysis, while the second one is. This, as we said in the discussion after Eq. (6.9), can possibly be traced back to the failure of the 'mean field' approximation that was used to link S_γ with the true probability of finding a nodal line [91]. We have hence learned that we must assume $a \gg 1/\Lambda$ for our results to hold. Equation (6.30) for $a \gg 1/\Lambda, 1/\lambda$, and $m = 0$ gives

$$\mathcal{E}_{\text{int}} = -\frac{\pi}{24a}, \tag{6.31}$$

yielding

$$\mathcal{P} = e^{\pi T/24a}. \tag{6.32}$$

The higher dimension ($d > 2$) case cannot be solved in general, due to its strong geometry dependence. The constant time section of γ can be any hypersurface representing disconnected conductors in space. The Casimir problem is the most generic one and we do not posses an efficient way of solving it. We know however how to solve the case of parallel, large (actually, infinite) $d-2$ hyper-planes (lines in $d = 3$.

planes in $d = 4$ etc.). The result for $m = 0$, $\lambda \to \infty$ is

$$\mathcal{E}_{\text{int}} \propto -\frac{S}{a^{d-1}} \tag{6.33}$$

where S is the $d-2$ dimensional area of the hyper-planes, a their separation and the proportionality constant depends on d.

One of the main problems of Casimir physics is to find effective (analytical or numerical) ways of calculating the Casimir energy for arbitrary configurations of perfect conductors. Despite recent developments [4, 96] this problem escapes analytical solution for all but the simple parallel plates case. We then expect to gain some insights from the other side of the duality, namely the nodal lines distributions.

6.5 Extensions and further developments

Extension to different spectra. It would be interesting to know how much of what we said in this chapter, based on the scalar field spectrum, is valid for other spectra (like the monochromatic spectrum). The monochromatic, as well as other kinds of isotropic spectra cannot be modelled by an Hamiltonian field theory, even thought their probability functional is gaussian. The high degree of non-locality of these spectra implies that the free energy F is not extensive. Hence we could not even define a T-independent quantity like the Casimir energy $\mathcal{E}$. It is hence of great interest for a field theorist to grasp some of the properties of these generalized free QFTs in terms of some, more intuitive perhaps, statistical properties of random waves.

Extension to codimension > 1. Generically nodal lines of real fields have codimension 1 (lines in the plane, etc.) because they are defined by a single condition, namely $\phi(x) = 0$. Codimension 2 or higher nodal lines are non-generic and have extremely low probability of occurring. For example the probability of having $\phi(x) = 0$ at an isolated point requires both $\phi(x) = 0$ and $|\nabla\phi(x)| = 0$ at the same point. This is *extremely* unlikely in the sense that it has measure 0, and would never show up in a Montecarlo simulation. We know in fact from [94] that conductors of codimension 2

and higher cannot be defined with $\lambda > 0$. They *must* be defined as a limit $\lambda \to 0^-$. However the generating functional $S_\gamma(\lambda)$ is not well-defined for $\lambda < 0$. It diverges badly. Actually, since $S_\gamma(\lambda) = \left\langle e^{-\lambda X_\gamma} \right\rangle$, for $\lambda < 0$ it is finite and only if the probability distribution of X_γ decays at infinity faster than $e^{\lambda X_\gamma}$. It turns out that one can take the limits ($\lambda \to 0^-$ and shrinking γ to codimension > 1) in such a way that this divergence and the infinitesimal probability of a codimension > 1 nodal line occurring compensate, giving a finite value for S_γ.

Extension to complex fields and phase singularities. A nodal line of a complex field is a more interesting object than that of a real field [88]. Complex field nodal lines are phase singularities whose strength can be interpreted as a topological charge [92]. Various correlation functions of this charges have been calculated by means of the Gaussian field technology. It would be interesting to see what the Casimir energy analogy has to say on these objects.

Numerics. One of the main reasons this duality is interesting is that it could lead to a more efficient numerical algorithm for computing Casimir energies of conductors of arbitrary shape. However this issue is beyond the scope of this thesis and we leave them for future work.

6.6 Conclusions

We have shown that there is a dual description of random waves in terms of quantum field theory. In particular we put forward and started the exploration of the duality between the probability of having a nodal line close to a given disconnected reference curve and the Casimir energy of a configuration of conductors.

We used this duality to infer some properties of the distribution of nodal lines and we proved that, for the scalar field spectrum, nodal lines induce other nodal lines in their proximity. This last statement just follows from the attractive nature of Casimir interactions.

This duality can be used in the other direction to gain information on the Casimir energy of an arbitrary configuration of conductors from the statistical properties of

the nodal line.

Bibliography

[1] H. B. G. Casimir and D. Polder, Phys. Rev. **73**, 360 (1948).

[2] S. K. Lamoreaux, Phys. Rev. Lett. **78**, 5 (1997).

[3] B. V. Derjagin, Kolloid Z. **69** 155 (1934), B. V. Derjagin, I. I. Abriksova, and E. M. Lifshitz, Sov. Phys. JETP **3**, 819 (1957); For a modern discussion of the Proximity Force Theorem, see J. Blocki and W. J. Swiatecki, Annals Phys. **132**, 53 (1981).

[4] R. L. Jaffe and A. Scardicchio, Phys. Rev. Lett. **92**, 070402 (2004); A. Scardicchio and R. L. Jaffe, Nucl. Phys. B **704**, 552 (2005); A. Scardicchio and R. L. Jaffe, Nucl. Phys. B **743**, 249 (2006)

[5] M. Born and E. Wolf, *Principles of Optics*, Cambridge Univ. Press. (1980).

[6] M. Kline and I. W. Kay, *Electromagnetic theory and geometrical optics*, Interscience, N.Y. (1965).

[7] O. Schroeder, A. Scardicchio and R. L. Jaffe, Phys. Rev. A **72**, 012105 (2005).

[8] N. Graham, R. L. Jaffe, V. Khemani, M. Quandt, M. Scandurra and H. Weigel, Nucl. Phys. B **645**, 49 (2002).

[9] M. Schaden and L. Spruch, Phys. Rev. **58**, 935 (1998); Phys. Rev. Lett. **84**, 459 (2000).

[10] L. S. Brown and G. J. Macay, Phys. Rev. **184**, 1272 (1969).

[11] D. Deutsch and P. Candelas, Phys. Rev. D **20**, 3063 (1979).

[12] R. P. Feynman, *Lectures on Physics*, Addison Wesley, (1970).

[13] J. B. Keller, J. Opt. Soc. Am.**52**, 116 (1962); J. B. Keller, in *Calculus of Variations and its Application* (Am. Math. Soc., Providence, 1958), p. 27; B. R. Levy and J. B. Keller, Commun. Pure Appl. Math. **XII**, 159 (1959); B.R. Levy and J. B. Keller, Can. J. Phys. **38**, 128 (1960).

[14] M. C. Gutzwiller, J. Math. Phys.**12**, 343 (1971); *Chaos in Classical and Quantum Mechanics*, Springer, Berlin (1990).

[15] S. A. Fulling, J. Phys. A **35**, 4049 (2002) .

[16] See, for example, V. M. Mostepanenko and Trunov, *Casmir Effects and Its Applications*, Oxford University press, (1997).

[17] J. S. Dowker and G. Kennedy, Journ. of Phys. **A11**, 895, (1978).

[18] For a discussion, see Appendix A in Ref. [8].

[19] R. P. Feynman and A. R. Hibbs, *Quantum Mechanics and Path Integrals*, McGraw-Hill, (1965).

[20] M. V. Berry and K. E. Mount, Reps. Prog. Phys **35**, 315 (1972).

[21] Y. A. Kravtsov, Sov. Phys.-Acoust. **14**, 1 (1968).

[22] L. S. Schulman, *Techniques and Applications of Path Integration*, John Wiley & Sons; (1981).

[23] J. H. Hannay and A. Thain, [arXiv:physics/0303093] (2003).

[24] R. S. Decca, E. Fischbach, G. L. Klimchitskaya, D. E. Krause, D. L. Lopez and V. M. Mostepanenko, Phys. Rev. D **68**, 116003 (2003).

[25] G. L. Klimchitskaya and V. M. Mostepanenko, private communications.

[26] T. Poston and I. Stewart, *Catastrophe Theory And Its Applications*. Dover. NY. (1996).

[27] M. V. Berry and C. Upstill, Progress in Optics XVIII, 257 (1980).

[28] R. Balian and C. Bloch, Ann. of Phys **69**, 401 (1970); **63**, 592 (1971); **69**, 76 (1972).

[29] R. Balian and B. Duplantier, Annals Phys. **104**, 300 (1977); Annals Phys. **112**, 165 (1978).

[30] T. H. Boyer, Phys. Rev. **174**, 1764 (1968).

[31] H. Feshbach, *Theoretical Nuclear Physics, Nuclear Reactions*, Wiley-Interscience; (1993).

[32] F. D. Mazzitelli, M. J. Sanchez, N. N. Scoccola and J. von Stecher, Phys. Rev. A **67**, 013807 (2003).

[33] N. Bleistein and R. A. Handelsman, *Asymptotic Expansions of Integrals*, Dover, NY (1975).

[34] S. C. Creagh and R. L. Littlejohn, Phys. Rev. A **44** 836 (1991).

[35] S. C. Creagh, Annals Phys. **248** 60 (1996).

[36] M. V. Berry, M. Tabor, Proc. Roy. Soc. Lond, **A349**, 101 (1976).

[37] M. Schaden, private communication.

[38] M. Schaden and L. Spruch, [arXiv:cond-mat/0304290] (2003).

[39] E. M. Lifshitz, Sov. Phys.-JEPT, **2**, 73 (1956); N. E. Dzyaloshinskii, E. M. Lifshitz and L. P. Pitaevskii, Sov. Phys.-Usp., **4**, 152 (1961); L. D. Landau, E. M. Lifshitz, *Electrodynamics of Continuous media*. Pergamon, Oxford, (1960).

[40] S. K. Lamoreaux, Phys. Rev. Lett. **78**, 5 (1997); M. Bordag, U. Mohideen and V. M. Mostepanenko, Phys. Rept. **353**, 1 (2001); G. Bressi, G. Carugno, R. Onofrio and G. Ruoso, Phys. Rev. Lett. **88**, 041804 (2002).

[41] R. Golestanian and M. Kardar, Phys. Rev. A **58**, 1713 (1998); T. Emig, T. Emig, Europhys. Lett. **62**, 466 (2003); R. Buscher and T. Emig, [arXiv:cond-mat/0401451].

[42] H. Gies, K. Langfeld and L. Moyaerts, JHEP **0306**, 018 (2003).

[43] A recent review for the mathematically minded reader is: A. Uribe, *Trace formulae*, in *First Summer School in Analysis and Mathematical Physics: Quantization, the Segal-Bargmann Transform and Semiclassical Analysis* (Contemp. Math. 260), ed. by S. Perez-Esteva and C. Villegas-Blas, American Mathematical Society, Providence, 2000, pp. 61-90.

[44] M. V. Berry, J. Phys. A **5**, 272-91 (1972).

[45] J. Feinberg, A. Mann and M. Revzen, Annals Phys. **288**, 103 (2001).

[46] N. D. Birrell and P. C. W. Davies, *Quantum Fields In Curved Space*, Cambridge Univ. Press, Cambridge (1982).

[47] See for example S. Weinberg, *The Quantum Theory of Fields*, Cambridge Univ. Press, Cambridge (1996).

[48] G. Barton, J. Phys. A **37** (2004) 1011–1049; R. L. Jaffe, AIP Conf. Proc. **687**, 3 (2003).

[49] S. Reynaud, A. Lambrecht and C. Genet in "Quantum Field Theory under the influence of external boundaries" ed. K. Milton (Rinton Press, 2004) pg. 36.

[50] R. L. Jaffe and A. Scardicchio, JHEP 06 (2005) 006, [arXiv:hep-th/0501171].

[51] M. Abramowitz and I. Stegun, *Handbook of Mathematical Functions*, Dover Publications, Inc., New York (1970).

[52] P. W. Milonni. *The Quantum vacuum: An Introduction to quantum electrodynamics*, Academic Press, London (1994).

[53] M. P. Hertzberg, R. L. Jaffe, M. Kardar and A. Scardicchio, Phys. Rev. Lett. **95**, 250402 (2005).

[54] H. A. Bethe and R. Peierls, Proc. Roy. Soc. **A 148**, 146 (1934).

[55] E. Fermi, In *Collected Papers* Edited by E. Segré, University of Chicago Press (1962). Vol. 1 pg. 943.

[56] S. N. Solodukhin, Nucl. Phys. B **541**, 461 (1999).

[57] S. Albeverio, F. Gesztesy, R. Hoegh-Krohn and H. Holden, *Solvable Models in Quantum Mechanics*, AMS Chelsea Publishing, (2000).

[58] Ya. B. Zel'dovich, Sov. Phys. JETP **11**, 594 (1960).

[59] F. A. Berezin and L. D. Faddeev, Sov. Math. Dokl. **2**, 372 (1961).

[60] R. Jackiw, *Delta-function potentials in two- and three-dimensional Quantum Mechanics*, in "M. A. B. Beg Memorial Volume" A. Ali, P. Hoodbhoy, Eds., World Scientific, Singapore (1991).

[61] M. Reed and B. Simon, "Methods of Modern Mathematical Physics. II. Fourier Analysis, Selfadjointness," Academic Press (1980).

[62] B. Allen and A. C. Ottenwill, Phys. Rev. D **42**, 2669 (1990); B. Allen, B. S. Kay and A. C. Ottenwill, Phys. Rev. D **53**, 6829 (1990);

[63] B. S. Kay and U. M. Studer, Commun. Math. Phys. **139**, 103 (1991).

[64] N. Graham, R. L. Jaffe, V. Khemani, M. Quandt, M. Scandurra and H. Weigel, Nucl. Phys. B **645**, 49 (2002);E. Farhi, N. Graham, P. Haagensen and R. L. Jaffe, Phys. Lett. B **427**, 334 (1998);N. Graham, R. L. Jaffe, V. Khemani, M. Quandt, M. Scandurra and H. Weigel, Phys. Lett. B **572**, 196 (2003). For a review, see N. Graham, R. L. Jaffe and H. Weigel, Int. J. Mod. Phys. A **17**, 846 (2002).

[65] W. D. Goldberger and M. B. Wise, Phys. Rev. D **65**, 025011 (2002).

[66] V. M. Mostepanenko and N. N. Trunov, "The Casimir effect and its applications," Oxford University Press (1997).

[67] J. Polchinski, "String theory. Vol. 1: An introduction to the bosonic string," Cambridge Univ. Press (1998).

[68] F. Quevedo, Class. Quant. Grav. **19**, 5721 (2002).

[69] N. Graham, R. L. Jaffe, M. Quandt and H. Weigel, Phys. Rev. Lett. **87**, 131601 (2001).

[70] L. Randall and R. Sundrum, Phys. Rev. Lett. **83**, 3370 (1999).

[71] R. Hofmann, P. Kanti and M. Pospelov, Phys. Rev. D **63**, 124020 (2001).

[72] M. G. Alford and F. Wilczek, Phys. Rev. Lett. **62**, 1071 (1989).

[73] M. T. Jaekel and S. Reynaud, Phys. Lett. A **167**, 227 (1992).

[74] N. D. Birrell and P. C. W. Davies, *Quantum fields in curved space*, Cambridge Univ. Press, 1982.

[75] Both kinds of divergences are discussed in detail in Ref. [77]

[76] See for example S. Weinberg, *The Quantum Theory of Fields*, Cambridge Univ. Press, 1996.

[77] N. Graham, R. L. Jaffe, V. Khemani, M. Quandt, O. Schroeder and H. Weigel, Nucl. Phys. B **677**, 379 (2004).

[78] N. Graham, R. L. Jaffe, M. Quandt and H. Weigel, Phys. Rev. Lett. **87**, 131601 (2001); Annals Phys. **293**, 240 (2001).

[79] J. Zorbas, Journ. Math. Phys. **21**, 840 (1980).

[80] R. Newton, *Scattering Theory of Waves and Particles* McGraw-Hill, New York, 1966; M. Goldberger and K. Watson, *Collision Theory* John Wiley & Sons, New York. 1964; K. Gottfried *Quantum Mechanics* W. A. Benjamin, New York, 1966.

[81] L. D. Landau and E. M. Lifshitz, *Quantum Mechanics: Nonrelativistic Theory* Pergamon Press, Oxford, England, 1997.

[82] M. V. Berry and K. E. Mount, Reps. Prog. Phys. **35**, 315 (1972).

[83] M. Abramowitz and I. Stegun, *Handbook of Mathematical Functions*, Dover Publications, Inc., New York, 1970.

[84] M. Bordag, U. Mohideen and V. M. Mostepanenko, Phys. Rept. **353**, 1 (2001).

[85] R. Bracewell, *The Hilbert Transform* in *The Fourier Transform and Its Applications*, 3rd ed. New York. McGraw-Hill, pp. 267-272, 1999.

[86] N. Graham, R. L. Jaffe, V. Khemani, M. Quandt, M. Scandurra and H. Weigel, Nucl. Phys. B **645**, 49 (2002).

[87] P. Hoodbhoy, [arXiv:quant-ph/0411031].

[88] M. V. Berry and M. R. Dennis, Proc. Roy. Soc. Lond. A **456**, 2059 (2000). Corrigenda in A **456**, 3048 (2000).

[89] A. Weinrib and B. I. Halperin, Phys. Rev. B **26**, 1362 (1982).

[90] M. V. Berry. J. Phys. A: Math. Gen. **10**, 2083 (1977).

[91] G. Foltin, S. Gnutzmann, U. Smilansky, J. Phys. A: Math. Gen., **37**, 11363 (2004); G. Blum, S. Gnutzmann, and U. Smilansky, Phys. Rev. Lett. **88**, 114101 (2002).

[92] B. I. Halperin, in R. Balian et al., eds. Les Houches, Session XXXV, pg. 813 (1980).

[93] E. Bogomolny and C. Schmit, Phys. Rev. Lett. **88**, 114102 (2002).

[94] A. Scardicchio, Phys. Rev. D **72**, 065004 (2005).

[95] M. V. Berry, J. Phys. A: Math. Gen. **35** 3025 (2002).

[96] H. Gies, K. Langfeld and L. Moyaerts, JHEP **0306**, 018 (2003).